Design and Development of a 7 Degree-of-Freedom Powered Exoskeleton for the Upper Limb

Joel C. Perry

A dissertation submitted in partial fulfillment of the requirements for the degree of

Doctor of Philosophy

University of Washington

2006

Program Authorized to Offer Degree: Department of Mechanical Engineering

University of Washington
Graduate School

This is to certify that I have examined this copy of a doctoral dissertation by

Joel C. Perry

and have found that it is complete and satisfactory in all respects,
and that any and all revisions required by the final
examining committee have been made.

Chair of the Supervisory Committee:

Jacob Rosen

Reading Committee:

Jacob Rosen

Blake Hannaford

Joseph L. Garbini

Date: 8.15.06

In presenting this dissertation in partial fulfillment of the requirements for the doctoral degree at the University of Washington, I agree that the Library shall make its copies freely available for inspection. I further agree that extensive copying of the dissertation is allowable only for scholarly purposes, consistent with "fair use" as prescribed in the U.S. Copyright Law. Requests for copying or reproduction of this dissertation may be referred to ProQuest Information and Learning, 300 North Zeeb Road, Ann Arbor, MI 48106-1346, 1-800-521-0600, to whom the author has granted "the right to reproduce and sell (a) copies of the manuscript in microform and/or (b) printed copies of the manuscript made from microform."

Signature 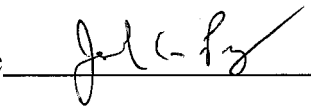

Date 10-13-06

University of Washington

Abstract

Design and Development of a 7 Degree-of-Freedom
Powered Exoskeleton for the Upper Limb

Joel C. Perry

Chair of the Supervisory Committee:
Research Assistant Professor Jacob Rosen
Electrical Engineering

An exoskeleton is an external structural mechanism with joints and links corresponding to those of the human body. With applications in rehabilitation medicine and virtual reality simulation, exoskeletons offer benefits for both disabled and healthy populations. A pilot database defining the kinematics and dynamics of the upper limb during daily living activities was among several factors guiding the development of an anthropomorphic, seven degree-of-freedom (DOF), powered arm exoskeleton. Additional design inputs include anatomical and physiological considerations, workspace analyses, and upper limb joint ranges of motion. Utilizing a seven DOF model of the human arm to calculate joint torques from measured arm kinematics, a pilot database defining typical ranges of motion and torque was compiled from 19 arm activities of daily living. A second ADL study including 6 subjects (N=6) and 24 daily actions confirmed prior result of the pilot study toward the definition of design requirements. Proximal placement of motors and distal placement of cable-pulley reductions were incorporated into the design, leading to low inertia, high-stiffness links, and back-drivable transmissions with zero backlash. The design enables full glenohumeral, elbow, and wrist joint functionality. Potential applications of the exoskeleton as a wearable robot include: (1) a therapeutic and diagnostics device for physiotherapy, (2) an assistive (orthotic) device for human power amplifications, (3) a haptic device in virtual reality simulation, and (4) a master device for teleoperation. Termed the CADEN-7 (Cable-Actuated Dexterous Exoskeleton for Neuro-rehabilitation), the exoskeleton arm offers remarkable opportunities as a versatile human-machine-interface and as a new generation of assistive technology.

TABLE OF CONTENTS

Page

LIST OF FIGURES

Figure Number Page

LIST OF TABLES

Table Number Page

LIST OF SYMBOLS

$\alpha, \ddot{\Theta}$	angular acceleration
α	neural activation
β	elbow lateral offset angle with respect to the upper arm
BW	bodyweight
cm	center of mass
ΔL	change in length
F	cable tension
F_m	cable tension at motor capstan
F_j	cable tension at joint
F_{CE}	force in the contractile element
f_l	force component factor based on muscle length
F_{max}	maximum voluntary contractile force of the muscle
F_{PE}	force in the parallel element
F_T	total force developed by a muscle
f_v	force component factor based on muscle velocity
$G(\Theta)$	7x1 vector of gravitationally dependent terms
i	index indicating the body segment number
I	arm segment inertia
j	index indicating joint number
K	arm segment radius of gyration
L	arm segment length
L_{CE}	instantaneous length of the contractile element
L_{CEo}	rest length of the contractile element
L_{max}	muscle rest length
L_{Ts}	tendon slack length
m	arm segment mass
$M(\Theta)$	7x7 mass matrix for upper arm, lower arm, and hand
r, R	attachment radius of cable or tendon
S	shape parameter relating to stiffness of the Hill model element
ϕ, θ, Θ	joint angular position
τ, T	joint torque
$V(\Theta, \dot{\Theta})$	7x1 vector of centrifugal and Coriolis terms
V_{CE}	velocity of the contractile element
u	normalized neural activation
$\omega, \dot{\Theta}$	angular velocity

GLOSSARY OF TERMS

Back-drivable: refers to a transmission that can be driven in either direction. Forces applied at either end of a back-drivable transmission will produce motion.

Cable: a wire rope constructed of twisted bundles of miniature wire strands. Higher strand counts yield cables that are more flexible

Capstan: a spool possessing a helical groove to maintain proper wrapping and alignment of cable. Capstans transmit rotary motion of motor shafts into cable travel.

Contractile Element (CE): element of the Hill-based model responsible for active shortening of the muscle

CE: Contractile Element

Distal: away from the midline of the body

Drive Pulley: the final "pulley" in a pulley transmission where cables terminate; the pulley that transmits torque about a joint

EF: Elbow Flexion-extension

Electrode: a non-corrosive, highly conductive metallic device responsible for measuring sEMG signals from underlying muscles.

Electromechanical delay (EMD): the time between the first synapse of neural intention and the mechanical response produced by the innervated muscle

Electromyography (EMG): the measurement of electrical signals that are produced by muscles during muscular contraction

EMD: Electromechanical delay

EMG: Electromyography

Exoskeleton: an external structural mechanism composed of joints and links corresponding to joints and links of the human body

FR: Forearm internal-external Rotation

Genetic Algorithm (GA): a method of deriving optimized solutions based on iterative "evolution" of an initial pool of "genes"

GA: Genetic Algorithm

Glenohumeral (G-H): refers to shoulder joint articulation between the head of the humerus and the glenoid fossa

G-H: Glenohumeral

Haptics: the study of touch and tactile sensation in the context of force-feedback mechanisms. From the Greek word *haptesthai* meaning "to touch".

HMI: Human-Machine-Interface

Human-Machine-Interface (HMI): a point of contact between the human and wearable device

Idler Pulley: a pulley located between the capstan and drive pulley for changing the direction of the cable route

Jacobian: a transformation matrix that converts

Kinematics: the study of motion

Kinetics: the study of forces that cause motion

Link: a structural member between two joints

Mapping Matrix: Matrix that 'maps' or transforms values from one coordinate system into another. See also Transformation Matrix.

mHMI: Mechanical HMI.

Myosignal: An electrical potential developed within the muscle during contraction, measurable from the surface of the skin.

Neuromuscular Disorder (NMD): A disorder effecting the neural or muscular system or both, characterized by one or more of the following: muscle weakness, denervation, muscle decay, spasticity, muscular pain, rashes, difficulty breathing, or difficulty swallowing.

nHMI: Neural HMI

NMD: Neuromuscular Disorder

Parallel Element (PE): A spring-like element operating in parallel with the contractile and series elements of the Hill Model, representing ligaments and other connecting tissues of the body that run in parallel to muscle.

PE: Parallel Element

Proximal: Characterized by close proximity to the midline of the body.

RAR: Robot-Assisted Rehabilitation

Reduction Pulley: A pulley in a cable-pulley system designed to lower or reduce the speed of the end-effector with respect to the driving element.

Robot-Assisted Rehabilitation (RAR): A recent modality of rehabilitation from injuries or impairments utilizing robotic technology to aid in the rehabilitation process.

SA: Shoulder Abduction-Adduction

Series Element (SE): A spring-like element operating in series with the contractile of the Hill Model, representing tendinous tissues of the body that run in series with muscle.

SF: Shoulder Flexion-extension

Singularity: a position of a mechanism where a degree of freedom is lost or compromised as a result of alignment between two joint axes.

Slack Length: Maximal length of an element without undergoing contraction or stretch.

SR: Shoulder internal-external Rotation

Transformation Matrix: Matrix that transforms or 'maps' values from one coordinate system to another. See also Mapping Matrix.

Trans-joint: Spanning across a joint, as in a trans-joint cable.

WD: Wrist radial-ulnar Deviation

WF: Wrist Flexion-extension

ACKNOWLEDGEMENTS

The author would like to thank the Departments of Mechanical and Electrical Engineering and the National Science Foundation for their long-term support over the duration of this project. Appreciation also goes to the University of Washington for harboring such cutting-edge research facilities as the Biorobotics Lab (Blake Hannaford), and for making possible the extent of inter-departmental collaboration necessary for continued advances in medical robotics. From the department of Rehabilitation Medicine, the author wishes to thank Dr. Stephen Burns for his extended collaborative efforts and Dr. Janet Powell for her interest and contributions to the work. The author also wishes to acknowledge the support of Michael Orendurff and Glenn Klute from the VA's Center of Excellence in Limb-Loss Prevention and Prosthetic Engineering, and Zoran Popovic, Stephen Spencer, and Seth Cooper from the UW's Graphics and Imaging Laboratory. Sincere appreciation is extended also to the following individuals who were involved significantly in aspects of data-collection, prototype development, real-time control environment setup, myoprocessor development, or exoskeleton component design (in reverse chronological order): Levi M. Miller, Trevor M. Bardine-Fowler, Ettore Cavallaro, Bobby Davis, Alan Sledd, Nathan Manning, and Alex Campbell.

The author would also like to thank Dr. Jacob Rosen for his countless contributions to the work. Undoubtedly, without his dedication, this work would not have taken place. He has been a mentor, an esteemed colleague, and a good friend. His unending support, insight, wisdom, perspective, and enthusiasm have been treasured and appreciated, and were vital to the completion of this work. It has been a sincere pleasure to collaborate with him, and an honor to be his first doctoral student.

Finally, to my wife and son: thank you for the many ways you have shown and continue to express your support. My appreciation for your devotion is beyond words.

DEDICATION

To my wife and child(ren)

CHAPTER 1: INTRODUCTION

Exoskeletons have existed in the minds of scientists and writers long before their realization as wearable devices. The term "exoskeleton" is derived from the words 'exo-', meaning "external", and 'skeleton', which refers to "a supporting structure or framework" [1]. The earliest well-documented exoskeleton, known as 'Hardiman', was developed in the 1960's by General Electric [2-4]. Weighing 1500 pounds, Hardiman's position-controlled hydraulic actuators were intended to produce amplifications of 25:1. However, only half of this strength was achieved and with only one arm. Unsupported walking was never accomplished, and the project was abandoned shortly thereafter.

Over the next 40 years, the state of exoskeleton research evolved to achieve much higher amplification ratios from devices that are, not surprisingly, both smaller and lighter than the 1965 prototype. Desired applications have increased from strictly human performance augmentation and military defense to haptic environment interaction and neuromuscular rehabilitation. Presently, there are more than 20 research facilities worldwide working to advance the state of upper-limb exoskeleton technology.

Adding to existing upper-extremity research, a new exoskeleton has recently been developed at the University of Washington Biorobotics Laboratory. The following sections present the objectives of the project, pertinent background information on neuromuscular rehabilitation and exoskeletons, and provide a detailed overview of the current exoskeleton project.

1.1. Exoskeleton Project Objectives

The primary objective of the University of Washington's exoskeleton project is to develop a seven degree-of-freedom (DOF) exoskeleton arm (see Figure 1.1) for use as a wearable force-reflecting device. An eventual objective, but not one that will be addressed in the scope of this document, is to demonstrate the feasibility of using a high-level control algorithm (myosignal-based) to control the developed seven DOF device.

This will extend the state of myosignal-based research four degrees of freedom beyond what has previously been controlled using this technology.

System development evolved in three stages. First, a period of assessment took place in which the requirements of the design were specified, followed by a 3-year period of mechanical design, fabrication, and assembly, and finally initial development of controllers and software structures. The developmental periods are discussed in Chapters 2, 3, and 4, respectively. A six subject ADL study was later performed to confirm previously assessed torque requirements (discussed in Chapter 5). Finally, a brief discussion of current stroke statistics and how exoskeleton technologies might satisfy present needs in the stroke population is presented in Chapter 6.

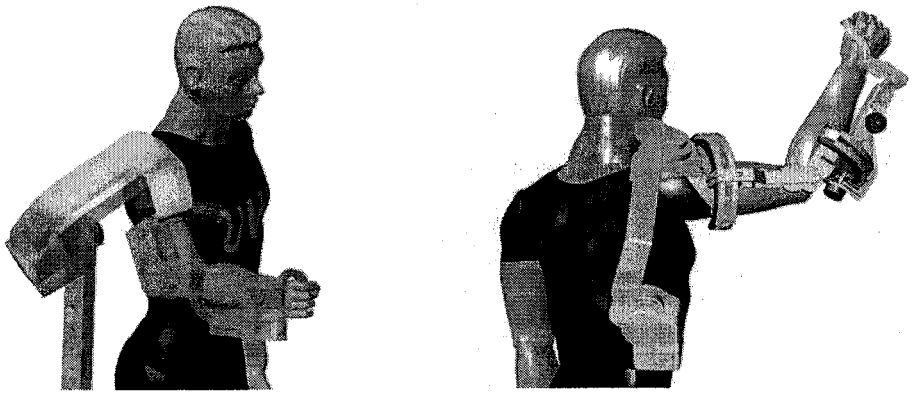

(a) (b)

Figure 1.1: Conceptual models of the exoskeleton structure: (a) covered view (b) exposed view

1.2. Background – Literature Review

Although the device has several intended applications, one of particular interest to the author is that for neuromuscular and stroke rehabilitation. For this reason, the background and literature review that follows is focused primarily on this application.

1.2.1. Significance – Population statistics

The most significant sources of muscular deficiency fall under two categories: neuro-muscular disorders and strokes.

1.2.1.1. Neuromuscular Disorders

Although exact population statistics are not known, results of a 1991 global survey estimate that more than one in every 3000 persons suffers the effects of a neuromuscular disorder (NMD) [5]. Neuromuscular disorders are diseases that can cause muscle weakness, muscle decay, cramps, spasticity, pain, rashes, difficulties with breathing and swallowing, as well as a number of other problems. Causes range from inherited or mutated genes to dietary deficiencies and unknown factors. Although there is a multitude of specific NMD's, they can be divided into three main categories: dystrophies, atrophies, and neuropathies. Muscular dystrophies alone contain over 60 variations of NMD's. Treatment varies widely depending on the disorder. Some neuropathies, such as carpal tunnel syndrome can be lessened via cortisone injections and surgery, whereas others, including muscular dystrophies and motor neuron diseases have no present cure or successful treatment.

1.2.1.2. Stroke Statistics

According to the American Heart Association, stroke is a leading cause of long-term disability in the US. Nearly 700,000 people sustain a first or recurrent stroke in the US each year leading to more than 5 million people currently live with the consequences of stroke. [6]. As such, stroke is considered the leading cause of disability despite advances in prevention and novel international treatments [7]. Improved medical treatment of the complications cause by acute stroke has contributed to decreased mortality, but 90% of the survivors have significant neurological deficits. Reducing the degree of permanent disability remains the goal of post stroke rehabilitation programs. Relying on the plasticity of the brain, new approaches to impairment reduction through managing sensorimotor treatment may contribute to reduced disability [8].

1.2.2. Current Rehabilitation Efforts

Classical approaches to rehabilitation fall under two categories: physical therapy and electrical stimulation. Methods are outlined in Table 1.1 and explained in further detail below.

1.2.2.1. Physical Therapy

Strength-based. Strength-based rehabilitation efforts have been the focus of many stroke rehabilitation studies. Some studies report the effect of simple muscular contractions against load on factors such as spasticity and functional performance [9-12] More recent studies examine the effects of feedback such as visual and auditory within the context of weight training regimes [13-15]. However, controversy still resides over the functional effectiveness of such strength-based approaches [13,15].

Table 1.1: Description of various types of motor deficit rehabilitation.

REHABILITATION TYPE	DESCRIPTION
Physical Therapy	
-Strength-based	Simple manual resistance to load
-Task-oriented	Functional task-related exercises
-Relaxation-based	Reduce spasticity by providing visual/auditory feedback during unwanted co-contraction, thereby training an awareness of spastic muscles
-Forced Use	Constraint-imposed use of deficient limb by restraint of the intact side
Electrical Stimulation	
-TES	Passive open-loop stimulation of musculature
-EMG-Stim	Muscle stimulation triggered by myosignal feedback
-FES	Pre-programmed muscular stimulation system for performing functional tasks
-FNS	Complex neuromuscular system which bypasses damaged length of spinal cord and is controlled entirely by user

Task-oriented. Several studies have considered a more task-oriented approach to rehabilitation, rather than focus solely on muscle strength. In these, a series of tasks/movements mimicking those useful for daily function are repeatedly performed by the subject [16-20]. Studies report reduced time to perform the tasks with training. Although improvements were seen in the non-paretic limb as well, substantially higher improvements were consistently seen in the paretic side.

Relaxation-based. Spasticity of the effected limb, a common symptom associated with NMD's, can be reduced through the application of confirmatory visual and/or

auditory feedback to subjects when they are able to relax non-agonist muscles during a contraction. Results show substantial neuromuscular improvements, although greater improvements were seen in patients who began treatment with a larger range of motion and less spasticity [21,22].

Forced-use. One of the leading methods of rehabilitation, with regard to lasting functional recovery, is that of forced use. The philosophy behind this approach is that non-use of the paretic limb is a learned activity that increases the deficit, promoting further non-use. By restraining the sound limb, and forcing subjects to use their paretic limb for periods of two weeks or more, significant improvements are made to the paretic limb that remain present more than one year post-treatment [23-25].

1.2.2.2. Electrical Stimulation

An alternate method of treatment, Electrical Stimulation has been utilized for therapeutic and functional use under a variety of modalities.

TES. The first report of the effects of Therapeutic Electrical Stimulation (TES) for treatment of spasticity in motor deficient patients was published in 1871 [26]. Results show lasting reductions in spasticity, however improvements on fiber size and strength have been inconsistent [27].

EMG-Stim. For patients capable of controlled motion but with minimal levels of force generation an emg-controlled biofeedback mechanism can boost muscle contractions under the subjects control. This form of treatment provides improved results over basic TES.

FES. In Functional Electrical Stimulation (FES), the electrical stimulus profile necessary to achieve specific functional tasks are pre-programmed and recalled on command. In this technique there is no element of control by the subject and, hence, no biological incentive to improve motoneuronal activity, although some reversal of muscle denervation is observed. FES has been in use since the 1970's [28].

FNS. Of increasing complexity, Functional Neuromuscular Stimulation includes systems that enable functional mobility in subjects suffering from complete transection of

the spinal cord. The more advanced of these systems are still in the theoretical stages of implementation.

Of the rehabilitation techniques presented above, those producing the best functional outcomes have been forced use and techniques aimed at improving other functional motor parameters in addition to strength [29,30]. Methods of rehabilitation from stroke and other conditions that affect the neuromuscular system have been changing slowly over the past decade, and are approaching of a new wave of technological advance. Starting with the introduction of the MIT Manus in 1992 [31], and others later [20,32-37], robot-assisted therapy [38-41] has gradually been making an appearance, changing the perceived limits of post-stroke rehabilitation and the optimal methodology for achieving those limits. Studies have shown robot-assisted therapy to have positive effects on impairment reduction and potential improvements over conventional treatment [38-41].

Among the electrical stimulation approaches, there is a clear benefit to an element of biofeedback as it provides the subject not only with increased control over the stimulation, but encourages the functional use of biological sensors and actuators [30,48,49]. Combining these favorable aspects of existing therapies and administering them through a wearable robot under the direct control of the user may lead to marked improvements over current rehabilitation efforts.

1.2.2.3. Myosignal-Based Treatment

Following the above definitions of different forms of electrical stimulation, it should be emphasized that myosignal-based control is not electrical stimulation. Rather, it involves passive superficial measurements of muscular activity. Contrary to treatment by electrical stimulation, no current flows into the human during myosignal-based (sEMG-based) control (Figure 1.2). Treatment regimes using sEMG-based methods eliminate the long-term effects of non-physiological muscle stimulation such as alterations of fiber type and intracellular matrix structures [50,51]. Additionally, direct control of assistive motor torques by the user enables rapid feedback of muscular activity and confirmation of correct or incorrect neurologic activity. The signals are processed individually to

obtain each muscle's envelope of activity, after which the envelopes are interlaced through a muscle model to predict the desired joint torques [52]. As a result, the device bridges the gap between intended and articulated motion of upper-limbs with mild to moderate neuromuscular impairment. It should also be noted that existence of some measurable sEMG activity from the user is essential for this particular mode of power assistance.

1.2.3. Existing Exoskeleton Systems

Several generic exoskeleton mechanisms and haptic devices were developed for various applications (e.g. [54-64]). Of particular interest, a seven DOF exoskeleton system for haptic interaction, developed at PERCRO [62], implements several design aspects worthy of note, including peripheral placement of singularities and open interface designs for axial rotations of segments.

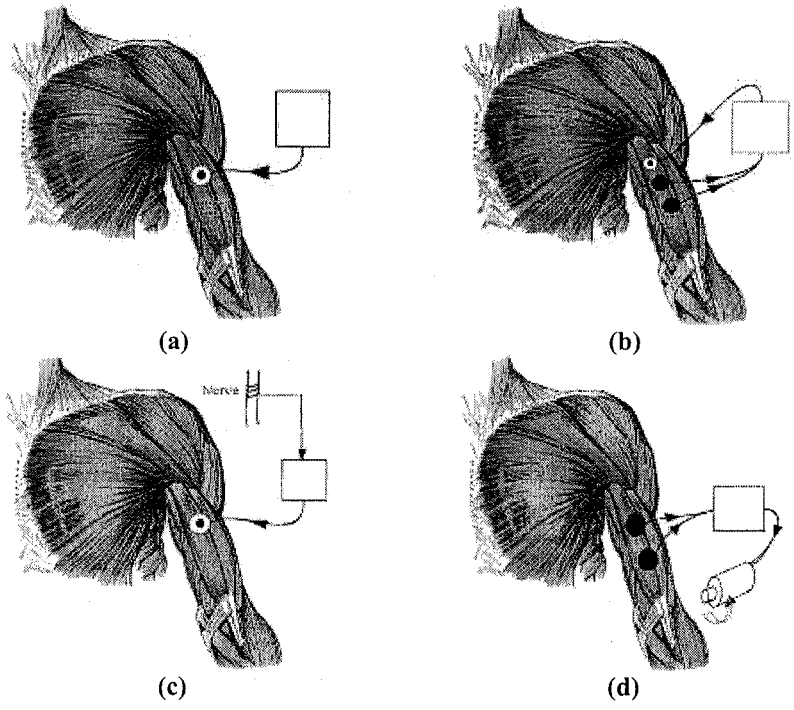

Figure 1.2: Electrical stimulation vs. sEMG-based control. In TES (a), EMG-Stim (b), and FES (c), current flows into the muscle denoted by the white circle with black center. SEMG-based control (d), however, muscle signals are only passively measured, shown by the black circles. Anatomical illustration from [53].

1.2.4. Previous Work

Over the past twelve years, three prototypes of an upper-limb powered exoskeleton have been developed. The first two prototypes, developed in Israel by Rosen et al. [65,66], were confined to a limited number of active degrees of freedom (Figure 1.3). These systems have demonstrated the feasibility of controlling 1-DOF and 3-DOF systems in a human augmentation mode using neural signals (sEMG) as the primary command to the system. The aim of these studies was to compare the performances of two types of muscle models (myoprocessors – Neural Network and Hill based Model) in terms of predicting the moments developed at human elbow and shoulder joint complexes based on joint kinematics and neuromuscular activity.

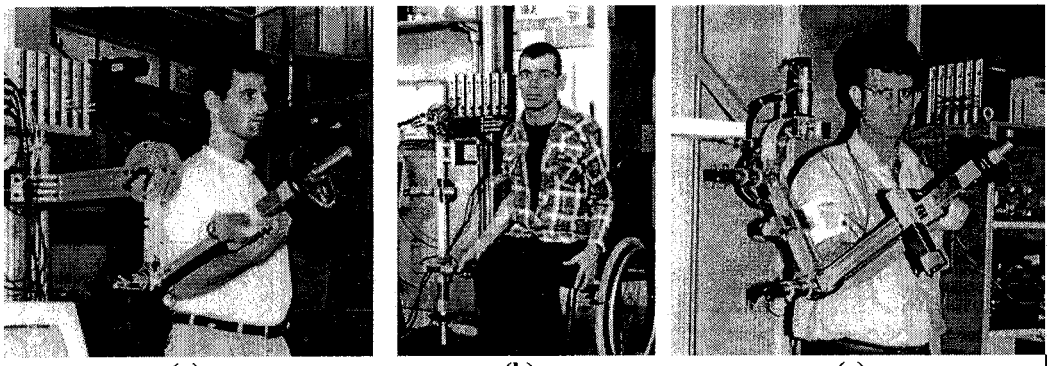

(a) (b) (c)

Figure 1.3: The first two prototypes of an upper limb powered exoskeleton. (a) One DOF (elbow joint) powered exoskeleton was developed as a proof of concept using myosignals as the primary command signals. (b) The one DOF exoskeleton system tested with disabled person suffering from Tay-Sachs. (c) The three DOF (2 shoulder joints, 1 elbow joint) powered exoskeleton was developed to study joint dependency during manipulation.

1.3. Exoskeleton Project Overview

Over the past 3 years (2002-2005), the third generation of an upper-limb powered exoskeleton has been under development, with the primary aim to help victims of stroke and neuromuscular disorders. The exoskeleton is an external structural mechanism with joints and links corresponding to those of the human body. Worn by the human, the cable-driven device transmits torques from proximally located actuators through rigid exoskeletal links to the human joints. Actuator current commands are computed by a

myoprocessor at each time-step based on measured sEMG signals. The total system is realized through the integration of both mechanical and software subsystems (Figure 1.4).

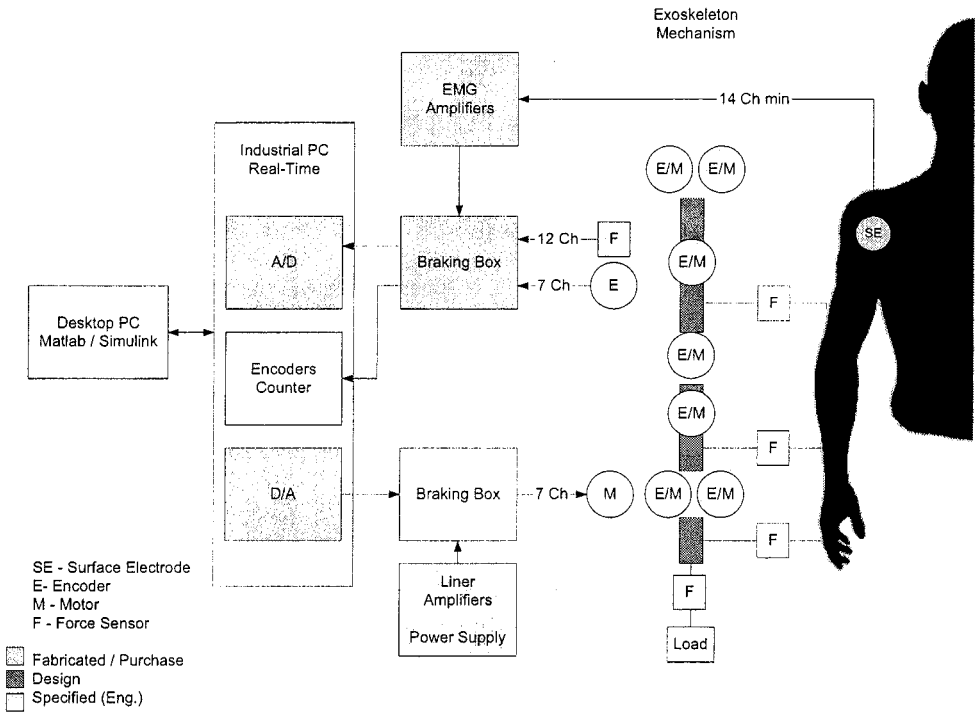

Figure 1.4: Project schematic showing relationship between exoskeleton and user and the software architecture

1.3.1. Mechanical Structure

The mechanical subsystems consist of the exoskeletal hardware, signal-acquisition and power hardware, and two personal computers. The exoskeleton hardware in Figure 1.4, consists of structural aluminum links, cables, and pulleys (shown in red); motors (M), encoders (E), force sensors (F), and surface electrodes (SE); signal acquisition and power hardware consists of a 64-channel EMG amplifier, and 5-volt, 12-volt, and 48-volt power supplies; a host computer (desktop PC) displays the Matlab and Simulink interface while a target computer (industrial PC) is equipped with digital-to-analog (D/A) and analog-to-digital (A/D) converters to perform real-time calculations based on acquired signals.

1.3.2. Software Structure

The real-time software structure consists of the following subsystems: 1) signal filtration, 2) the myoprocessor, 3) plant models, and 4) space mapping. Noise in acquisition signals makes it necessary to filter potentiometer and force-sensor signals prior to command signal calculations. The myoprocessor block is composed of three distinct modules that calculate muscle force using a Hill-based model, muscle length and moment arms from kinematic data, and muscle activation from sEMG signals (explained in Section 2.2.1.2). The plant model is a representation of the exoskeleton system to predict system behavior from given inputs. Space mapping refers to both kinematic and dynamic mapping from motor space to joint space and vice-versa (Section 4.1). The following section discusses the four modes under which the exoskeleton is designed to operate.

1.3.3. Applications – 4 Modes of Operation

The same device with different control algorithms may be used in four fundamental modes of operation:

1) power amplification
2) haptic virtual reality (VR) interface
3) active/passive power-assistance
4) master teleoperative control

The first mode can utilize the exoskeleton as a human power amplifier. The human provides control signals for the exoskeleton, while the exoskeleton actuators provide most of the power necessary for performing the task. The human becomes part of the system and applies a scaled-down force compared with the load carried by the exoskeleton.

In the second mode of operation, the exoskeleton can be used as a haptic device. Employing the exoskeleton as a haptic device is a relatively new technology aiming to simulate human interaction with virtual objects simulated in virtual reality. Immersed in a virtual environment, the operator can touch virtual objects while the exoskeleton structure and its actuators provide force-feedback, simulating aspects of realism such as

mechanical stiffness, weigh, and texture [67,68]. In this mode, the exoskeleton simulates an external environment and adds the sense of touch (haptics) to the otherwise purely graphical virtual environment.

The third mode is a hybrid mode including passive and active modes of assistance. In this mode, the exoskeleton may passively move the operator's arm or any other body part and gradually shift to an active assistance mode as previously define by the first mode. As a passive assistance device, the exoskeleton acts as a physical therapist to provide proper motions and treatment regimes to increase patient range of motion. As the assistance becomes more active, possibly controlled by the user sEMG signals, the mode describes the exoskeleton's role in neuromuscular rehabilitation.

In the forth mode the exoskeleton can be utilized as a master device for a teleoperated system enabling the operator to control a robotic arm (slave) form a distance. In a bilateral mode, the forces applied on the robotic arm by the environment are reflected back to the master and applied by the exoskeleton structure and actuators on the operator's arm. In this setup, the operator feels the interaction of the robotic arm tool-tip with the environment [69,70].

While all of these modes for controlling an exoskeleton are relevant to rehabilitation medicine, the one of particular interest to the author is power assistance as it applies to the disabled community. In this mode, the exoskeleton will assist users either as a wheelchair-mounted device or in a treatment center as a wall-mounted rehabilitation robot. As a result, the proposed study will focus primarily on aspects related to the third mode of operation.

1.3.4. Novel Control Strategy

As previously mentioned, one of the main objectives of the work is to demonstrate the feasibility of a high-level control strategy using sEMG signals as the primary command signals. This would elevate the controller to the neural level, increasing speed of response and overall feeling of oneness with the device. A recent workshop on medical robotics [71] noted, "At higher [command] levels, there need to be more robust techniques to interpret a patient's intentions." Part of robustness is maintaining stability

at higher gains, a feat shown achievable using sEMG commands [65,66] due to the nature of the signal, which can be measured 20-100 ms prior to force generation [72-74]. This advanced measurement of the command signal effectively increases the phase margin, affording greater stability and robustness at higher gains.

CHAPTER 2: PRELIMINARY INVESTIGATION

In this chapter, the results of two pilot studies on the human arm are presented. The first study, entitled "Activities of Daily Living", explores the kinematics and dynamics of the human arm while performing daily tasks, such as opening a door, picking up a phone, or eating with a spoon. The second pilot study, entitled "Surface EMG to Joint Torque Mapping", examines electromyographic signals that result from single joint motions under known loading conditions.

2.1. Pilot Study 1: Activities of Daily Living

The first pilot study was conducted on a single subject at the VA Puget Sound Health Care System's Center of Excellence in Limb-Loss Prevention and Prosthetic Engineering gait lab.

2.1.1. ADL Study – Methodology

The study on activities of daily living (ADL) consisted of, first, the collection of kinematic data according to the experimental protocol, and second, post-processing of kinematic data to calculate kinetics of motion throughout the recorded activities.

2.1.1.1. Kinematics – Experimental Protocol

The kinematic data of the human arm of a single subject during daily activities were collected using the VICON motion capture system (Vicon Inc.) at a sampling frequency of 120 Hz. Reflective markers were attached to a subject at key anatomical locations (Figure 2.1a). The subject was instructed to perform three repetitions of the same arm activity. The arm activities were divided into two subgroups: (1) general motions, and (2) actions (daily activities). Selecting the specific human arm actions was based on previous surveys of the disabled community indicating the desired tasks and functionality of powered orthotic devices and rehabilitation robots [75-77]. The general motion included a movement through a full range of motion of each of the human arm joints in a standing posture. The human arm actions during daily activities were performed in either standing or sitting body posture depending on the nature of the activity. During these activities, the

subject interacted with various small objects as dictated by each activity in an unconstrained environment. All motions and activities were performed using the subjects' right (dominate) arm. Given these conditions, no external forces or torques were applied on the human. Every action and general motion started from an initial arm position in which the arm was fully extended along the body. The following arm activities were included in the experimental protocol:

Actions

1. Arm in lap
2. Arm reach to head level
3. Arm reach to right, head level
4. Arm reach to left, head level
5. Arm reach right, move object to left side
6. Open door
7. Open Drawer/Close Drawer
8. Move object at waist level
9. Pick up phone on table/hang up
10. Pick up phone on wall/hang up
11. Eat with fork
12. Eat with spoon
13. Eat with hands
14. Drink with cup
15. Eat with spoon
16. Pour from bottle
17. Brush teeth
18. Comb hair
19. Wash face
20. Wash neck
21. Shave
22. Eat with fork (power – disabled grasp)
23. Eat with spoon (power – disabled grasp)
24. Full workspace motion

General Motions

1. Elbow flexion/extension
2. Elbow rotation (pronosupination)
3. Shoulder adduction/abduction
4. Shoulder flexion/extension
5. Shoulder interior/exterior rotation
6. Wrist flexion/extension
7. Wrist ulnar/radial deviation
8. Shoulder horizontal flx/ext
9. Full-range shoulder free motion

The arm action associated with eating with a spoon and a fork had two variations. Actions 11 and 12 involved normal fork/spoon handling (Figure 2.1c) where the fingers were used to orient the fork and spoon. In actions 22 and 23, a power gasp of the

fork/spoon along with maximal wrist joint flexion (Figure 2.1d) was used to emulate a method of fork/spoon handling commonly exhibited by patients who suffer from one of several neurological disorders.

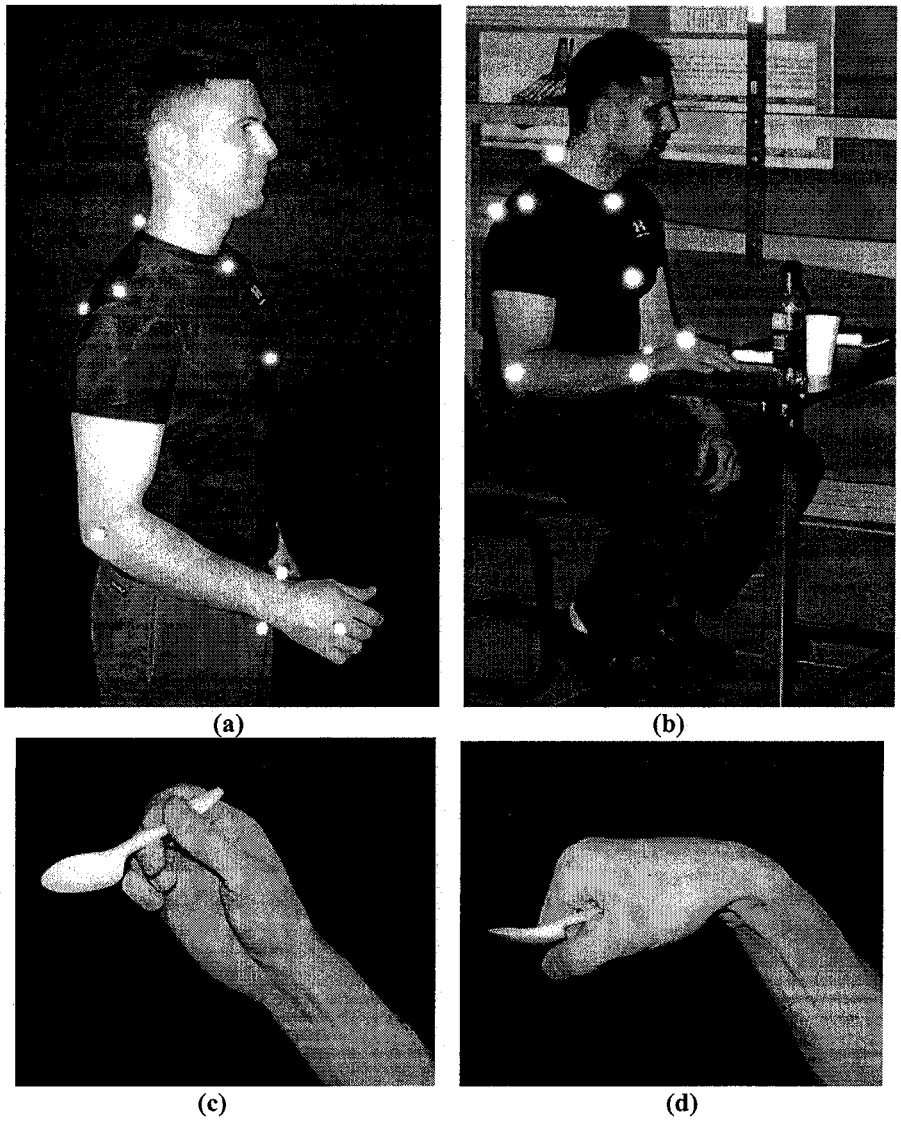

Figure 2.1: ADL pilot study experimental setup: (a) Reflective markers of a motion capture system attached to a subject at key anatomical locations (b) Motion capture of a subject's upper arm kinematics interacting with objects in daily activities (c) Holding a spoon with normal hand grasp (d) holding a spoon using a power grasp along with full wrist joint flexion, a typical pathology developed among several neurological disorders.

For each arm motion, Euler joint angles for the seven degrees of freedom (DOF) of the human arm were calculated based on the Cartesian coordinates of each marker. This transformation was performed based on an inherent model of the body that is incorporated into the Vicon system. The model incorporates anthropometric data that was measured directly from the subject under study. Each action was videotaped synchronously with the data collection performed by the Vicon system. A simulation of collected data using the human model within the Vicon system was compared with the video clip to ensure the appropriate transformation between marker coordinates and the calculated joint angles.

2.1.1.2. Dynamics – Post Processing

The human arm dynamics were studied using analytical and numerical approaches. A model of the human arm with seven DOF's was developed. Analytical expressions of the seven equations of motion were developed using Autolev (OnLine Dynamics Inc.). In addition, the dynamics of the human arm was simulated numerically using a numerical model within COSMOS/Motion, powered by the ADAMS® simulation engine. COSMOS/Motion is a virtual prototyping package for use with Solidworks CAD software. The coordinate systems that were assigned to each link of the human arm are depicted in Figure 2.2.

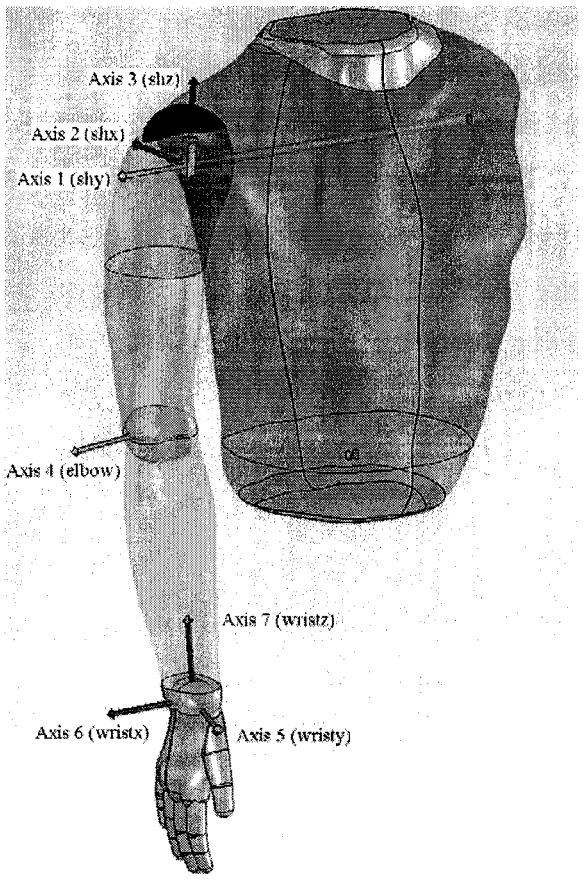

Figure 2.2: The human arm model and coordinate system assignments for each link of the human arm. Arm and torso model from BodyWorks (Zetec Ltd.).

The general form of the equations of motion is expressed in Equation 1.

$$\tau = M(\Theta)\ddot{\Theta} + V(\Theta, \dot{\Theta}) + G(\Theta) \qquad \textbf{Equation 1}$$

where $M(\Theta)$ is the 7x7 mass matrix, $V(\Theta, \dot{\Theta})$ is a 7x1 vector of centrifugal and Coriolis terms, G(Θ)is a 7x1 vector of gravity terms, and τ is a 7x1 vector of the net toques applied at the joints. Given the kinematics of the human arm $(\Theta, \dot{\Theta}, \ddot{\Theta})$ the net joints toque (τ) vector was calculated with and without the gravitational effect. These two parallel calculations allow one to examine the contribution of gravity in comparison to the combined effects on net torque from inertial, centrifugal, and Coriolis forces. In this case, the contributions from gravity could not be computed directly due to the size and complexity of involved equations.

2.1.2. ADL Study – Results

Figure 2.3 depicts typical time histories of the seven rotation angles, angular velocities, angular accelerations, and joint axes torques associated with one repetition of action 2 - Arm reach to the head level. In Figure 2.4, the statistical distribution of the same information depicted in Figure 2.4 is plotted. Similar statistical distributions for two other actions are plotted in Figure 2.5, including (1) moving an object at the waist level – action 8, and (2) picking up a phone on a wall – action 10.

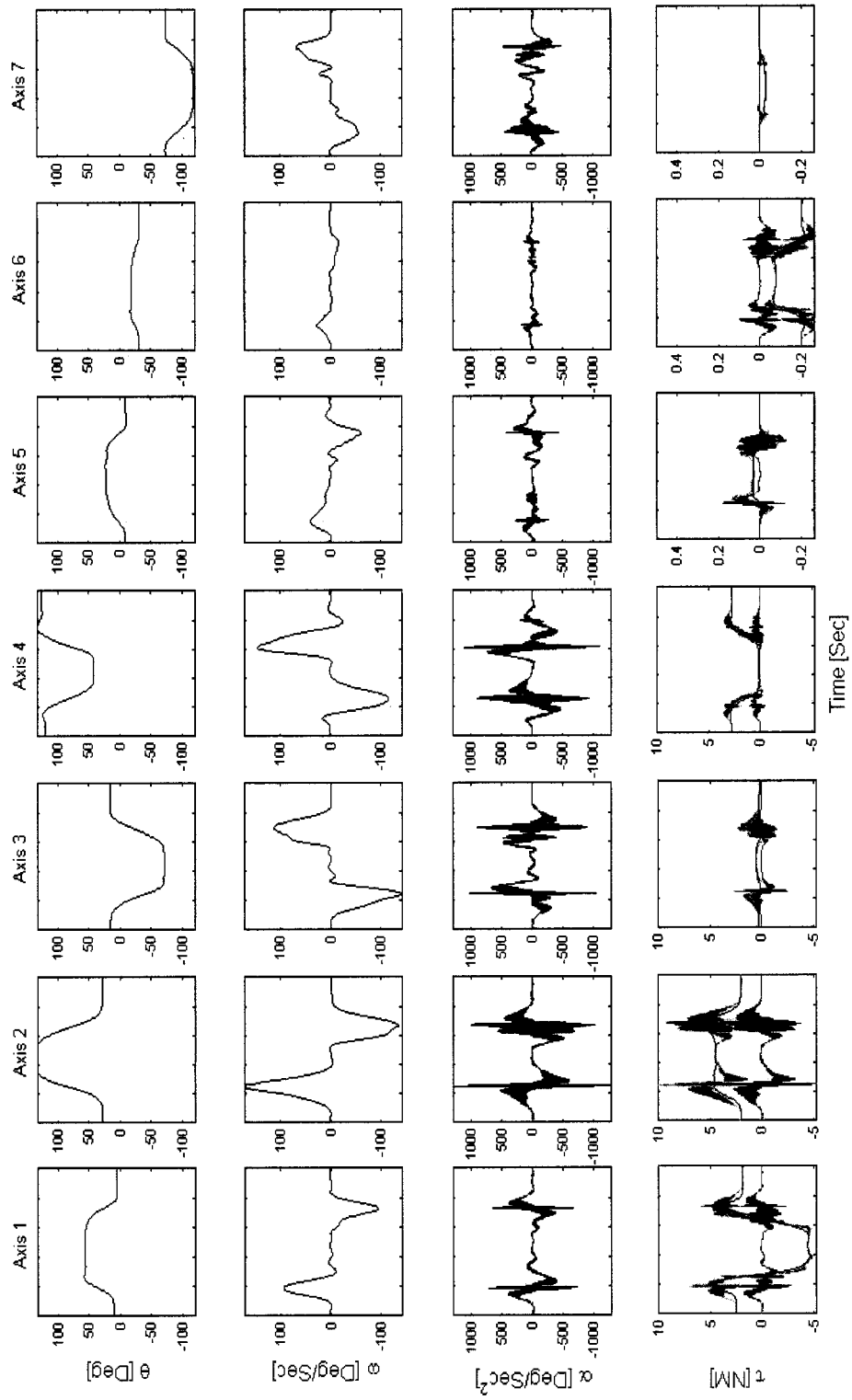

Figure 2.3: Time histories of the joint kinematics and dynamics of the human arm during an arm reach to head level (action 2). The three torque curves (bottom) illustrate the total joint axis torque (cyan), in comparison to the gravitational torque (black) and the combined torque due to inertial, centrifugal, and coriolis terms (magenta).

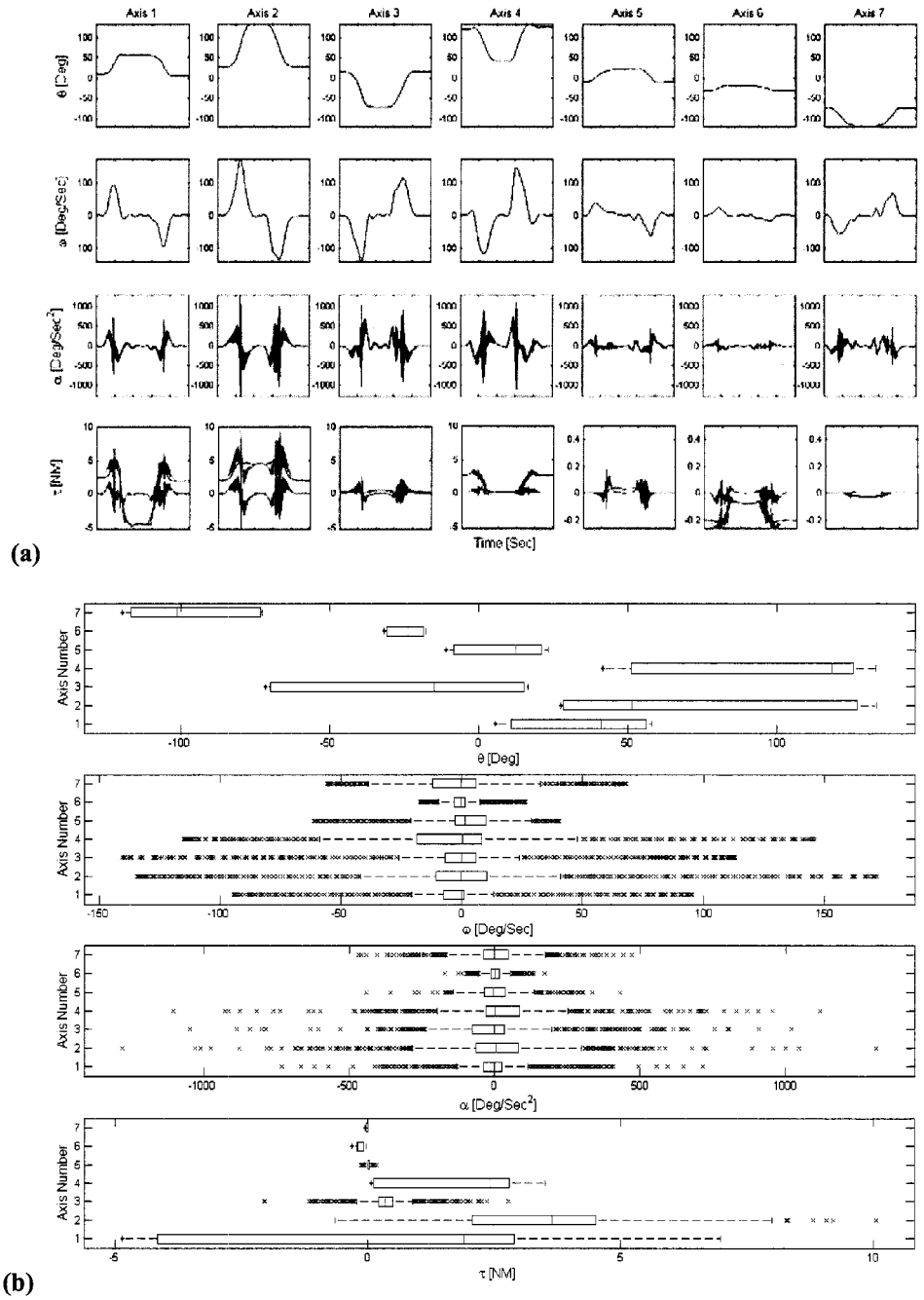

Figure 2.4: Time histories and statistics of the kinematics and dynamics of the human arm during an arm reach to head level (action 2): (a) Time histories of the joint kinematics and dynamics (b) Statistical distribution of the joint kinematics and dynamics. The line box plots of (b) indicate the lower quartile, median, and upper quartile values. The dashed lines extend beyond the upper and lower quartiles by one and a half times the interquartile range. Data that lies outside of this range is displayed with the symbol 'x'. Figure (a) is repeated from Figure 2.3, reshown here for easier comparison to representation (b).

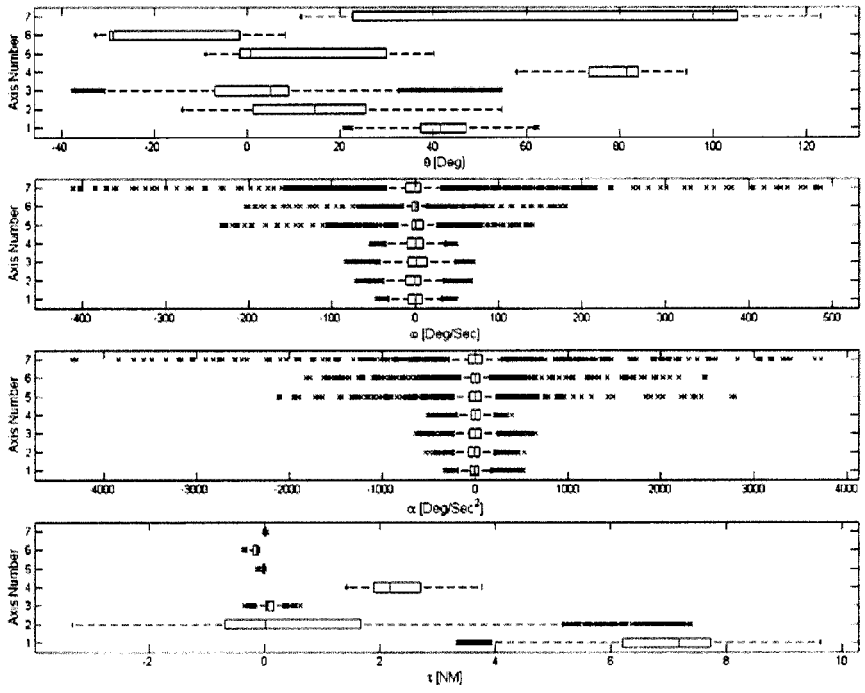

(a)

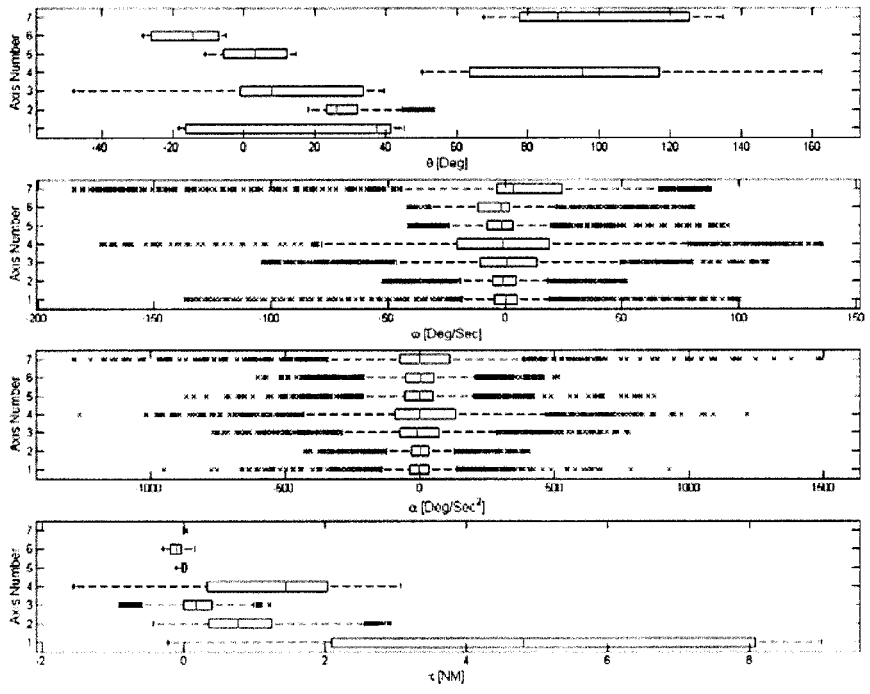

(b)

Figure 2.5: Statistics of the kinematics and dynamics of the human arm during various upper arm daily activities: (a) Statistical distribution of the joint kinematics and dynamics while moving an object at waist level (action 8), and (b) Statistical distribution of the joint kinematics and dynamics while picking and then hanging up a wall-mounted phone (action 10). See Figure 2.4 caption for explanation of box plot features.

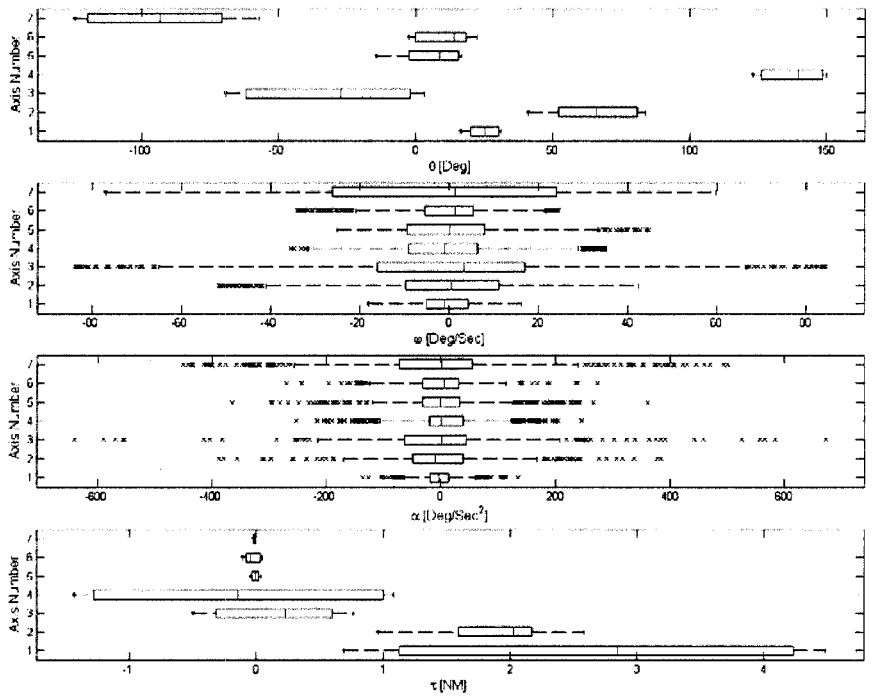

(a)

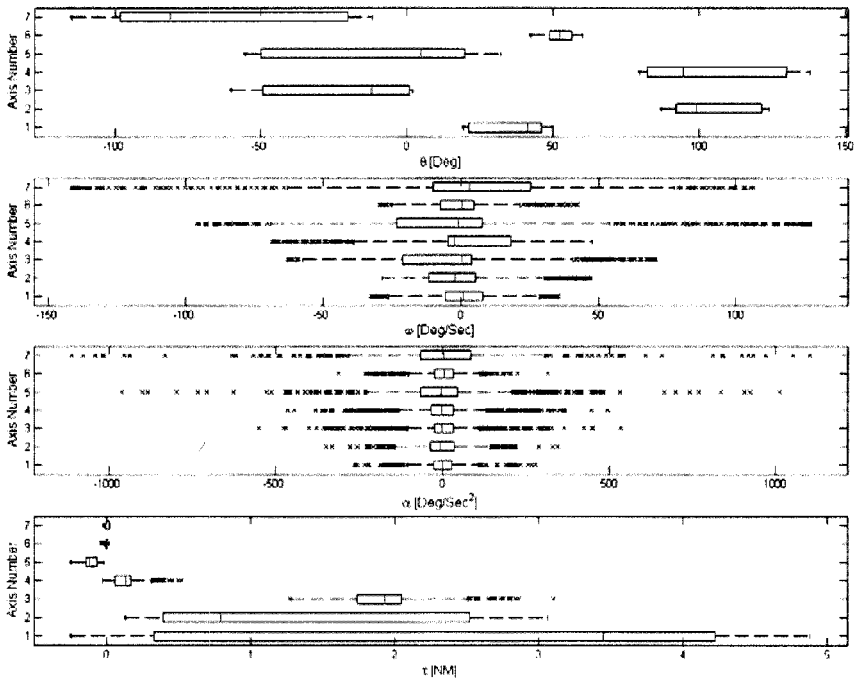

(b)

Figure 2.6: The human arm kinematics and dynamics statistical distribution while eating with a spoon using (a) normal spoon grasp – action 12, and (b) power spoon grasp, a typical pathology developed among several neurological disorders – action 23. See Figure 2.4 caption for explanation of box plot features.

These three actions represent three subgroups of actions including gross position actions (e.g. action 2), fine manipulation actions (e.g. action 8), and combined gross and fine manipulation (e.g. action 10). The results indicate that higher joint velocities of the shoulder and the elbow joints (axes 1-4) occur during gross positioning compared to lower velocities of the wrist joint (axes 5-7) – Figure 2.4b. This relationship of velocity magnitudes between the two joint groups (axes 1-4 and axes 5-7) is inverted during fine manipulation. One may note that the velocity magnitudes of axes 5-7 during the fine manipulation tasks exceeded the velocity magnitudes of axes 1-4 during the gross positioning tasks. In the actions involving both gross positioning and fine manipulation, the maximal axis velocities were similar.

Figure 2.3 (last row) depicts, for each joint, the total joint axis torque as well as the gravitational terms and the inertial, centrifugal, and Coriolis terms combined. In general, the magnitude of joint torque is small for the distal joint and higher for the proximal joints. Regardless of the joint location, the joint torque component that compensates the gravitational loads is significantly larger than the inertial, centrifugal, and Coriolis terms combined (Figure 2.4a). In fact, the overall shape of the joint axis torque during the selected daily activities is dictated solely by the low frequency gravitational term.

Comparison of kinematics and dynamics of the human arm while eating with a spoon in a normal and emulated disabled spoon grasp indicates a significant increase of the shoulder joint range of motion and joint torque during the emulated disabled spoon grasp. These phenomena are also associated with lower magnitudes of shoulder joint axis velocities in the case of the emulated disabled spoon grasp (Figure 2.6).

As a concluding result, Table 2.1 summarizes magnitude ranges of all kinematic and dynamic ranges along with mean and median values for actions 2, 8, 10, 12, and 23. Note the relative size between mean joint torques with and without gravitational components; total joint torques (torTot) are larger than the equivalent torques without gravity (torAV) by an order of magnitude or more. Comparing normal and power grasp methods of eating with a spoon, kinematic alterations are made to accommodate the abnormal grasp; severe pronation and ulnar deviation lead to additional shoulder adduction and elbow extension.

Table 2.1: Summary of all the kinematic and dynamic ranges along with mean and median values for actions 2, 8, 10, 12, and 23. Data includes min, max, mean, and median values for angles (deg), angular velocities (deg/s), angular accelerations (deg/s^2), and torques (mNm) at each joint. Two torque values are provided, the total joint torque (torTot) and the velocity/acceleration-dependent torque (torAV), i.e., the torque required to position the arm without the presence of gravity. For correlation between joint label and corresponding axis label (for example shy = axis 1), see Figure 2.2.

		shy				shx				shz				elbow				wristy				wristx				wristz			
		min	max	mean	median	min	max	mean	median	min	max	mean	median	min	max	mean	median	min	max	mean	median	min	max	mean	median	min	max	mean	median
act02	theta	5.7	58.2	33.9	41.0	27.5	133.6	71.7	51.5	-71.7	16.7	-23.9	-14.8	41.7	133.1	94.6	118.6	-23.3	11.0	-8.0	-12.4	17.6	31.7	24.7	24.0	-119.8	-72.8	-97.2	-101.5
	vel	-94.6	95.0	-0.9	-0.1	-134.1	171.5	0.0	-0.2	-140.7	113.0	0.2	-0.1	-115.4	145.8	1.3	0.5	-40.2	61.1	0.0	-1.4	-26.5	17.3	0.0	0.2	-55.8	67.9	-0.1	-0.5
	accel	-732.7	715.4	2.6	-0.4	-1282.7	1311.7	-1.7	4.5	-1049.0	1020.3	3.2	-1.2	-1104.7	1117.5	6.0	2.2	-429.5	441.8	-3.6	5.0	-171.9	171.6	-1.1	-0.4	-466.9	471.2	-2.5	-1.0
	torTot	-4869.4	6990.1	297.8	1904.1	-640.4	10057.0	3609.1	3650.0	-2040.8	2791.2	368.8	341.2	73.2	3513.6	1704.1	2413.0	-173.0	128.6	-12.1	0.0	21.8	307.1	157.1	197.7	-40.6	3.2	-9.9	-1.7
	torAV	-2854.9	2276.5	5.3	-5.1	-5210.1	5492.0	53.1	19.0	-2416.6	2426.4	14.8	1.7	-516.5	1050.1	129.3	1.7	-179.1	118.3	-6.8	0.0	-100.4	119.9	8.7	0.2	-20.9	6.7	-0.3	-0.1
act08	theta	20.8	62.3	42.3	41.6	-14.0	54.6	16.7	14.6	-37.8	54.6	5.3	4.9	58.0	94.4	78.3	81.5	-40.1	9.1	-10.8	-0.6	-8.1	32.7	19.6	29.0	11.5	123.2	74.7	95.7
	vel	-46.9	48.9	0.1	0.0	-71.9	67.2	0.2	-0.8	-83.7	70.0	-0.5	1.5	-53.2	49.6	0.4	0.3	-141.2	232.9	-0.4	-0.4	-180.4	203.9	-0.3	-0.2	-412.8	486.3	-0.4	-0.3
	accel	-330.5	517.1	-0.4	-3.2	-534.7	531.7	-1.4	-8.6	-640.3	657.3	6.3	1.3	-507.7	398.6	-4.0	1.3	-2790.1	2116.2	-1.1	-2.5	-2476.2	1822.4	-0.1	0.5	-4343.6	3715.5	-1.6	2.5
	torTot	3344.7	9626.0	6841.9	7169.9	-3344.3	7377.1	947.9	17.9	-348.5	610.4	95.6	61.7	1417.4	3763.1	2271.1	2171.1	-21.9	132.4	23.2	11.6	83.2	373.8	160.2	147.9	-21.7	43.5	2.8	-0.1
	torAV	-1694.0	3245.1	-16.1	-17.9	-2344.5	2504.7	1.5	-7.4	-582.9	437.8	-18.9	-0.8	-610.2	1081.3	13.5	15.6	-43.0	42.8	-1.2	-0.3	-80.6	169.6	-0.3	0.8	-8.7	11.7	0.0	0.0
act10	theta	-18.3	45.0	20.1	37.3	18.2	53.2	29.2	26.2	-48.1	39.5	6.0	8.0	50.3	162.9	99.0	95.3	-14.6	10.8	-3.0	-3.3	5.1	28.3	15.7	14.4	67.6	134.9	98.1	88.3
	vel	-136.7	99.9	0.1	0.5	-51.9	51.5	0.2	-0.8	-103.4	112.0	-0.8	1.0	-172.8	135.7	1.1	-0.8	-95.2	40.9	0.3	1.4	-80.3	41.4	0.9	1.5	-184.7	87.6	1.6	3.7
	accel	-949.7	924.4	-0.2	-3.1	-426.1	403.3	-0.8	3.7	-767.0	773.3	-9.6	-9.3	-1266.1	1214.3	12.1	-1.4	-868.7	868.2	-1.1	0.0	-512.4	602.1	3.5	-2.4	-1288.0	1494.7	7.3	0.0
	torTot	-216.9	9029.5	4717.1	4807.1	-432.3	2914.4	873.9	763.6	-896.8	1212.9	113.8	177.1	-1561.3	3073.1	1076.9	1449.0	-56.3	95.5	-1.1	2.2	-153.9	282.5	88.3	98.7	-5.4	39.4	4.8	3.0
	torAV	-6049.8	4172.2	25.3	26.1	-2533.3	1505.9	-21.5	12.1	-994.9	690.7	-16.2	4.6	-1440.7	1383.0	36.8	18.1	-62.2	84.5	1.8	0.6	-193.7	149.9	1.8	1.9	-15.2	21.0	0.4	0.0
act12	theta	16.7	31.3	24.9	25.5	41.3	84.0	65.4	65.8	-69.2	3.0	-31.6	-27.4	123.2	150.1	137.7	139.7	-16.4	14.3	-6.1	-8.8	-2.4	22.3	10.6	14.1	-124.6	-57.0	-94.4	-93.4
	vel	-17.9	16.2	-0.5	-1.0	-51.6	42.4	-1.4	0.6	-84.0	84.5	0.0	3.3	-35.5	35.0	-1.0	-1.0	-44.7	25.1	-1.1	-0.2	-34.0	24.5	-0.3	1.4	-76.9	59.8	-0.3	1.3
	accel	-136.0	134.6	-1.6	-3.9	-388.6	383.4	-0.2	-9.3	-640.7	672.8	-1.9	2.9	-253.1	245.5	5.7	0.6	-361.2	365.2	-2.2	0.8	-270.1	273.3	-1.9	6.5	-450.6	500.2	-5.8	1.9
	torTot	693.4	4490.7	2677.5	2852.9	964.0	2584.0	1885.2	2027.1	-505.8	763.1	125.7	228.9	-1439.2	1082.2	-139.5	-149.9	-35.1	43.7	8.2	7.8	-109.8	44.1	-27.9	-46.7	-23.1	-7.6	-16.7	-18.7
	torAV	-435.6	338.4	-0.6	-10.6	-687.9	646.9	3.4	-16.7	-367.7	258.8	-7.7	-7.4	-236.9	378.4	27.4	20.2	-8.3	3.7	-0.8	-0.5	-27.0	32.6	2.1	1.5	-2.4	5.6	0.2	0.0
act23	theta	19.3	49.8	35.8	41.3	87.0	123.9	104.7	98.9	-59.9	1.9	-22.3	-12.1	79.5	138.1	103.5	94.6	-32.2	55.2	9.2	-4.7	-60.1	-42.3	-51.8	-52.3	11.7	114.9	65.8	81.0
	vel	-32.5	35.4	1.0	1.1	-28.6	47.2	-0.7	-2.2	-62.9	70.6	0.0	0.3	-68.6	47.7	-0.5	-2.2	-127.2	95.9	-0.3	0.8	-42.5	29.6	0.6	-0.2	-106.4	141.7	0.1	-3.2
	accel	-263.2	278.4	0.5	0.8	-348.8	343.8	-1.4	-6.8	-550.8	533.7	2.6	-0.6	-464.5	495.4	-0.4	-1.7	-1011.9	963.6	2.0	4.4	-316.0	310.4	0.0	-5.3	-1103.3	1114.0	-1.2	-3.2
	torTot	-247.5	4883.8	2538.0	3447.3	128.9	3063.5	1282.8	788.4	1273.8	3100.8	1890.0	1931.3	-29.0	518.0	129.6	130.6	18.3	245.8	108.4	121.0	-14.6	39.6	1.8	-2.4	-20.8	18.2	-1.9	3.7
	torAV	-691.4	662.1	-2.7	3.4	-534.8	485.2	-17.9	-16.8	-710.0	704.3	-9.4	2.7	-173.2	216.3	4.9	2.8	-79.4	58.6	-2.0	-0.5	-15.4	21.4	-0.3	0.1	-4.6	6.3	0.2	0.2

2.1.3. ADL Study – Discussion

Developing a powered exoskeleton that would serve a human operator adequately during daily activities requires a profound understanding of the kinematics and dynamics of the human arm during these activities, and is beyond the anthropometric information that has been widely known for several decades [78,79]. The aim of this study was to study the kinematics and dynamics of the human arm and to provide the engineering specification to facilitate the design of a seven degree-of-freedom powered exoskeleton. Three important observations resulted.

2.1.3.1. Gravitational Dominance

As expected, the joint torques decrease as we move from the proximal end of the arm to the distal end, which is also correlated with the muscular mass of the arm. Analyzing the contribution of individual terms of the arm's equations of motion indicate that the low frequency gravitational term is the most dominant term in these equations. The magnitudes of this term across the joints and the various actions is higher than the inertial, centrifugal, and Coriolis terms combined. These results justify using only the gravitational terms of the equations of motion as compensator in part of the control system.

2.1.3.2. 3 Types of Manipulation

The results indicate that the various joints' kinematics and dynamics change significantly based on the nature of the task. Gross position is usually achieved by utilizing the shoulder and the elbow joints with relatively low joint velocities. However, fine manipulations are performed by the wrist and forearm rotations with higher joint velocities.

2.1.3.3. Influence of Grasp

Studying two different ways in which a human hand grasps an object (e.g. spoon or fork) while eating shows indicates that despite similar starting points, ending points, and tip paths, the arm joint kinematics and dynamics are different. The shoulder joint that is usually used for gross manipulation was utilized to compensate for the reduced flexion/extension of the wrist as well as the fine manipulation of the spoon by the fingers

due to the power grasp. The shoulder joint compensations were pronounced by an increased range of motion as well as decreased velocity magnitudes. This result suggests that the exoskeleton might be utilized differently by a disabled person compared to a healthy operator due to specific and inherent disability regarding the range of motion of a specific joint or the method in which an object is grasped.

2.2. Pilot Study 2: Surface EMG to Joint Torque Mapping

The second pilot study was conducted on a single subject at the University of Washington Intramural Activities (IMA) facility. Surface electromyographic (sEMG) signals as well as joint position and load were recorded for a series of isolated-motion weightlifting exercises.

2.2.1. sEMG Study – Methodology

The following subsections outline the experimental protocol, development of the myo-processor, and parameter optimization of the myoprocessor for the sEMG Study.

2.2.1.1. Experimental Protocol and Preliminary Data Processing

The experimental protocol included flexion/extension movements of the elbow joint (0 - 145° range) using the "Arm Curl" VR2 Cybex (Cybex International, Inc) exercise machine (Figure 2.7). Each movement was repeated three times with three different loads (4.54, 6.80, 9.07 Kg) moving at three angular velocities (average values of 1.8 ± 0.26, 1.4 ± 0.13, 0.7 ± 0.04 rad/s, further referred to as fast, medium and slow). The joint angle was measured using a potentiometer (Midori America Corp., CA) attached on the Cybex machine aligned with the rotation axis. sEMG signals were collected using Silver-Silver Chloride surface electrodes (In Vivo Metric) from 28 individual right upper-limb, chest, and back muscles (Figure 2.7). Electrodes were located for optimal signal detection based on [80,81]. Maximal voluntary muscle activations were recorded during isometric contractions. The sEMG signals were amplified by analog amplifiers (Teledyne Inc.) and the data were sampled at 1KHz by a 14-bit A/D card (United Electronic Industries) using the Matlab Real-time workshop toolbox (Mathworks Inc.).

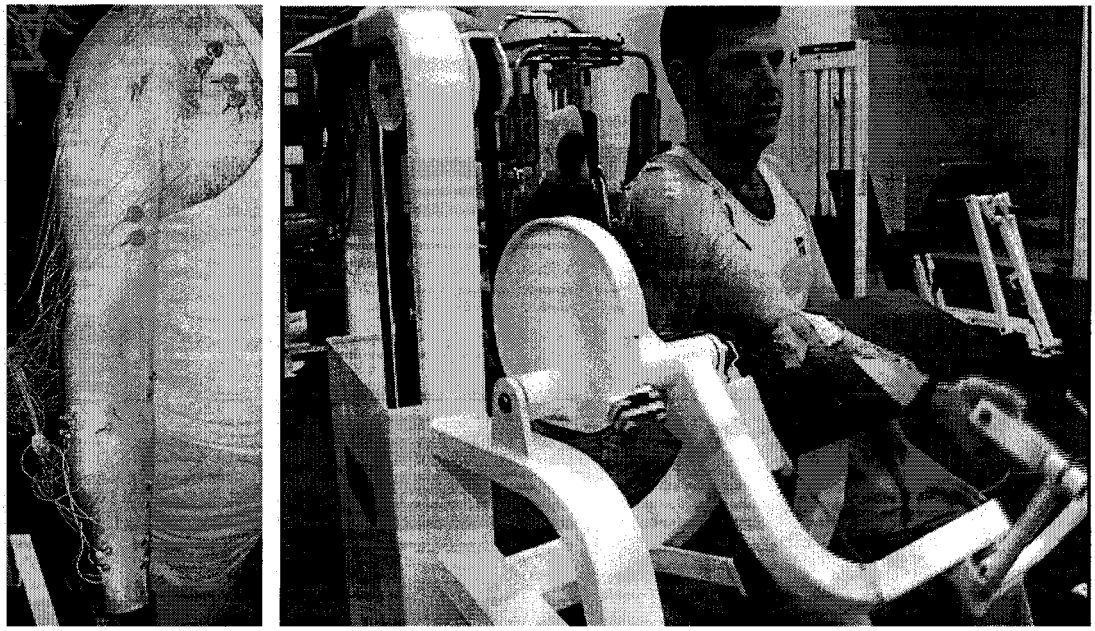

(a) (b)

Figure 2.7: sEMG pilot study experimental setup: (a) Surface electrodes attached to the subject measuring EMG signals from 28 muscles simultaneously, (b) Flexing and extending the elbow joint under different loads using a Cybex exercise machine while recording the joint position and muscle EMG signals.

The moments applied on the joint as a function of time by the external load were calculated based on the measured joint kinematics, and the Cybex machine geometry and mechanical model.

2.2.1.2. The Myoprocessor

The myoprocessor, depicted in Figure 2.8a, is composed of three modules: (i) a module that estimates the degree of neural activation based on measured sEMG signals, (ii) a module that computes the force exerted by the muscle using the activation level and the muscle length and shortening velocity, and (iii) a module that calculates the muscle lengths and moment arms given the joint angles and limb kinematics.

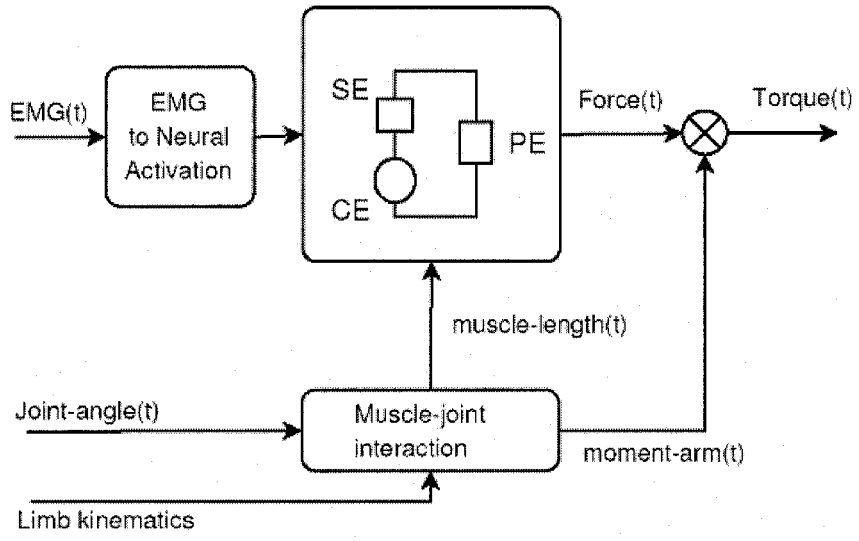

(a)

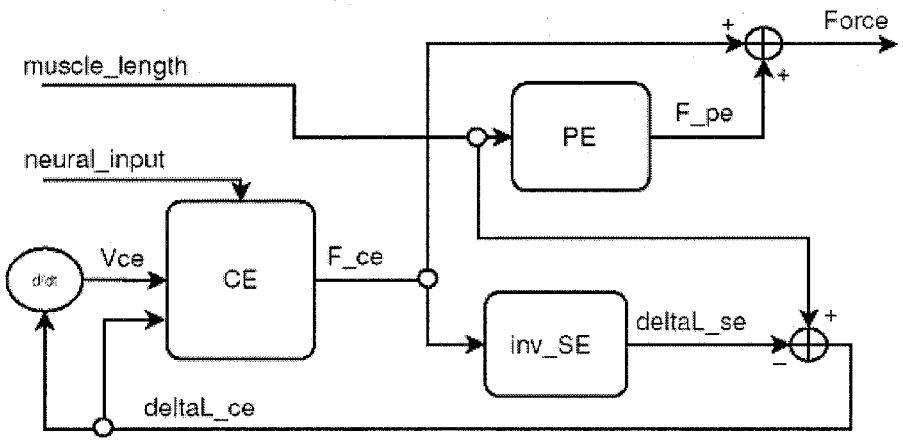

(b)

Figure 2.8: Muscle modeling block diagrams: (a) Myoprocessor Block diagram. (b) Detail of the Hill model implementation (see Eq. 2-7); the "inv_SE" block represents eq. 2 solved for ΔL given F_{CE} (equal to F_{SE}) as input.

Finally, the torque contribution from each muscle is computed as the product of force and the corresponding moment arm. A Myoprocessor for each of the seven muscles and sub-muscle groups (head) involved in flexion/extension of the elbow joint was implemented in the Matlab/Simulink environment (MathWorks Inc.). The modeled muscles are: Brachialis (BRS); Biceps Brachii long head (BLH); Biceps Brachii short

head (BSH); Brachioradialis (BRD); biceps Brachii long head (TLgH); Triceps Brachii medial head (TmH); and Triceps Brachii lateral head (TLtH).

The module converting sEMG to neural activation levels consists of a cascade of digital filters (with a causal implementation – using only past samples of the input) and nonlinear blocks: (1) Butterworth 4th order high-pass filter (10Hz cut-off frequency); (2) Butterworth 4th order notch filter (60 Hz); (3) full wave rectification; (4) Butterworth 4th order low pass filter (5 Hz cut-off frequency); (5) normalization with respect to the maximal voluntary muscle activation levels [1].

As previously indicated in the literature [82,83], the moment arm and the length-angle relation have a profound effect on the joint moment model prediction. For this reason a model of the muscle-joint interaction based on [84-86], has been implemented. The model in [84-86] takes advantage of data derived from the Visible Human Project. For each muscle, origin and insertion points are provided, together with fixed via points, i.e. points that constrain the muscle path. In order to provide better matching with the physiological path, muscles are allowed to wrap around obstacles that simulate other anatomical structures such as muscles, soft tissues, or bones. The obstacles are modeled as spheres, cylinders, or combination of these two basic elements. The muscle path is then calculated as the shortest path from origin to insertion while maintaining obstacle constraints.

The Hill model of the muscle is a phenomenological model commonly used for its relative computational simplicity. The model presents two elements arranged in series - the passive serial element (SE) and the active contractile element (CE) - and a passive element (PE) arranged in parallel to the previous two elements. The development of the Hill-based muscle model in this work follows previous research efforts [87-89]. An extensive review of literature has been presented by Yarden [89]. The functions describing the three principal elements of the model are defined by Equations 2-6 [87-89].

The force generated by PE or SE is defined as

$$F_{PE,SE} = \left(\frac{F_{\max}}{e^{S}-1}\right)\left(e^{\left(S\cdot\frac{\Delta L}{\Delta L_{\max}}\right)}-1\right) \qquad \textbf{Equation 2}$$

where ΔL is the change in length of the element with respect to the slack length, S is a shape parameter (related to the stiffness of the element), F_{max} is the maximum force exerted by the element for the maximum change in length ΔL_{max}, and $F_{PE,SE}$ is the passive force generated by the PE or the SE element depending on the set of parameters used.

The force generated by the CE element is defined as

$$F_{CE} = u \cdot f_l \cdot f_v \qquad \textbf{Equation 3}$$

$$f_l = \exp\left(-0.5\left(\frac{\frac{\Delta L_{CE}}{\Delta L_{CE_0}} - 0.05}{0.19}\right)^2\right) \qquad \textbf{Equation 4}$$

$$f_v = \frac{0.1433}{0.1074 + \exp\left(-1.3\sinh\left(2.8\frac{V_{CE}}{V_{CE_0}} + 1.64\right)\right)} \qquad \textbf{Equation 5}$$

$$V_{CE_0} = 0.5(u+1)V_{CE_{\max}} \qquad \textbf{Equation 6}$$

Finally, the total force, F_T, developed by the muscle is:

$$F_T = F_{CE} + F_{PE} \qquad \textbf{Equation 7}$$

In these equations u $\in$ [0, 1] is the normalized neural activation, V_{CE_0} is the maximal CE velocity when $F_{CE} = 0$, f_l is the F_{CE} when $V_{CE} = 0$ and $u = 1$, $V_{CE_{\max}}$ is V_{CE_0} when the activation is maximum (u = 1), L_{CE_0} is the optimal fiber length.

Although seven muscles are represented in the model, sEMG signals were recorded only from five of the muscles due to anatomical limitations in accessing these muscles using non-invasive techniques. In order to estimate the unmeasured neural activation

levels, the following assumptions were made: (i) the neural activity of the two heads of the Biceps, measured by a single pair of electrodes, was assumed to be the same except for a scaling factor; (ii) similarly, the Brachialis was assigned a scaled version of the Brachioradialis activation level [90,91].

2.2.1.3. Myoprocessor Parameter Optimization

A genetic algorithm (GA) was used in order to tune parameters of the model. GAs are commonly used as optimization techniques [92,93]. Their advantage over other techniques lies in their capability to handle very large search spaces, minimizing the risk of finding solutions that are only locally optimal. Given an optimization problem, defined by a certain (usually high) number of parameters, GAs find an optimal solution by using simulated evolution processes. The optimal parameters search begins from an initial random population of "chromosomes", each one representing a potential solution. The "survival of the fittest" criterion and "genetic operators" are used to reach a final population of best solutions [94]. Further details of the optimization routine can be found in [52].

In this study, the chromosome has been designed with 38 genes. Each gene represents a scaling factor γ with respect to the reference parameters shown in Table 2.2. A gene with a value of one preserves the reference value of the parameter it represents. For each muscle, 5 genes were used with bounded values including: optimal fiber length ($\gamma L_{CE0} \in$ [0.8, 1.2]), maximum force for the optimal fiber length when velocity is zero ($\gamma F_{CEmax} \in$ [0.5, 1.5]), fast fiber percentage ($\gamma_{\alpha} \in$ [0.5, 1.5]), shape factor for PE ($\gamma S_{PE} \in$ [0.8, 1.2]), and shape factor for SE ($\gamma S_{SE} \in$ [0.8, 1.2]). In addition, three other global parameters were defined: a scale factor for the activation of biceps long head with respect to the short head ($\gamma_{ebi} \in$ [0.8, 1.2]), a scale factor Brachialis / Brachioradialis activation level ($\gamma_{ebr} \in$ [0.5, 4]), and a geometric scale factor for the skeletal parameters ($\gamma_g \in$ [0:8; 1:2]).

The remaining parameters of the model (used in Eq. 2-7) not listed in Table 2.2 were computed as follows in Equations 8-12 [82,89]:

Table 2.2: Nominal parameters for the myoprocessor model based on [85,89]

Muscle	L_{max} [cm]	L_{CE_0} [cm]	L_{T_s} [cm]	$F_{CE_{max}}$ [N]	α [%]	S_{PE}	S_{SE}
BSH	40.46	13.07	22.98	461.76	56	9	2.8
BLH	41.94	15.36	22.93	392.91	56	9	2.8
TLgH	40.29	15.24	19.05	629.21	66	10	2.3
TMH	18.95	4.90	12.19	619.67	66	10	2.3
TLtH	28.22	6.17	19.64	1268.87	66	10	2.3
BRD	35.35	27.03	6.04	101.58	75	9	2.6
BRA	13.01	10.28	1.75	853.90	38	9	3

$$V_{CE_{\max}} = 2 \cdot L_{CE_0} + 8 \cdot L_{CE_0} \cdot \alpha \qquad \textbf{Equation 8}$$

$$F_{PE_{\max}} = 0.05 \cdot F_{CE_{\max}} \qquad \textbf{Equation 9}$$

$$\Delta PE_{\max} = L_{\max} - (L_{CE_0} + L_{T_S}) \qquad \textbf{Equation 10}$$

$$F_{SE_{\max}} = 1.3 \cdot F_{CE_{\max}} \qquad \textbf{Equation 11}$$

$$\Delta SE_{\max} = 0.03 \cdot L_{T_S} \qquad \textbf{Equation 12}$$

where α is the percentage of fast fibers in a muscle, L_{T_S} is the tendon slack length (other symbols have been previously defined). Given the experimental protocol, the data collected in one of the repetitions (namely the first repetition, medium velocity, 6.80 Kg load) was used for optimizing the model, whereas the other repetitions were used to evaluate the overall model prediction. In addition, the model predictions were assessed with respect to the actual moments using three criteria: maximum error (Eq. 13), root mean squared error (Eq. 14) and correlation coefficient (Eq. 15). The root mean squared error was also used as a fitness function for the GA.

$$E_{\max} = \max_i \left| T[i] - \tilde{T}[i] \right| \qquad \textbf{Equation 13}$$

$$E_{rms} = \sqrt{\frac{1}{N} \sum_{i=1}^{N} (T[i] - \tilde{T}[i])^2} \qquad \textbf{Equation 14}$$

$$\rho = \frac{C_{T\tilde{T}}}{\sigma_T \sigma_{\tilde{T}}} \qquad \textbf{Equation 15}$$

where T represents the actual torque, $\tilde{T}$ is the torque computed by the model, N is the number of sample points, $C_{T\tilde{T}}$ is the covariance coefficient, and σ_T and $\sigma_{\tilde{T}}$ are standard deviations.

2.2.2. sEMG Study – Results

Figure 2.9 depicts typical kinematics (joint angles), dynamics (joint torques), and the neural activation levels of the flexor/extensor muscles as a function of time. The joint kinematics and the neural activation levels of the muscles were used as inputs to the myoprocessor whereas the external joint load was used to optimize the model parameters and to assess the myoprocessor predictions.

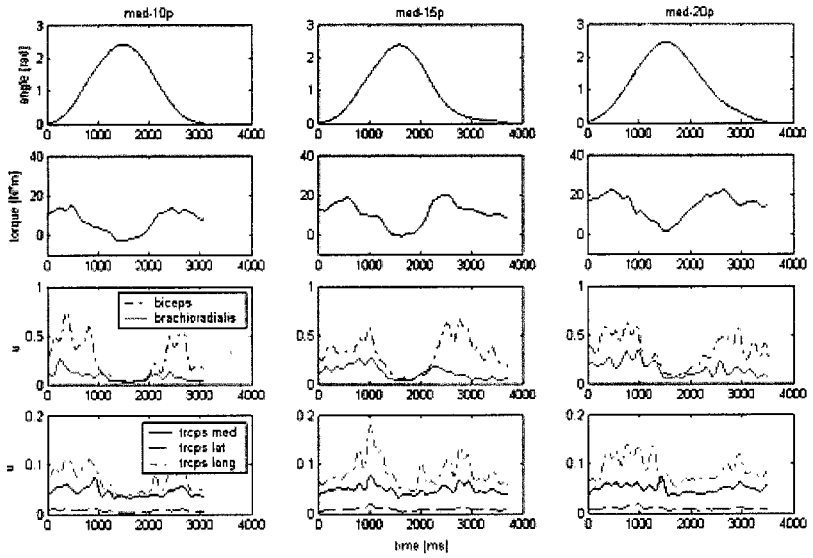

Figure 2.9: Typical datasets recorded as part of the experimental protocol for various loading conditions during flexion/extension of the elbow joint.

Typical joint torques as a function of time are plotted in Figure 2.10. The data depicted represents two repetitions of full flexion/extension of the elbow joint with the following loading conditions: (i) Figure 2.10 (top) - medium velocity, 6.8 Kg - data that

were used for optimizing the muscle parameters (ii) Figure 2.10 (bottom) - fast velocity, 9.07 Kg - data that were used for evaluate the myoprocessor predictions. Each plot includes three torques: (1) the actual torque as computed by using the kinematics and the dynamics of the Cybex exercise machine (actual), (2) the myoprocessor predictions with nominal model parameters (non optimized), and (3) with optimized parameters (optimized) using the GA.

The results of Figure 2.10 (top) indicate that the myoprocessor can predict the actual measured data with a maximum error of E_{max} = 6.5Nm, a root mean squared error of E_{RMS} = 2.67Nm, and a correlation coefficient of ρ = 0.91. The peak-to-peak torque excursion was 19.8 Nm. Conversely, the non-optimized model yielded values of E_{max} = 14.64Nm, E_{RMS} = 7.78Nm, and ρ = 0.79. The test data set depicted in the bottom plot yielded optimized E_{max} = 12.6Nm, E_{RMS} = 5.2Nm, ρ = 0.90 and non-optimized E_{max} = 23.4Nm, E_{RMS} = 11.4Nm, ρ = 0.82.

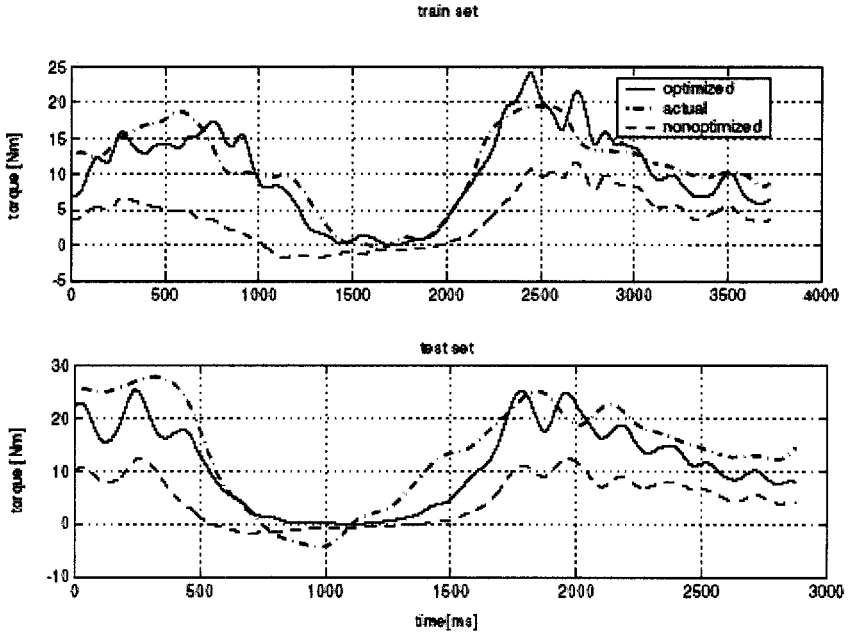

Figure 2.10: Actual (dash-dotted), non-optimized (dashed), and optimized (solid line) moments at the elbow joint during flexion/extension movements as measured and predicted by the myoprocessor. Top panel - the optimization set (medium velocity, 6.8Kg); bottom panel - one of the data sets used for evaluation (fast velocity, 9.07Kg).

Table 2.3 summarizes the experimental results using the metrics defined in Equations 13-15. The results were averaged over the two repetitions that were not used for the model optimization.

Table 2.3: Averaged results for the test data sets

trial	ρ	E_{rms} [Nm]	E_{max} [Nm]	total escursion [Nm]
fast, 4.54Kg	0.935	4.13	10.20	33.80
fast, 6.80Kg	0.895	4.97	12.85	31.93
fast, 9.07Kg	0.905	5.25	11.95	29.8
med, 4.54Kg	0.855	3.28	14.40	19.72
med, 6.80Kg	0.915	3.41	9.05	27.30
med, 9.07Kg	0.860	6.00	11.40	20.15
slow, 4.54Kg	0.780	3.08	9.78	8.89
slow, 6.80Kg	0.825	4.05	10.28	12.98
slow, 9.07Kg	0.695	7.15	12.30	12.20

As part of the optimization process using the GA, the myoprocessor internal parameters deviated from the nominal values presented in Table 2.2. Figure 2.11 depicts the parameters' scaling factors (nominal values are defined as zero) of all the internal model parameters. The most significant optimized scaling factors are: (1) the Brachioradialis to Brachialis sEMG scaling factor (~3.5); (2) the geometrical scaling factor (~1); (3) the maximum force of the three head of the triceps (lowered to the maximum extent); and (4) the fast fiber percentage scaling factors (greater than one for all the muscles).

The resulting optimal set of parameters (best chromosome) was obtained by using a population of 90 chromosomes and 500 generations. Additional details of mutations between generations can be found in [52].

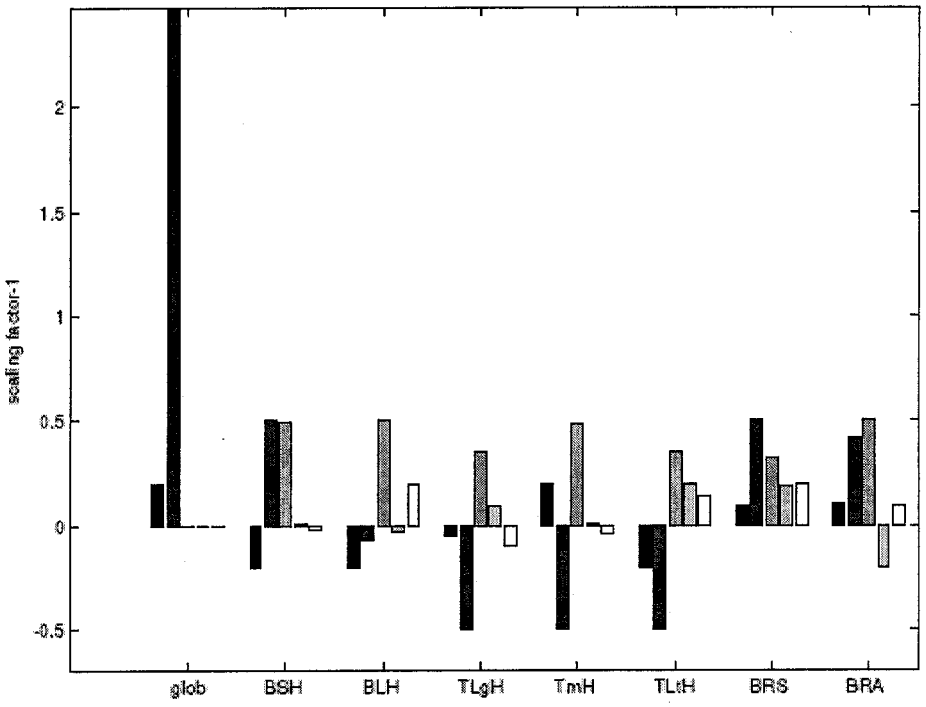

Figure 2.11: Scaling factors of the nominal values of the muscle models parameters obtained by the Genetic Algorithm optimization. The nominal values are defined in Table 2.2. For readability purposes, the scaling factor are presented here with an offset of one unit in the vertical direction. Hence, a value of zero indicates that no change was made to the nominal value of the parameter. The first three genes are 1) scaling factor for biceps long head sEMG, 2) scaling factor for brachialis sEMG, 3) geometrical scaling factor. For each muscle, the parameters are: 1) optimal fiber length, 2) maximum force at the optimal length, 3) fast fiber percentage, 4) S_{PE} parameter, and 5) S_{SE} parameter.

2.2.3. sEMG Study – Discussion

The objective of this study was to develop a myoprocessor to be used as an elbow joint moment predictor for an upper limb exoskeleton. As a central element of a neural-controlled exoskeleton, the myoprocessor should be robust, providing accurate torque predictions over broad loading conditions in real-time.

In order to achieve adequate performance and robustness, the myoprocessor has been developed with internal parameters that preserve close ties with physiological parameters of the muscles while maintaining the required simplicity to allow real-time operation. At its core, the myoprocessor is a Hill-based muscle model working in unison with a three-dimensional anatomical representation of the upper limb based on the Visible Human

Project [84-86]. Along with the experimental database obtained for various loading conditions, genetic algorithms were used to optimize a large set of internal parameters for the myoprocessor. This methodology allows one to modify the nominal generic internal parameters and tailor them for specific individuals. As indicated by the results, the ability of the myoprocessors to accurately predict the joint moment increased significantly with an optimized set of internal parameters.

The results indicated that the model is limited in predicting the joint moments for slow movements, particularly when the elbow joint approaches full flexion. This phenomenon could be explained by the lack of measured sEMG data for predicting the Brachialis muscle activation levels. Neural activation of the Brachialis was estimated as a percentage of the Brachioradialis activation level [90]. It was previously indicated that the Brachialis is more active during isometric elbow flexion, compared to dynamic elbow flexion, where the biceps plays a major role [91]. When the elbow joint approaches maximum flexion, the moment arm of the Brachialis reaches its maximal value and the joint angular velocity decreases until it reaches a value of zero at the end of the flexion movement. Therefore, it is reasonable to assume that the Brachialis contributes to the overall joint moment. As a result, an approximation of the Brachialis neural activity based only on the Brachioradialis may lead to some discrepancies in the overall model prediction in these specific conditions. The importance of the Brachialis is confirmed by the relatively high scaling factor (~ 3.5) obtained with respect to the Brachioradialis.

Also evident from the optimization algorithms was the tendency to lower the maximum force of the Triceps muscle. During the elbow flexion movement the Triceps muscle acts as a joint stabilizer, which decreases the net joint torque generated by the flexor muscles. Since joint stabilization through co-contraction is not part of the optimization criteria, the optimization process decreases the Triceps muscle contribution to the net joint torque. In future studies, more accurate extensor muscle parameters should be obtained by also including active extension movements in the optimization data set.

It is evident from the results (Figure 2.11) that no global geometrical scaling was necessary. This result is validated by a close match between the anthropometrical data of the subject under study and the visible human database that was incorporated into the model.

The fast fiber percentage (α) increase that was obtained after the optimization, even if not physiologically satisfactory, could be explained based on the effect it has on $V_{CE_{\max}}$ (Eq. 8) and consequently on the shape of the f_v curve (Eq. 5). From the corresponding equations, it can be seen that an increase in α causes an increase in $V_{CE_{\max}}$ such that greater values of force could be achieved at a given velocity, during concentric contractions.

CHAPTER 3: MECHANICAL DESIGN

Chapter 3 details critical aspects of the mechanical design, such as design requirements, joints, cabling schemes, speed-reductions, and placement of motors and singularities.

3.1. System Requirements

The design and development of a high performance robotic device is a process with numerous competing factors. The mechanism weight and stiffness exist at opposite ends of the spectrum, the goal being to achieve the highest structural rigidity while maintaining the lowest segmental inertias. Contributing to these underlying requirements are factors such as the operational workspace, desired joint torques, motor placement, link design, and cable selection. Since the device will operate in direct contact with humans, additional requirements emerge regarding comfort and safety of operation.

3.1.1. Kinematic and Dynamic Requirements

In order to promote high performance while ensuring safe operation, the requirements must be realized and understood both from their technical as well as functional aspects. To better understand the kinematic and dynamic requirements of an exoskeleton arm for functional use, a pilot study was first performed. Motions of the human arm were recorded during 24 activities of daily living (ADL) using a motion capture system. Further details of the pilot study are described in Section **2.1**. The results of joint position and joint torque about each axis have been condensed from the ADL pilot study to a single set of histograms and plotted in Figure 3.1 and Figure 3.2, respectively. While some distributions appear quite normal in shape, others possess a bi-modal or even tri-modal form where the centers of modes correspond to key anthropomorphic configurations. These configurations are positions of the arm that occur commonly throughout daily activities, often where joint velocities remain near zero at the initial or final periods of motion trajectories. Mean and median values, as well as static modes for position and torque are reported in Table 3.1.

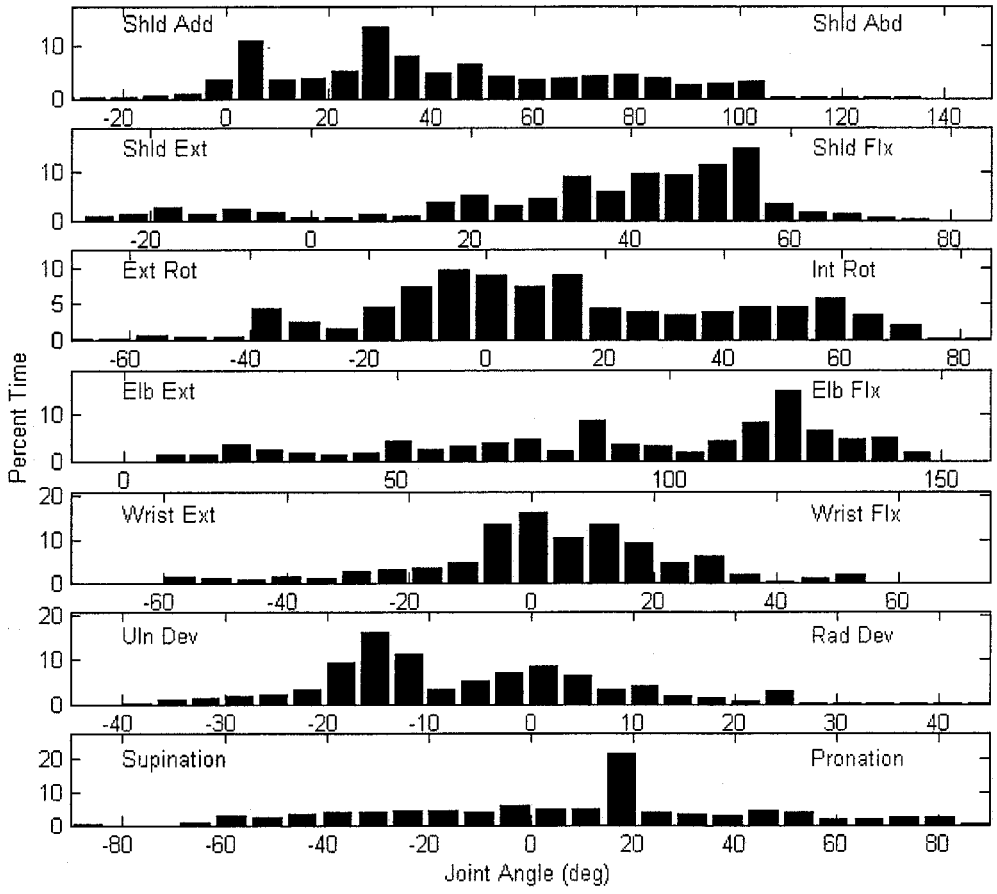

Figure 3.1: Statistical distribution of human arm joint angles during 19 activities of daily living. Histograms are plotted sequentially from the top: Vicon axes 1 through 7.

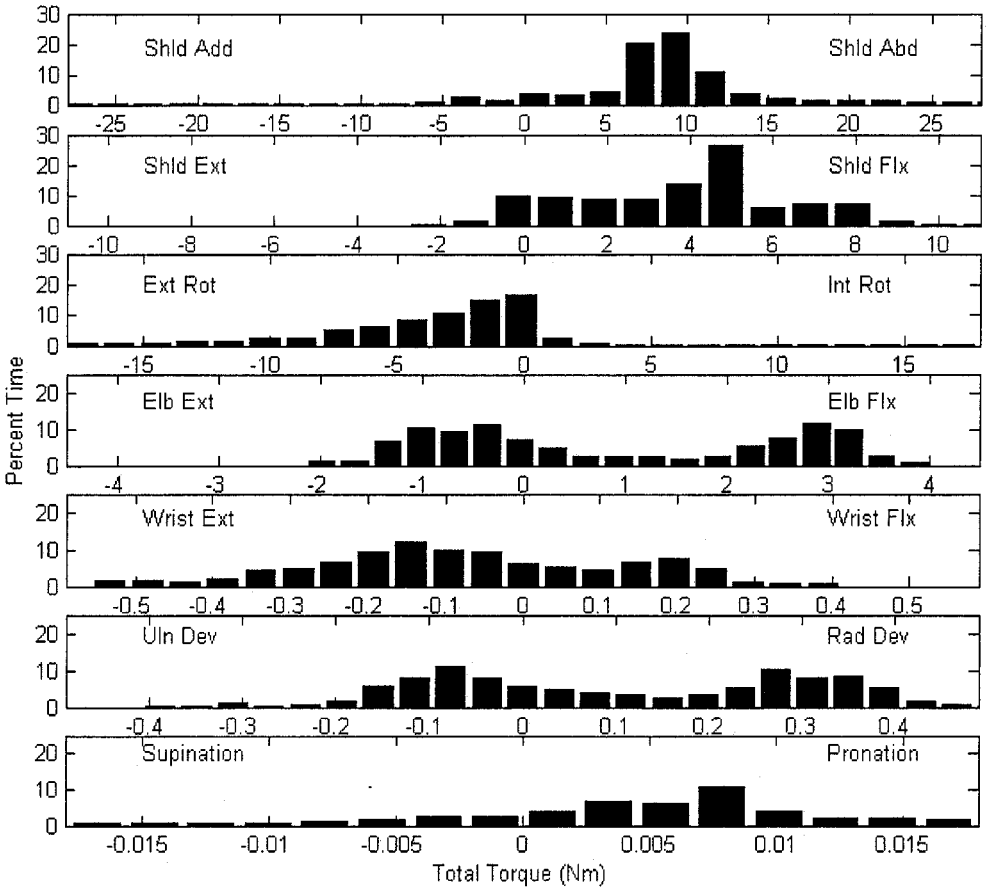

Figure 3.2: Statistical distribution of human arm joint torques during 19 activities of daily living. Histograms are plotted sequentially from the top: Vicon axes 1 through 7.

Table 3.1 Values for joint motion and torque about each Vicon axis during 19 recorded activities of daily living.

MEASURE		VICON AXIS						
		1	2	3	4	5	6	7
Anlge (deg)	ROM	110	100	135	150	115	70	150
	Mean	42.0	35.4	13.1	92.1	3.1	-4.8	11.7
	Median	35.1	41.4	9.1	98.6	3	-9.3	15.9
Torque (Nm)	Mean	7.5	3.8	-4.1	0.90	-0.07	0.10	0.01
	Median	8.6	4.3	-3.0	0.35	-0.09	0.08	0.01
	RMS	14.3	4.8	12.9	1.9	0.28	0.23	0.10

3.1.2. Physical Human-Machine-Interfaces

The mHMI's are the physical components that mechanically couple the human arm and the exoskeleton structure and enable force transmission between them. With awareness that one intended population of users will possess varying levels of muscular and functional impairment, an emphasis was placed on designing an interface that can easily be attached to the user. For patients of stroke and cervical spine injury, unassisted elevation of the arm is difficult if not impossible.

To achieve axial rotation of exoskeleton limbs, three primary exoskeletal configurations are conceivable, illustrated in Figure 3.3. The first two configurations involve a single-DOF bearing with its axis of rotation aligned collinearly with the approximate anatomical axis of rotation of the segment, while the third configuration involves a first axis that is displaced from the anatomical axis and a minimum of two additional non-collinear axes. In the first two configurations, the exoskeleton joint can be placed at either end of the long axis of the segment (Figure 3.3a) or axially between the ends of the segment (Figure 3.3b), using a bearing of minimum radius, r_b, greater than the maximum anthropometrical radius, r_a, about the corresponding segment axis. The additional axes of the third configuration are required to correct for non-collinearity of the first axis with respect to the rotating segment.

Configuration 3a (Figure 3.3a) offers a simple solution that allows for proximal placement of heavy components such as bearings and actuators, reducing inertial effects on power consumption, however, the placement is undesirable due to human-machine interferences during shoulder abduction. Configuration 3c (Figure 3.3c) can avoid the interferences by displacing the joint axis laterally from the segment axis of rotation. However, the two additional joints, adding undesired weight and complexity to the design, are necessary to maintain proper rotation as was achieved in previous configurations through the use of a single joint. The second configuration (Figure 3.3b) offers an alternative single-DOF solution where the human-machine interferences associated with configuration 3a can be removed. Full 360-degree bearings in this arrangement interfere with the torso when the arm is at rest or during motions that place distal arm joints near the body. Alternatively, these interferences can be removed through substitution of the full bearing with a partial bearing where the bearing track is affixed to the proximal exoskeleton link.

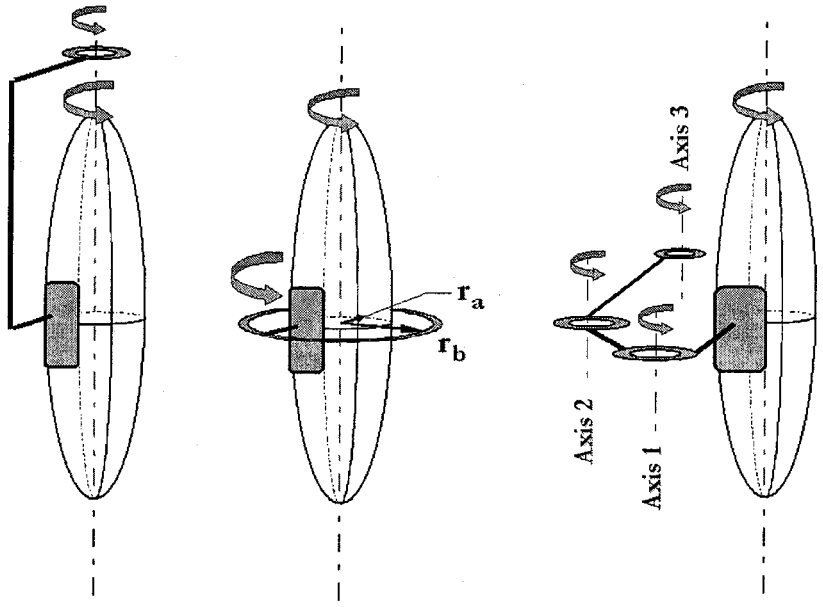

Figure 3.3: Three exoskeleton configurations that achieve rotation about the long axis of a limb segment, involving (a) a proximally placed single DOF, (b) a circumferentially placed single DOF, and (c) three parallel, non-collinear DOF's.

Current strength-to-weight limitations of available hardware necessitate non-mobile platforms for immediate upper-limb exoskeleton technologies, and consequently, more user-friendly mHMI's. Strength-to-weight ratios of existing materials and electric motors, as well as energy-to-weight ratios of power supplies are not yet at the level necessary to support development of mobile platforms for partial-body upper-limb exoskeletons. As a result, a full body exoskeleton is required to support the existing weight of state-of-the-art power supplies, onboard controllers, and other upper-limb hardware.

In the use of non-mobile platforms for therapy applications, positioning the device relative to an immobile arm to facilitate sleeve-like donning through closed (360-degree) bearings is less desirable, and joint configurations should be carefully selected and designed to minimize strain or discomfort to the user. Optimal designs for functionally impaired users enable attachment of the arm and device with minimal movement of the impaired limb. Given a configuration that meets this criteria, additional co-dependent considerations such as link excursion, energy consumption, and collision avoidance with the body should be taken into account.

3.1.3. Safety Requirements

Paramount to all human-machine-interfaces (HMI) is the guarantee of safe operation. Safety precautions have been implemented on three levels, built into the mechanical, electrical, and software designs.

In the mechanical design, physical stops prevent segments from excessive excursions that could hyperextend or hyperflex individual joints. In addition, pulleys in some joints are driven purely by friction. This allows the transmission to slip if ever the force between the user and device were to exceed a limit.

The electrical system is equipped with three emergency shutoff switches: an enable button that terminates the motor command signal upon release, a large e-stop button for complete power shutoff by the observer, and a similar e-stop foot switch for the user.

Ideally, the above safety measures would go unused as a result of adequate safeguards at the software level. Redundant position sensors (Midori, Fullerton; Maxon,

Switzerland), one at either end of the power train, monitor both joint motion as well as motor position. Differentiation of position provides knowledge of velocity and acceleration, both of which can be incorporated into the control structure to prevent undesirable effects when approaching the joint limits. Redundancy of position sensing also enables software to monitor power transmission integrity. Any slip occurring between the motors and end-effector will result in a position discrepancy and lead to immediate system shutdown. Software limits will also be implemented on commanded motor currents, i.e. motor torques.

3.1.4. Modeling the Human Arm

Anthropomorphic joint approximations can be modeled at varying degrees of accuracy and complexity [84,115,116]. The level of complexity needed for a suitable representation depends highly on the desired tasks to be performed and replicated using the model. Shoulder motion, for example, composed of glenohumeral (G-H), acromioclavicular, and sternoclavicular articulations, can be represented largely by the G-H joint for a variety of arm activities involving up to 90 degrees of arm elevation. With minimal activity exceeding this range, a simplified model of the shoulder was deemed appropriate for the study. The G-H movement can further be simplified to a ball and socket joint composed of three orthogonal axes intersecting at the center of the humeral head, although the true center of rotation is known to vary with arm orientation [115,116]. Rotations about these orthogonal axes may be treated as Euler rotation. The order of flexion-extension and abduction-adduction about the first two axes is arbitrary, but should be noted, while the third rotation corresponds to internal-external rotation.

The elbow can be represented as a single-axis hinge joint where the hinge rests at an oblique angle with respect to both upper and lower arm segments under full arm extension as shown in Figure 4. Of the three elbow types identified in [115], Type-I (Fig. 4a) is the most common and was assumed in this analysis to represent the population. The hinge offset accounts for lateral deviation of the forearm during supinated activities. Under full elbow extension and forearm supination, angular differences, β, of up to 10 degrees exist between the midlines of the upper and lower arm segments, and decrease

with pronation. In the present study, an assumed offset of zero degrees has achieved sufficient results and significantly reduced complexity of the resulting dynamic equations of motion.

Pronosupination of the forearm has been treated interchangeably in literature as a freedom of the elbow and as a freedom of the wrist. In either case, it should be considered directly adjacent to the forearm, occurring after elbow flexion and before either wrist flexion or deviation, with the axis of rotation running approximately through the 5th metacarpal-phalangeal joint [115].

The wrist can be modeled as two orthogonal axes with a fixed offset between them [115]. The proximal and distal axes of the wrist correspond to wrist flexion-extension and wrist radial-ulnar deviation, respectively.

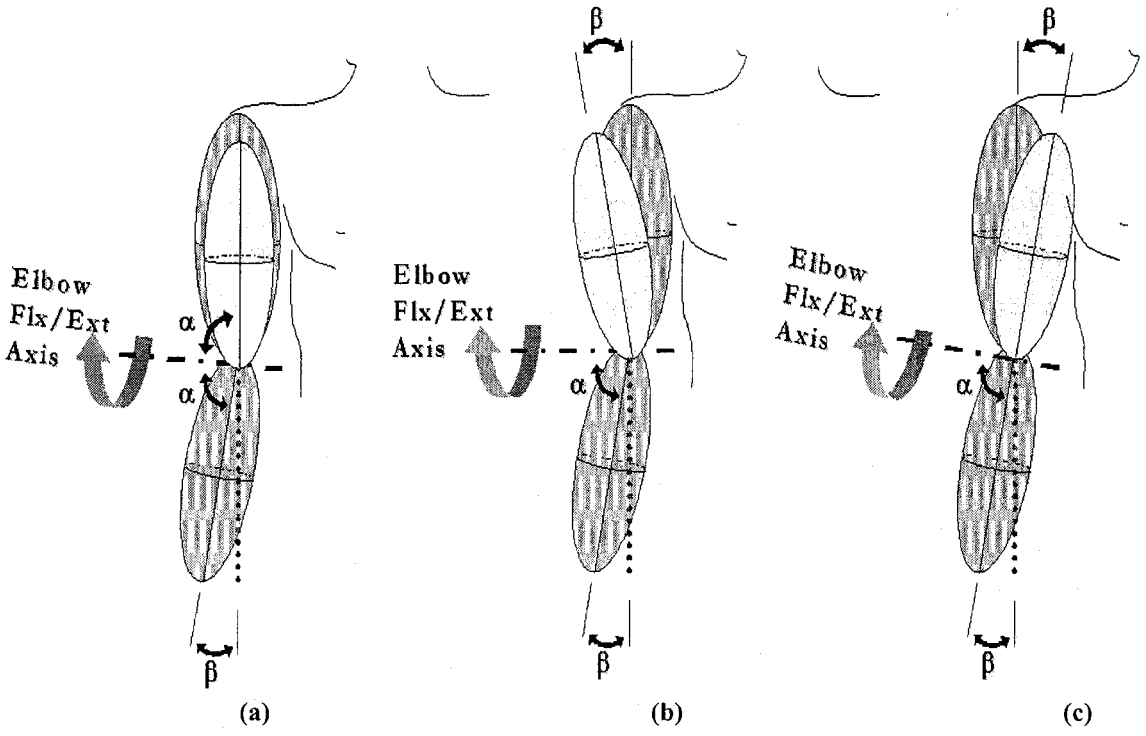

Figure 3.4: Angular variations between elbow flexion-extension and pronosupination axes, α, result in different elbow flexion kinematics. Type I individuals (a) are most common in which the elbow axis is symmetric with respect to both upper and lower arm segments. Types II (b), and III (c) are less common. Figure and Type I-III designations adapted from [115].

3.1.5. Performance

A widely used quantitative measure to evaluate system performance is bandwidth. Systems having a higher bandwidth are controllable under higher frequency command signals. Limited by the system's lowest natural frequency, the bandwidth is a measure of how successfully trade-offs between weight and stiffness are made. A target bandwidth of 10 Hz was selected based on the achievable frequency range of the human arm, which resides between 2-5 Hz [98-99]. Additional target values for the design are outlined in Table II. The actual weight was 3.5 kg and 6.3 kg for link 1 and links 2-7, respectively.

Table 3.2: Target values for design performance

PROPERTY	TARGET VALUE
Weight (moving links)	6.8 kg (15 lbs)
Static Payload (max)	2.5 kg (in hand)
Angular Deflection (max)	2 degrees per joint
Bandwidth	0-10Hz

3.2. Exoskeletal Joint Design

Articulation of the exoskeleton is achieved about seven single-axis revolute joints: one for each shoulder abduction-adduction, shoulder flexion-extension, shoulder internal-external rotation, elbow flexion-extension, forearm pronosupination, wrist flexion-extension, and wrist radial-ulnar deviation. The exoskeletal joints are labeled 1 through 7 from proximal to distal in the order shown in Figure 3.5. Note that the order and orientation of some joints are different from axes presented in Figure 2.2. Orientation is further addressed in section 3.2.4.

3.2.1. Anthropomorphic Joints

In the design of the current exoskeleton, three joint configurations emerged. The configurations can be classified as one of the following: a) 90-degree, b) 180-degree, or c) axial. The distinguishment pertains to the relative alignment of adjoining links when the joint is approximately centered within its range of motion. While some joints of the body articulate about their mid-ROM when adjoining links are near orthogonal (Figure

3.6a), others do so when the links are near parallel (Figure 3.6b). A third configuration emerges in axial rotation of both the upper and lower arm segments (Figure 3.6c). As shown in Figure 3.6d, exoskeleton joints 1 and 7 are modeled as 180-degree joints (Figure 3.6b), joints 2, 4, and 6 are 90-degree joints (Figure 3.6a), and joints 3 and 5 are axial joints (Figure 3.6c). Joint ROM in configurations (a) and (b) can be increased either by increasing the central radius, r, or decreasing the link width, w (Figure 3.6a). Adjusting the link offset distance, d, shifts the joint limits, illustrated with red circles, and effectively 'tunes' the joint's mid-ROM.

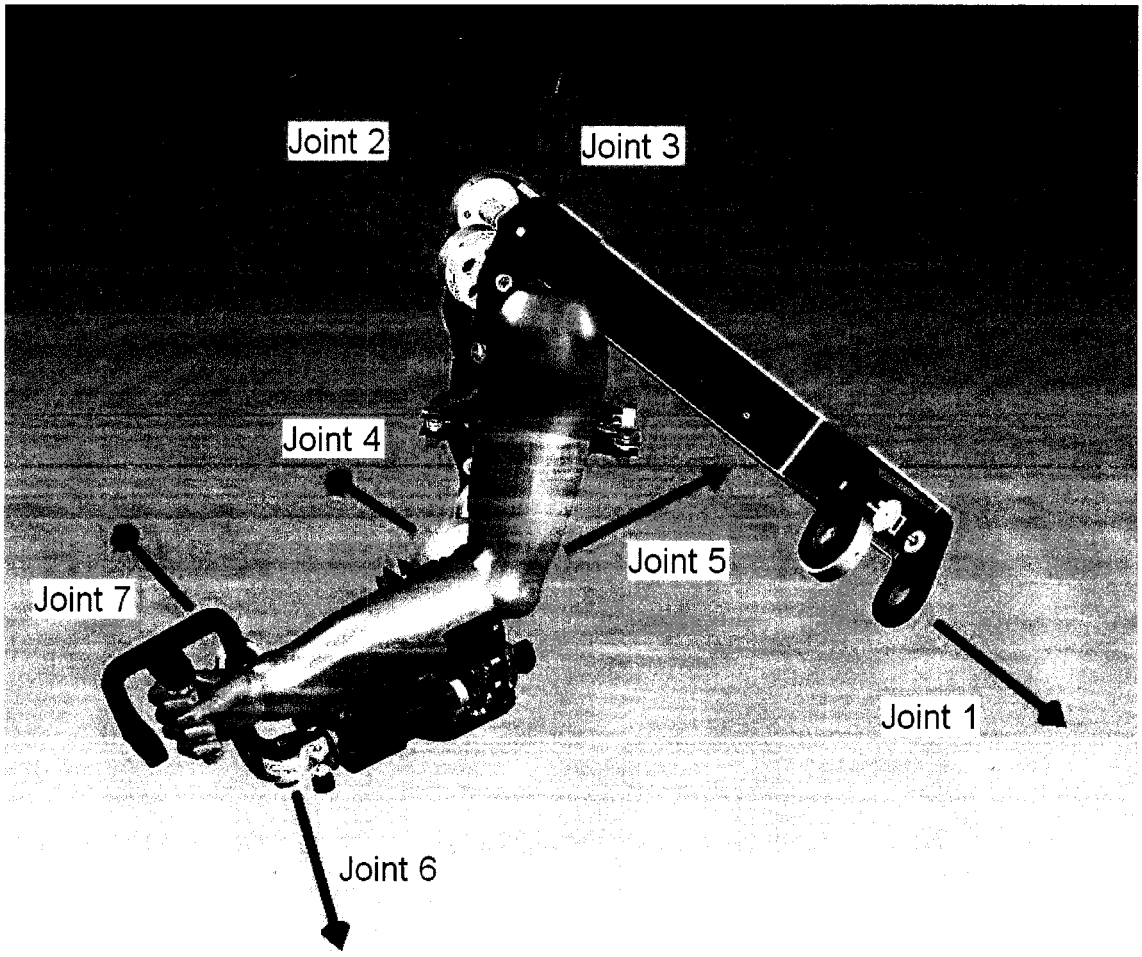

Figure 3.5: Exoskeletal axes assignment in relation to the human arm. Positive rotations about each joint produce the following motions: 1) combined flexion/abduction, 2) combined flexion/adduction, 3) internal rotation, 4) elbow flexion, 5) forearm pronation, 6) wrist extension, and 7) wrist radial deviation.

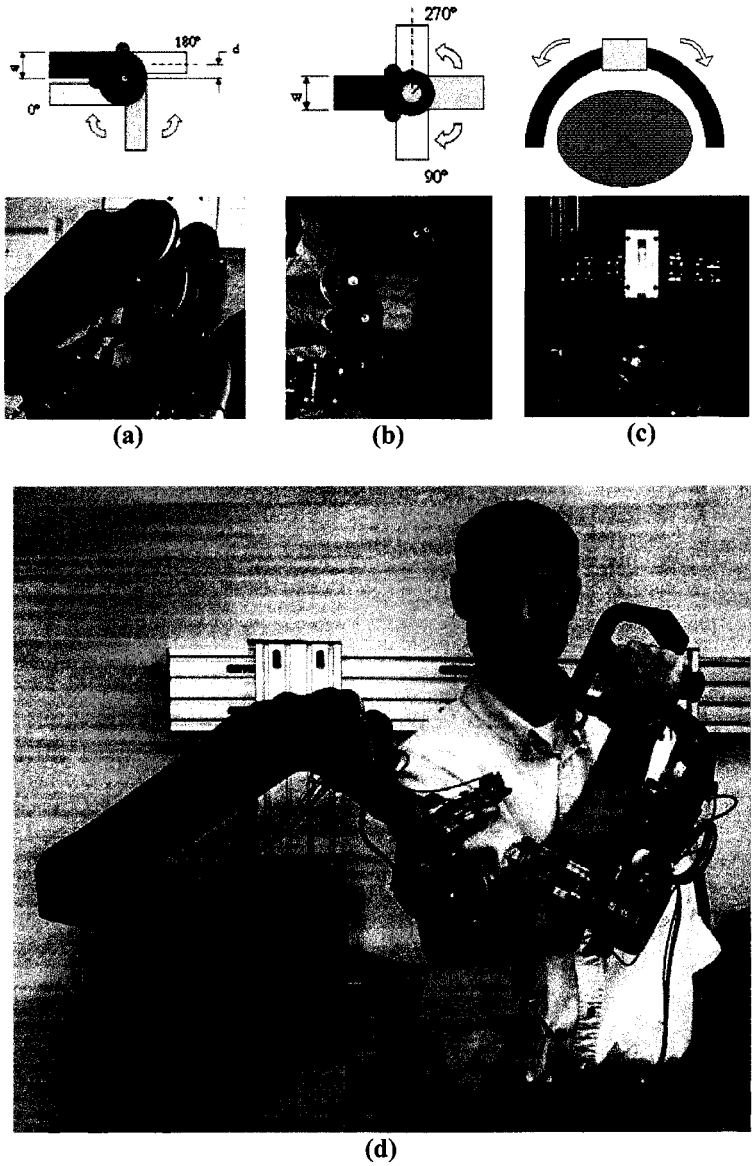

Figure 3.6: The exoskeleton is composed of three joint configurations: 90-degree joints (a), 180-degree joints (b), and axial joints (c). Together the joints produce an exoskeleton structure that achieves full glenohumeral, elbow, and wrist functionality (d).

Consistent with other exoskeleton research, the shoulder complex is reduced to the glenohumeral (GH) joint articulation [55-57,60,62], and the GH joint is considered a spherical joint composed of 3 individual axes intersecting at its center. The elbow is modeled by a single axis orthogonal to the third shoulder axis. A joint stop prevents the joint from hyperextension. Exoskeletal pronosupination takes place midway between the elbow and wrist joints as it does in the physiological mechanism. And finally, two intersecting orthogonal axes represent the wrist. Although anthropometrically it would be more accurate to incorporate a slight offset between the flexion-extension and radial-ulnar deviation axes, this offset has been neglected for simplicity.

Table 3.3 summarizes the ranges of motion achievable with the exoskeleton arm.

Table 3.3: The exoskeleton achieves 99% of the ranges of motion required to perform daily activities.

Joint	Motion	ADL ROM (deg)	EXO ROM (deg)
Shoulder	Flx-Ext	110	180
	Abd-Add	100	180
	Int-Ext Rot	135	166
Elbow	Flx-Ext	150	150
Wrist	Flx-Ext	115	120
	Rad-Uln Dev	70	60
	Pron-Sup	150	155

3.2.2. Mechanical Human-Machine-Interfaces

Joint configuration (c) presents special challenges in design because the human arm occupies the joint axis of rotation, represented by the elliptical shape in Figure 3.6. Previous exoskeleton designs have utilized internal-external rotation joints and prono-supination joints that fully enclose the arm, requiring the user to insert his/her arm from the end and slide it axially down the length of the arm [55,57,60-63]. This can be a difficult and even uncomfortable task depending on the severity of impairment.

The current exoskeleton mHMI uses a semi-circular bearing design to allow users to don the device without strain or discomfort. The semi-circular guides are composed of three 60-degree curved-rail-bearing segments (THK, Tokyo Japan)

3.2.3. Joint Cable Routing

Achieving mechanical joint ranges of motion that match those of the human arm is a challenging task, especially for cable-driven devices where the cables must either be routed through or around joint axes while maintaining constant cable length. Both trans-joint routing schemes (routing 'through' or 'around' joints) possess inherent advantages and disadvantages over the other.

Routing 'through' the joint requires a pulley on either side of the axis mounted relative to each link with the cable between them traversing the axis of rotation. The main drawback to this approach is that the pulleys, arranged with their largest dimension parallel the axis, take up significant space radially from the joint center. Additionally, since radial distance from the limb should be minimized for inertial reasons, the short length of cable remaining between the pulleys is subjected to twisting during relative rotation of the links. However, with the 'through' joint cabling approach ensures a constant cable length without inducing coupling effects between joints.

On the contrary, although routing cables 'around' the joints induce no twisting on the cable and lead to a more compact spatial solution, it results in mechanical coupling of both the joint kinematics and dynamics. Despite future complications to the controller induced by the presence of coupling, the later scheme was chosen for its smaller size and inertia.

The cable routing methods utilized are illustrated in Figure 3.7. In 90-degree and 180-degree configuration, the cable is wrapped around a pulley, called the 'joint idler pulley', which is concentric with the axis of revolution (Figure 3.7a). Axial joints are represented by a series of nine pulleys each located at a constant radius from the axis of revolution, together acting as a single larger-diameter joint idler pulley (Figure 3.7b).

To maintain constant cable length, the cable must remain in contact with the joint pulley at all times. The sequence shown in Figure 3.7a shows the extent of joint motion

using three equi-diameter cables. In the extreme positions, the shorter length of cable is tangent with the joint pulley and is therefore defined as the joint limit. Figure 3.7b illustrates the effect of increasing the joint pulley radius, r, on the amount of clockwise rotation before reaching the joint limit.

Figure 3.7d depicts a 90-degree exoskeleton joint and illustrates how an increased joint pulley radius *r* and offset *d* equal to *r* allow links to fold to an angle of zero. Each pulley actually represents a stack of two pulleys per DOF passing through the joint. Two DOF's, for example, would require a stack of four pulleys (Figure 3.7e), two representing the agonist muscle group and two for the antagonist group.

To enable bilateral routing of cables, as well as for lightweight strength, mechanical links were designed with high-stiffness I-beam cross-sections.

Joint motions that cause significant changes in length will result in one of two undesirable effects: either excessively high cable tension, reducing the life of the cables and bearings, or excessively low tension, potentially developing slack, transmission backlash, or even cable derailment. To prevent such occurrences, trans-joint pulley arrangements are kept in contact with the joint pulley at all times, and lateral deviations of the cable at all termination sites were limited to 2.5 degrees.

3.2.4. Singularity Placement

A singularity is a device configuration where a degree of freedom is lost or compromised as a result of an alignment of two rotational axes. In the development of a 7-DOF exoskeleton, the existence of singularities will depend on the desired reachable workspace. For devices that require large ranges of motion, motions greater than or equal to 180 degrees in at least one joint, singularities cannot be eliminated. In this case, the challenge is to place the singularity in an unreachable, or near unreachable location, such as the edge of the workspace.

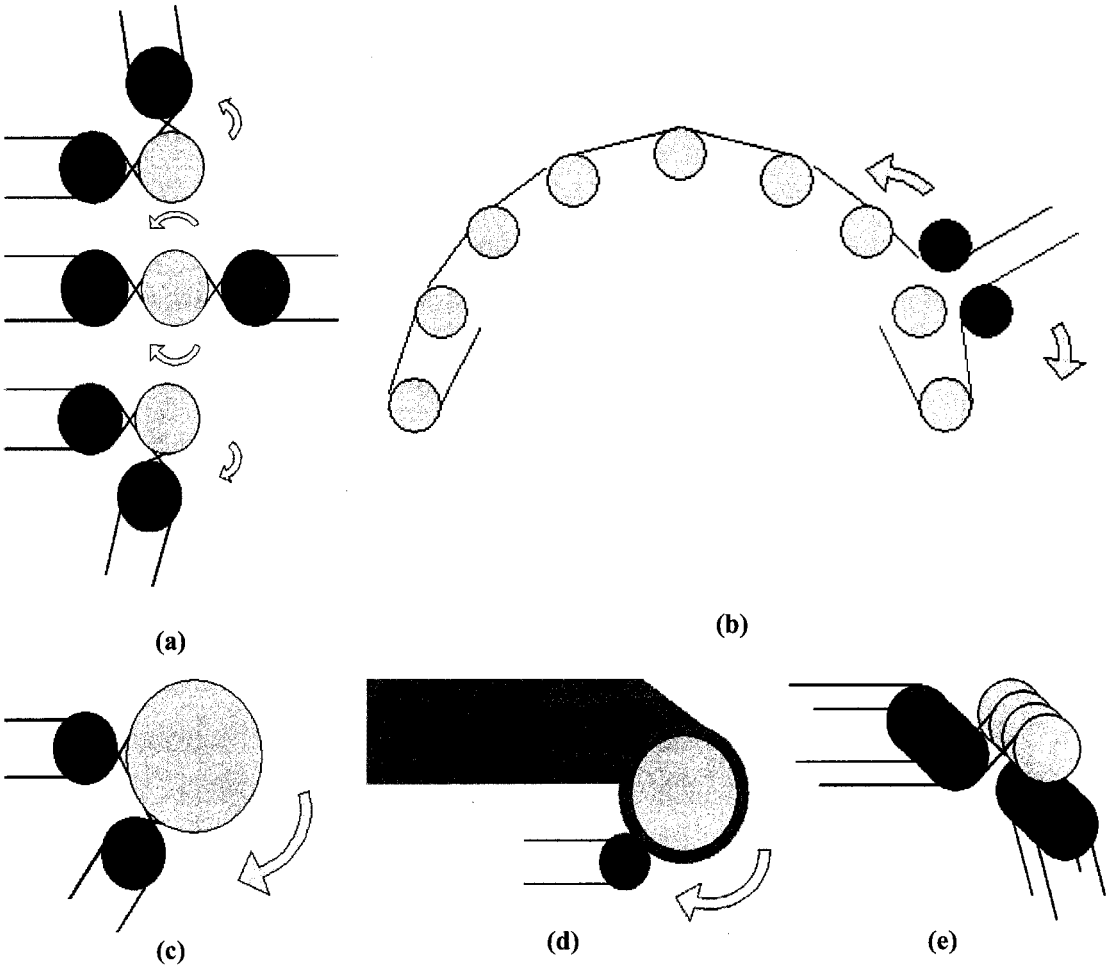

Figure 3.7: Joint cable routing and the effects on ROM using: three equi-diameter pulleys (a), an enlarged joint pulley (c), or an enlarged joint pulley with link offset (d). Also 9-pulley arrangement for axial joints (b), and cabling of stacked pulleys (e).

For the exoskeleton arm, singularities occur when joints 1 and 3 or joints 3 and 5 align. To minimize the frequency of this occurrence, the axis of joint 1 was positioned such that singularities with joint 3 take place only at locations that are anthropometrically hard to reach. To allow some user-specific flexibility in the design, the singular position is movable in 15-degree increments. For the placement shown in Figure 3.8, the singularity can be reached through simultaneous extension and abduction by 47.5 and 53.6 degrees, respectively (Figure 3.8c). Similarly, the same singularity can be reached through flexion and adduction of the upper arm by 132.5 and 53.6 degrees, respectively

(Figure 3.8d). The singularity between joints 3 and 5 naturally occurs only in full elbow extension (Figure 3.8e), i.e. on the edge of the forearm workspace. With each of these singularity vectors at or near the edge of the human workspace, the median of the workspace is free of singularities.

Another aspect to consider when placing singularities is mechanical isotropy. For optimal ease of movement in any direction, singular axes should be placed orthogonal to directions where isotropy is of highest importance. For the singularity placement shown, isotropy will be maximized in 42.5 degrees of shoulder flexion and 26.4 degrees of shoulder abduction, values that lie in the median of shoulder ROM from the ADL study.

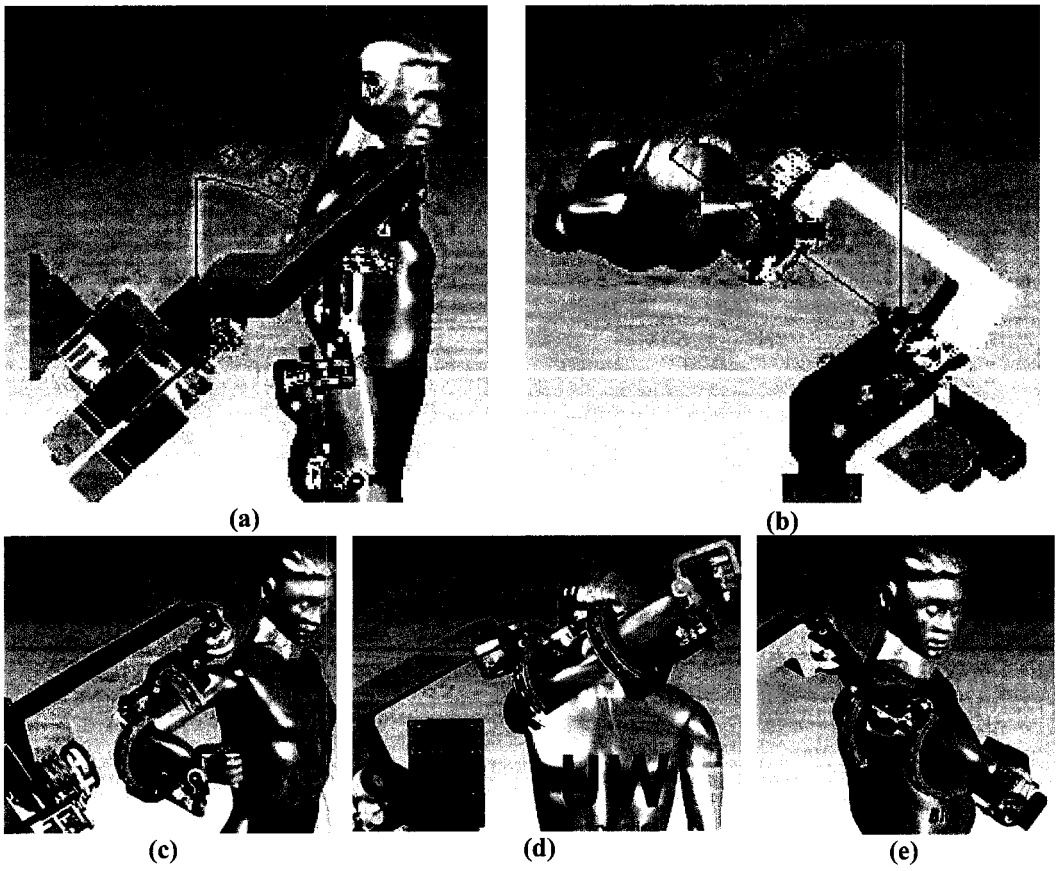

Figure 3.8: Mechanical singularities between axes 1 and 3 occur around the shoulder internal-external rotation axis in configurations (c) and (d). A singularity between axes 3 and 5 also occurs in full elbow extension (e).

3.3. Power Transmission

To date, the transmission of power from one location to another is achieved through a variety of means such as shafts, cables, fluid lines, and gear trains. Each method has specific applications where its characteristics are best suited. In the field of wearable robotics, weight is a critical factor that frequently must be sacrificed for the sake of strength or rigidity. However, development of a rigid structure that lacks adequate bandwidth is as ineffective a tool as one that is lightweight but lacks structural rigidity. To achieve both rigidity and bandwidth, critical decisions were made regarding transmission type and placement of actuators.

3.3.1. Cable-Drive Systems

Cable drive systems have been in use on larger scale devices long before their introduction into the world of biorobotics and microsurgery. Their biggest strength lies in their ability to transmit loads over long distances without the friction or backlash inherent to gears. The absence of backlash is achieved through the structural continuity of the cable, enabling a direct link between the driving shaft and the shaft or link being driven. For these reasons, a cable-driven design was selected.

Bimimmetically referred to as 'tendon-driven' systems [100,101], cable-drives are common in robotic applications for their low backlash, and have been used by Salisbury et al. to achieve back-drivable speed reductions that increase the stiffness of the robotic structure [102]. This concept is explained further in section 3.3.3.

3.3.2. Selection and Placement of Actuators

As the heaviest components in the design, placement of the motors was a crucial decision. Motors for joints 1-4 were mounted on the stationary base, achieving a 60% reduction in overall weight of the moving parts. The remaining three motors, whose torque requirements are substantially less, were positioned on the forearm. As each motor carries the weight and inertia of the more distally placed motors, the importance of high power-to-weight ratio increases from shoulder to wrist. Shoulder and elbow joints are

each driven by a high torque, low power-to-weight motor (6.2 Nm, 2.2 Nm/kg), while wrist joints are driven by a lower torque, high power-to-weight motor (1.0 Nm, 4.2 Nm/kg). Motors are rare earth (RE), brushed motors (Maxon Motor, Switzerland). The respective power-to-weight ratio of each motor is graphed in relation to three product lines in Figure 3.9. Note: the author does not recommend use of the RE 75 motors for quiet applications due to an audible high-frequency brush noise at low RPM.

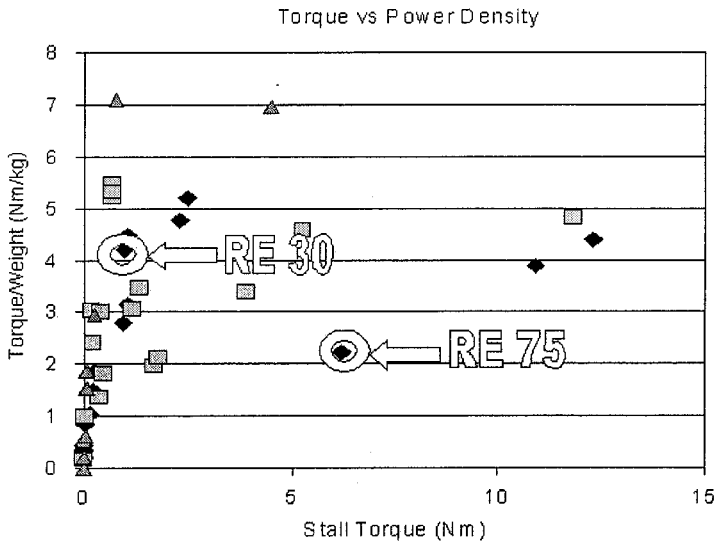

Figure 3.9: Torque-to-weight ratio vs. rated stall torque of RE series (diamonds), EC series (squares) and EC Flat series (triangles) motors available from Maxon Motor. The selected motors for exoskeleton joints 1-4 (RE75) and joints 5-7 (RE30) are circled.

3.3.3. Two-Stage Pulley Reduction

Pulleys arrangements can be used to create speed reductions in cable transmissions. Neglecting frictional losses, power throughout the transmission remains constant while tradeoffs between torque and angular velocity can be made. At the motor, required torque is low while angular velocity is high, whereas at the joint, torque is high and angular velocity is low. Lower torque corresponds to lower cable tension in stage 1 (Figure 3.10a), resulting in less strain, and therefore, less stretch per unit length of cable. Minimizing the length of stage 2 and routing the cable in stage 1 through the majority of the exoskeleton structure maximizes the overall transmission stiffness. Two-stage pulley reductions (Figure 3.10b) have been implemented in joints 1-4, whereas reductions at the

wrist are composed of a single-stage pulley reduction following a single-stage planetary gear reduction. Total reductions for each joint are as follows: ~10:1 (Joints 1-3), ~15:1 (Joint 4), ~30:1 (Joints 5-7).

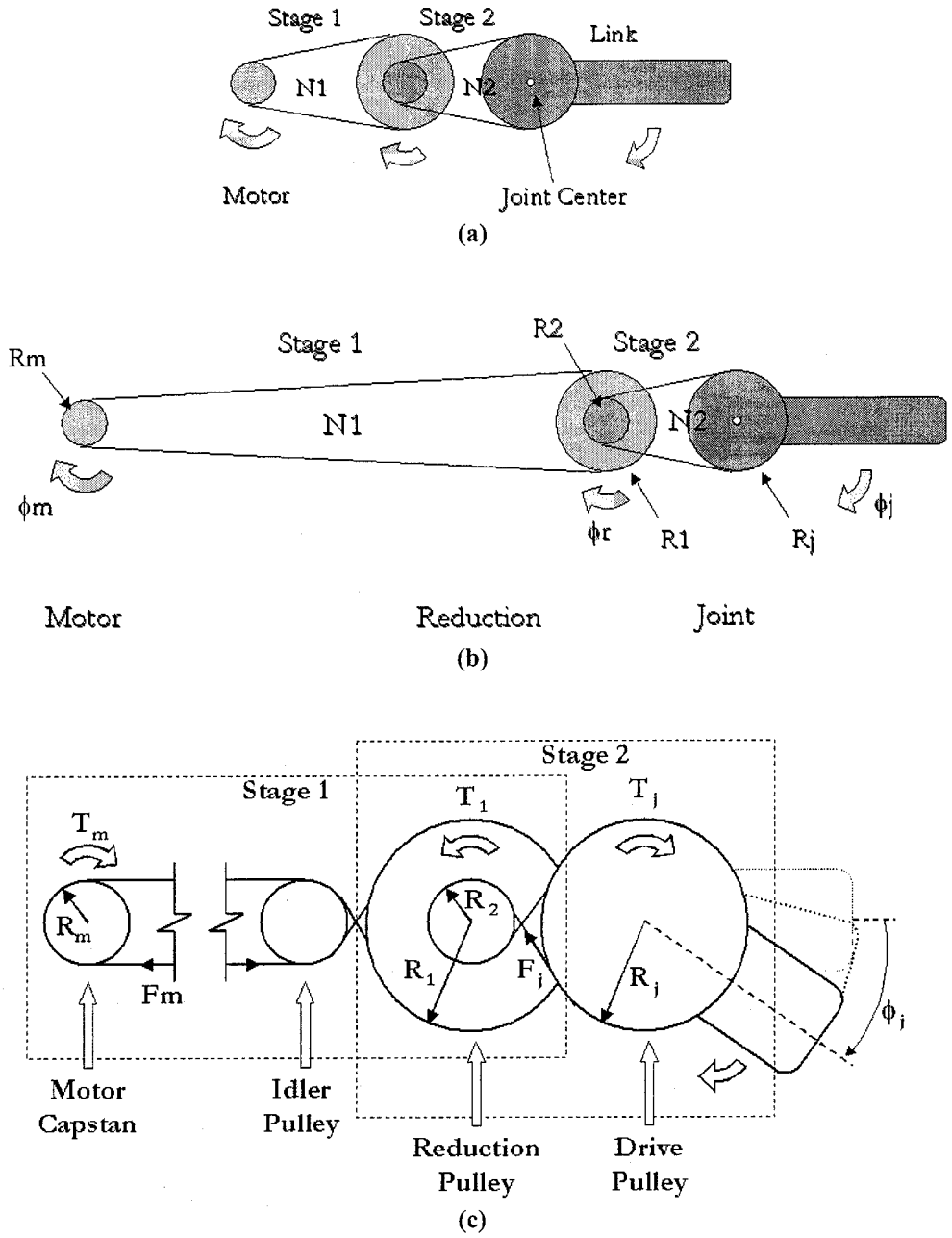

Figure 3.10: Transmission stiffness in two-stage pulley reductions (a), can be maximized by minimizing the length of cable in the high-tension stage 2 (b). Cable routing through the majority of the exoskeleton is represented by the gap between the motor capstan and idler pulley shown in (c).

3.4. Discussion

From the condensed study results presented in section 3.1.1, the largest ROM experienced by a joint during the selected daily activities is 150 degrees. Although some studies report joints to achieve ranges of motion exceeding 180 degrees, most joints can only reach such excursions with contributions from neighboring joints. The G-H joint, for example, appears to provide over 180 degrees of motion about all three axes, however this is due largely to scapular motion. As a result, joints capable of providing 180 degrees of motion, or less, using the three configurations described above are sufficient to develop an arm exoskeleton with full G-H, elbow, and wrist joint functionality.

Previous exoskeleton designs have utilized internal-external rotation joints and prono-supination joints that fully enclose the arm, requiring the user to insert his/her arm from the end and slide it axially down the length of the arm. This can be a difficult and even uncomfortable task depending on the severity of impairment. In the current exoskeleton design, the use of open mHMI's for both upper and lower arm segments eliminates this difficulty.

Due to the unique placement of the shoulder singularity, as described in section 3.2.4, pure shoulder flexion is achieved through a combination of rotations about joints 1 and 2. Additionally, this unique placement moves the region of highest shoulder joint isotropy into the area of the workspace most often utilized during functional tasks. This confirms that the singularity has been placed in an anthropometrically desirable location.

At the wrist level, although anthropometrically it would be more accurate to incorporate a slight offset between the flexion-extension and radial-ulnar deviation axes, this offset has been neglected for simplicity.

As mentioned in section 3.2.3, significant changes in cable length will result in either excessively high or excessively low cable tensions, both sources of undesirable effects. For this reason, care must be taken at all cable termination sites to ensure constant cable length as it wraps either around a reduction pulley, drive pulley, or capstan. The tension that results, and therefore the amount of length change allowable, are dependent upon the length of cable in the particular stage. Lengthy cable runs can endure higher amounts of

cable stretch without undergoing significant increases in tension. This, combined with a large gear reduction, can result in significant lateral travel of the cable as it wraps around the motor capstan. The nearest idler pulley should be located sufficiently far from the capstan to maintain proper alignment (less than ~2.5 degrees offset) between the cable and helical grooves in the capstan.

CHAPTER 4: CONTROLLER DEVELOPMENT

In earlier studies [65,66], sEMG signals were used to control 1-DOF and 3-DOF exoskeleton designs. One of the ultimate goals for the current exoskeleton project is to show the efficacy of this novel control strategy as it applies to higher degrees of freedom, in this case a 7-DOF exoskeleton arm. Toward the realization of this goal, two of four critical steps have been completed, including system identification and compensation controller development.

4.1. System Identification

Accurate identification of the system is imperative to the later development of a working and robust controller. Identification in this context refers to the modeling of kinematic and dynamic coupling between joints as a result of cable routing configurations. To maintain constant cable length in trans-joint cables, cables can either be routed around joints, as they were for the developed exoskeleton, or they can be routed through the joint axes of rotation (see section 3.2.3 on Joint Cable Routing). Whenever cables are routed around as opposed to through a joint, mechanical coupling between joints is introduced into the mechanism's kinematic and dynamic operation. With the presence of coupling, a transformation matrix, or 'mapping' matrix, must be calculated to 'map' inputs at the motors to outputs at the joints. A separate matrix exists for mapping each position (kinematic mapping) and torque (dynamic mapping) from motor space to joint space.

4.1.1. Motor Space to Joint Space Kinematic Mapping

Mapping the position information from motor space to joint space takes into account kinematic effects of individual joint motions on all distal joints that are driven by trans-joint cables passing through the particular joint being moved. Joints that are proximally located with respect to the joint being moved are unaffected by the motion, while antagonistic cable pairs will shorten and lengthen, respectively, by equal amounts in distal joints. The amount of cable shortening in the agonist cable will always be offset by

an equivalent lengthening in the antagonist cable. The trade-off in cable lengths is achieved through rotation of the motor capstans, effectively reeling in one cable and simultaneously letting out the other. For successful actuation of joint 1 while maintaining constant angles in joints 2, 3, and 4, requires actuation of all four motors. To actuate only joint 2 while maintaining the other joint angles at constant values will require actuation of motors 2-4. Motor 1 need not be actuated, as its corresponding joint is proximal to the actuated joint. As such, the transformation matrix from motor space to joint space for the current design yields a 7x7 matrix composed of two lower triangular matrices: a 4x4 lower triangular matrix and a 3x3 lower triangular matrix corresponding to motors 1-4 and 5-7, respectively (Eq. 16).

$$[\theta_i]^{7x1}_{joint} = \begin{bmatrix} k_{11} & 0 & 0 & 0 & 0 & 0 & 0 \\ k_{21} & k_{22} & 0 & 0 & 0 & 0 & 0 \\ k_{31} & k_{32} & k_{33} & 0 & 0 & 0 & 0 \\ k_{41} & k_{42} & k_{43} & k_{44} & 0 & 0 & 0 \\ 0 & 0 & 0 & 0 & k_{55} & 0 & 0 \\ 0 & 0 & 0 & 0 & k_{65} & k_{66} & 0 \\ 0 & 0 & 0 & 0 & k_{75} & k_{76} & k_{77} \end{bmatrix} \cdot [\alpha_i]^{7x1}_{motor} \qquad \textbf{Equation 16}$$

4.1.2. Motor Space to Joint Space Kinetic Mapping

Transformation of the torques from motor space to joint space accounts for kinetic effects of individual joint torques on all proximal joints through which the corresponding cables pass. Joints that are distally located with respect to the actuated joint are unaffected by the applied torque. Torques are transmitted from proximally located motors to distally located joints through two-stage cable and gear/cable combination reductions for motors 1-4 and 5-7, respectively. At each joint, the resulting torque is the differential cable tension $(F_1 - F_2)$ multiplied by the pulley radius r, summed for each trans-joint cable and driving cable, as illustrated in Equation 17.

$$\tau_i = \begin{cases} \sum_{j=i}^{4} (F_1 - F_2)_j \cdot r_j \quad , & for\ i \in \{1,2,3,4\} \\ \sum_{j=i}^{7} (F_1 - F_2)_j \cdot r_j \quad , & for\ i \in \{5,6,7\} \end{cases}$$ **Equation 17**

The resulting 7x7 transformation matrix from motor space to joints space is a matrix composed of two upper triangular matrices: a 4x4 upper triangular matrix and a 3x3 upper triangular matrix corresponding to motors 1-4 and 5-7, respectively. (See Eq. 18).

$$[\tau_i]_{joint}^{1x7} = \begin{bmatrix} d_{11} & d_{12} & d_{13} & d_{14} & 0 & 0 & 0 \\ 0 & d_{22} & d_{23} & d_{24} & 0 & 0 & 0 \\ 0 & 0 & d_{33} & d_{34} & 0 & 0 & 0 \\ 0 & 0 & 0 & d_{44} & 0 & 0 & 0 \\ 0 & 0 & 0 & 0 & d_{55} & d_{56} & d_{57} \\ 0 & 0 & 0 & 0 & 0 & d_{66} & d_{67} \\ 0 & 0 & 0 & 0 & 0 & 0 & d_{77} \end{bmatrix} \cdot [\tau_i]_{motor}^{1x7}$$ **Equation 18**

4.2. Controller Development

The controller is being developed in a modular framework where one or several controllers can be enabled at a time. There are two controllers designed to compensate for undesired effects of gravity and friction, which can currently be enabled under three modes of operation.

4.2.1. Compensation Controllers

The core of each compensation controller is a model of a particular aspect of plant dynamics, in this case either gravitational or frictional effects. Each model is responsible for the prediction of the particular effect on the exoskeleton in its present state.

4.2.1.1. Gravity Compensation

The controller responsible for gravity compensation is developed from a subset of the equations of motion, accounting only for the joint torque due to changes in angular position. It emerges from setting $\dot{\Theta}$ and $\ddot{\Theta}$ equal to zero in Equation 1. The resulting

gravity compensation equation is of the form $\tau = G(\Theta)$. To map the resulting joint torques to motor space, the transformation from Equation 18 is applied. Based on the instantaneous state of the device, gravity compensating torque values are updated in the command signal, summing with torque calculations for friction compensation and desired link accelerations. Further details of the gravity compensation controller are expressed in [103].

4.2.1.2. Friction Compensation

Accurate modeling of frictional effects including static, coulomb, and viscous friction can be rather complex. Though more sophisticated models can be realized for future work, at the current stage in the project a simple linear model representing coulomb and viscous friction has been sufficient. A more advanced friction model was also developed and tested on joint 4 of the exoskeleton [104].

4.2.2. Control Modes

The exoskeleton has been designed with the intent of operation under three modes: position control, impedance control, and sEMG control. Initial testing was carried out under position control, validating motor and potentiometer connections, as well as motor to joint space transformation matrices. A second (impedance-based) control law was developed and tested for the shoulder using the upper-arm load cell with a preliminary mHMI design. The sEMG controller remains under development.

4.2.2.1. Position Control

Under position control, an open-loop control law directs joint angles to predetermined locations. Here, the position control law runs in parallel with both the friction compensator and the gravity compensator. Negligible steady-state offsets from commanded positions are observed.

4.2.2.2. Impedance Control

Impedance, or velocity-based, controllers produce an output velocity in proportion to a measured signal, in this case a measured force. One advantage to such a control scheme is that no force is required to maintain a given position. A measure of zero force produces a velocity of zero, which simply maintains the present configuration of the arm. The

applied motor torque, and hence applied motor velocity, is computed by multiplying the joint-to-motor transformation matrix, the tip-to-joint Jacobian transpose, and the forces measured by the force-sensor.

A closed-loop controller structure was tested initially on the shoulder using force on the upper-arm load cell as the impedance-based command signal. Although operationally successful under ideal conditions, the working principle of the load cell proved unforgiving of arm exoskeleton misalignments. To improve robustness of the impedance controller, a redesign of the mHMI is in order and currently underway.

4.2.2.3. Myosignal-Based Control

To date, the novel control scheme set forth is section 1.3.4 has only been used to control up to three active degrees of freedom. The critical component in this strategy is a myoprocessor (see section 2.2.1.2 for details) that uses measured sEMG signals to predict desired joint torques. The desired torque vector will then be pre-multiplied by the joint-to-motor torque transformation matrix and converted to a current command signal before being sent to each motor. The work described in this document has paved the way for this concept to be extended to a robot possessing seven active degrees of freedom.

CHAPTER 5: ADL INVESTIGATION (N=6)

5.1. Methods and Tools

5.1.1. Experimental Protocol

The kinematics of the human arm were collected during 24 daily activities from six subjects ranging in age from 20 to 41 years. Mean height, weight, and age for the subjects were 1.72 +/- 0.08 meters, 76.2 +/- 23.1 kg, and 26.2 +/- 7.7 years, respectively. Of the six subjects, three subjects were male and three were female. Arm kinematic data was collected using a VICON motion capture system (Vicon Inc.) at a sampling frequency of 120 Hz. Raw optical data was captured synchronously from 12 cameras and filtered with a Woltring quintic spline filter having a mean square error of $20mm^2$.

Reflective markers of 14mm diameter were attached to the right (dominant) arm of each subject at seven key anatomical locations (Figure 5.1). Markers for the shoulder (SHO), elbow (ELB), and wrist (WRA, WRB) were placed respectively on the acromio-clavicular joint, lateral epicondyle of the elbow, and at the radial (WRA) and ulnar (WRB) approximate centers of rotation for wrist flexion/extension axis. The upper arm (UPA), forearm (FRA), and finger (FIN) markers were respectively placed between SHO and ELB markers, between ELB and wrist markers, and on the dorsal side of the hand just below (proximal) the head of the second metacarpal. Individual models were calibrated for each subject and marker set for use during Vicon post-processing of subject data.

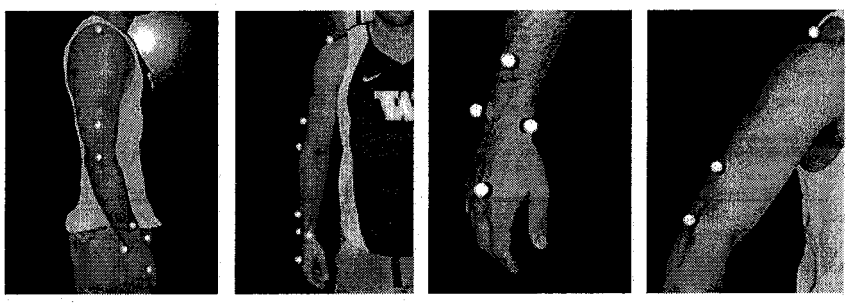

Figure 5.1: Retroreflective markers were placed on the subjects at the following 7 key anatomical locations: acromioclavicular joint, lateral upper arm, lateral elbow epicondyle, lateral forearm, medial and lateral wrist epicondyles, and between the 2nd and 3rd metacarpals.

The subject was instructed to perform three to six repetitions of each arm activity. The 24 arm activities were divided into four subgroups: (i) 7 reaching tasks, (ii) 8 Functional ADL tasks, (iii) 4 eating and drinking tasks, and (iv) 5 hygiene tasks. Specific human arm activities in each subgroup were selected based on previous surveys of the disabled community indicating the desired tasks and functionality of powered orthotic and robotic rehabilitation devices [75,76]. Seven actions were repeated each for six trials to look at intra- and inter-subject variations during reaching, functional, and eating tasks. All subgroup tasks with the exception of action 8 (opening and closing a door) were performed from a seated position; action 8 was performed in a standing posture with the midline of the body comfortably aligned with the doorknob. During seated tasks, the subject sat at a desk and manipulated objects in the workspace between predefined desk (D) and shelf (S) locations (Figure 5.2). Desktop locations were distally divided into three regions (D0, D1, and D2) with lateral components at the D1 level (D1L, D1R). Additional desktop locations were specified for objects used during specific tasks such as drinking from a cup (Dc), picking up a phone or pitcher (Dp), or the resting location of the hand (Dh). Left, central, and right positions were located 0.25 m to the left of the midline of the body, at the midline of the body, and 0.30 m to the right of the midline, respectively. The leftmost target position was chosen such that it placed the object directly in front of the lateral edge of the left shoulder for a 99^{th} percentile individual. D0, D1, and D2 locations were placed 0.10 meters, 0.25 meters, and 0.46 meters, respectively each from the front edge of the desk. Shelf locations are labeled S2L, S2, and S2R, for the left, central, and right positions (Figure 5.2, bottom-right). All objects were placed with respect to each desk or shelf location such that the center of the handgrip during object grasping and releasing was positioned vertically over each specified location. Desk and shelf heights were 0.76 and 1.20 meters, respectively, from the floor. Additionally, all individuals sat in the same chair with a fixed seat-to-floor height of .50 meters to properly represent the effect of individual subject height on joint kinematics and dynamics while operating in a typical fixed environment.

Opening and closing a door was simulated using an actual doorknob fixed 0.77 meters from the hinge, at a height of 0.95 meters with respect to the floor, and was allowed 45 degrees of travel to the 'open' state. The cupboard doorknob was position 0.38 meters above the desk, 0.38 meters from the front of the desk, 0.14 meters to the right of the midline, and was allowed about 95 degrees of travel to the 'open' state. The drawer was placed along the midline at a distance 0.38 meters from the front of the desk. Drawer motion underwent 0.35 meters of travel in the negative x-direction to the 'open' state. The drawer handle was 76 mm above the desktop, having a cylindrical gripping surface of 6.3 mm diameter by 57.1 mm length. Without instruction, all subjects naturally gripped the handle using an over-handed grasp.

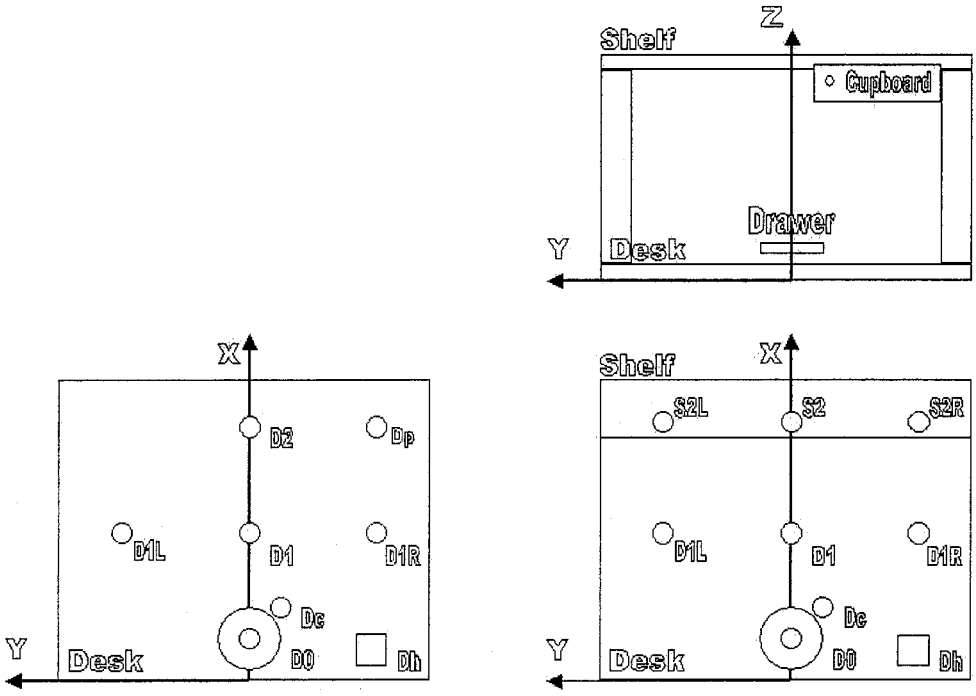

Figure 5.2: Desk (D) and shelf (S) location as defined in the ADL study were in general divided into three medial-lateral, three anterior-posterior, and two superior-inferior positions. A top view of the desktop (left) shows eight target desk locations, more heavily concentrated in the right hand plane. The three shelf locations were located at the same x-coordinate as desk locations D2 and Dp, only 0.44 meters above the desktop in the positive z-direction (bottom-right). Also attachable to the desk and shelf were a wood drawer, a cupboard, and a door (top-right).

The selected tasks from each subgroup and the variations for each task are illustrated as follows:

1. Reaching (action01-action07): placing hand on desk (RP to Dh), moving an object between desktop positions (D1R to D1L, D0 to D2), moving an object between shelf positions (S2L to S2R), combination shelf/desktop object motions (D1R to S2L, D1L to S2R, D1 to S2),
2. Functional ADL's (action08-action15): opening and closing a door / cabinet / drawer, answering a table-mounted phone (Dp), overhand/underhand stirring with a utensil (D1), pouring from a pitcher to a cup (Dp to Dc), and pouring from a cup to a pitcher (D1R to D1).
3. Eating and drinking (action16-action19): normal eating with a fork (D0), powered grasp eating with a fork (D0), eating with right hand (D0), and drinking from a cup (Dc).
4. Hygiene (action20-action24): combing the hair, washing the face, shaving the face, brushing the teeth, and washing the neck.

During the majority of these activities, the subjects interacted with various small and unconstrained objects as directed by the nature of each activity, and in a few cases interacted with partially constrained objects. It is assumed that all motions were made in accordance with the existing object constraints (e.g., door and cupboard hinges) such that no external forces or torques, other than those due to inertial and gravitational effects, were applied on the human by the object. During contact with constrained objects, although it is possible for large external forces to be applied on the arm if the constraint-induced trajectory is not followed, the data acquisition system and the mathematical dynamic model have no knowledge of this phenomenon. The dynamic model computes net joint torques based on measured angular position, velocity and acceleration about the 7 degrees of freedom. To minimize the potential for un-modeled dynamics, subjects were allowed to fully explore all constrained objects to familiarize themselves with the resulting constraint-induced motion.

With the exception of action01 and action08, every action began from an initial arm position in which the hand was resting at Dh and the upper and lower arm were relaxed. For reaching tasks and functional opening/closing tasks, the hand begins from rest at Dh, moves the object from the object starting position (position 1) to a second position (position 2), returns to rest at Dh for 1 second, and then performs the action in reverse, moving the object from position 2 back to position 1. In the case of opening and closing actions, positions 1 and 2 refer to the closed and open states, respectively, of the object. The objects used during each action and the positions associated with each action are shown in Table 5.1. Information about segments listed in the table and the segmentation process are further explained in Section 5.1.2.

The arm actions associated with eating with a fork had two variations. Action16 involved normal fork handling where a three-fingered grasp was used to orient the fork (a). In action17, a powered grasp of the fork (Figure 5.3b) was used to emulate a type of grasp often necessary for patients who suffer from one of several neurological disorders. The handle of the fork in this case was fitted with a typical buildup used to facilitate grasping in the patient population having such disorders.

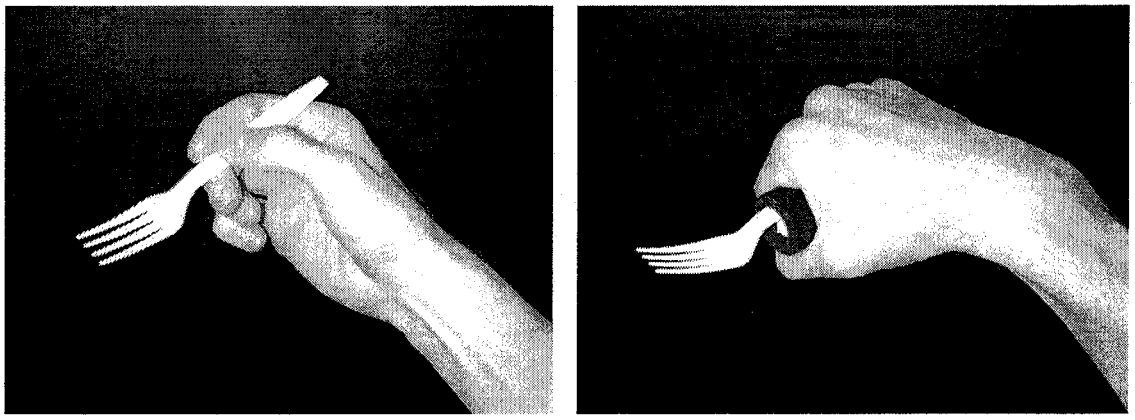

(a) (b)

Figure 5.3: During action 16, normal eating with a fork, subjects were instructed to eat using a standard three-fingered grasp (a), while in action 17, subjects used a fork that had been fit with a standard grip buildup to aid in myopathic grasp.

Table 5.1: Objects, target locations, and segmentation information associated with each action. For each action, an object was moved in the workspace from position 1 (Pos. 1) to position 2 (Pos. 2) and back to position 1. Data was segmented in either one or two segments (No. Segments), where the start and stop of each segment was triggered by motion of the object (Segment Trigger) listed.

Action No.	ADL Type	Object	Pos. 1	Pos. 2	No. Segments	Segment Trigger
1	Reaching	Hand	RP	Dh	2	Hand
2	Reaching	Cup	D1R	D1L	2	Cup
3	Reaching	Cup	D0	D2	2	Cup
4	Reaching	Cup	S2L	S2R	2	Cup
5	Reaching	Cup	D1R	S2L	2	Cup
6	Reaching	Cup	D1L	S2R	2	Cup
7	Reaching	Cup	D1	S2	2	Cup
8	Functional	Door	Closed	Open	2	Door
9	Functional	Cupboard	Closed	Open	2	Cupboard
10	Functional	Drawer	Closed	Open	2	Drawer
11	Functional	Table Phone	Dp	Right Ear	1	Phone
12	Functional	Short Utensil	Dh	D1	1	Hand
13	Functional	Long Utensil	Dh	D1	1	Hand
14	Functional	Pitcher	Dp	Dc	1	Hand
15	Functional	Cup	D1R	D1	1	Hand
16	Eating	Fork	Dh	D0	1	Hand
17	Eating	Fork	Dh	D0	1	Hand
18	Eating	Hand	Dh	D0	1	Hand
19	Drinking	Cup	Dc	Mouth	1	Cup
20	Hygiene	Comb	Dh	Hair	1	Hand
21	Hygiene	Hand	Dh	Face	1	Hand
22	Hygiene	Manual Razor	Dh	Face	1	Hand
23	Hygiene	Toothbrush	Dh	Mouth	1	Hand
24	Hygiene	Hand	Dh	Neck	1	Hand

For each arm motion, Euler joint angles for the seven degrees of freedom (DOF's) of the human arm were calculated based on the Cartesian coordinates of each marker. This transformation was performed by the Vicon system by matching marker trajectories to a 7-DOF model of the arm. The arm model incorporates anthropometric data, such as segment lengths and epicondylar widths, which were measured directly from the subject under study, and then allows the calibration to optimize model parameter based on a calibration trial. The order of Euler angle rotations in the model is as follows: shoulder flexion-extension (SF), shoulder abduction-adduction (SA), shoulder internal-external rotation (SR), elbow flexion-extension (EF), forearm rotation (FR), wrist flexion-extension (WF), and wrist radial-ulnar deviation (WD). Here, the rotation about the long axis of the forearm was considered a rotation of the forearm at the elbow, rather than a rotation of the hand at the wrist. This election is further addressed in the discussion.

The motion capture software (Vicon iQ 2.5, VICON) offers a real-time reconstruction fit of the markers with the calibrated subject arm model. The real-time model reconstruction was then directly compared with the subject under study during each trial capture with the Vicon system to ensure the appropriate transformation between marker coordinates and the calculated joint angles.

5.1.2. Post Processing – Kinematics

Kinematic data of the human arm was output in local Euler coordinates directly from the Vicon software. Position data was filtered using a 4^{th}-order Butterworth filter with a cutoff frequency of 5 hertz. Joint velocities and accelerations were each computed as two-point differences from raw position and computed velocity data, respectively, and then filtered with the same 4^{th}-order Butterworth filter. Actions 2 and 3 from the reaching subgroup, action 9 from the functional subgroup, and eating actions 16 and 17, each composed of six trials underwent similar analyses. The six trials from each action were combined to compute a mean curve as well as curves representing mean plus and mean minus standard deviations (stdev) over the action duration (Figure 5.4). Action durations for each trail were normalized over the trial length, and depending on the specifics of the action were composed of either one or two data segments (Table 5.1). Actions involving

movement of an object from position 1 to position 2 and then back were deemed to have two separate segments, each beginning and ending with the onset and disappearance of motion of an object (i.e., the cup, cupboard, or hand). The data was then resampled using a polyphase FIR filter and the two segments were concatenated together. Resampling took place prior to concatenation to eliminate side lobe effects of the resample process and was performed such that each trial contained 1000 data points. Mean and standard deviation curves for each action could then be computed both for individual subjects and across all six subjects.

Figure 5.4 shows an example of various data segmentations where Figure 5.4a has been segmented beginning and ending with the onset and cessation of hand motion, whereas Figure 5.4b has been segmented based on the onset and cessation of motion of the object, in this case the cupboard door. The first half of each plot depicts arm kinematics during opening the cupboard door, while the second half of each plot shows kinematics of the closing action. The vertical lines in Figure 5.4a illustrate the approximate potion of the data during which the cupboard door is in motion, and correspondingly matches with the concatenated segments of Figure 5.4b.

Additionally, the collective ADL position and torque data, represented previously in Figure 3.1 and Figure 3.2 from the ADL pilot study, were recreated using the first three trails of each action for each of the six subjects. As a result of the segmentation described above, biases in the histogram due to specified start and stop positions are significantly reduced.

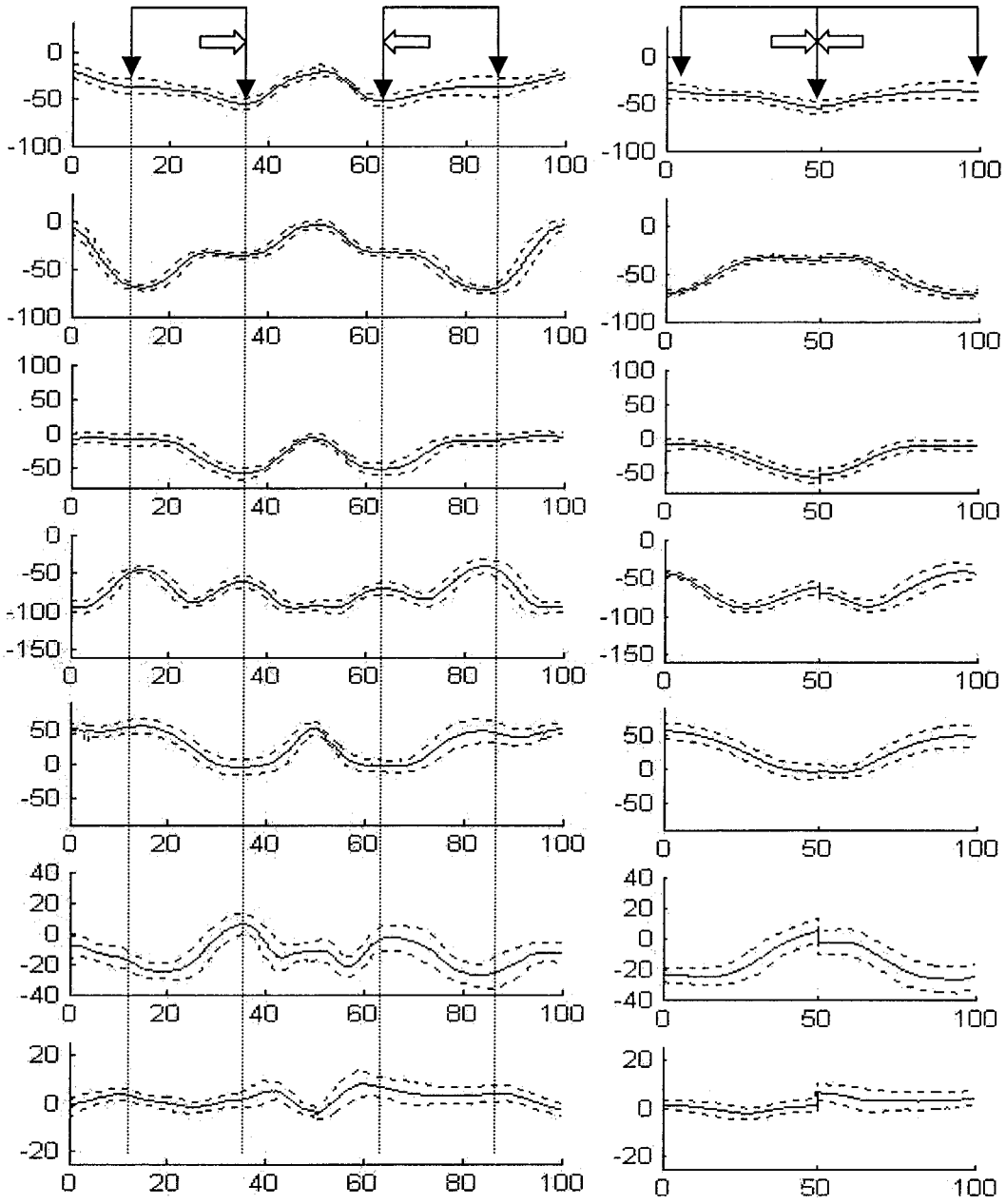

Figure 5.4: Mean +/- stdev data (N=6) of subjects opening and closing a cupboard, action 9, (a) segmented based on motion of the hand, and (b) segmented based on motion of the cupboard door.

5.1.3. Post Processing - Dynamics

The human arm dynamics were studied using an analytical approach. A mathematical model of the human arm with 7 DOF's, consistent with the 7-DOF Vicon model used

during data collection, was developed using Mathematica (Wolfram Research, Inc.). The Power of Exponentials approach [105] was used to eliminate potential singular effects at the shoulder, a common problem associated with the use of Euler angles. Analytical expressions of the seven equations of motion were derived from the model and converted to Matlab syntax for single-syntax post-processing.

The general form of the equations of motion is expressed in Equation 19.

$$\tau = M(\Theta)\ddot{\Theta} + V(\Theta, \dot{\Theta}) + G(\Theta) \qquad \textbf{Equation 19}$$

where $M(\Theta)$ is the 7x7 mass matrix, $V(\Theta, \dot{\Theta})$ is a 7x1 vector of centrifugal and Coriolis terms, $G(\Theta)$ is a 7x1 vector of gravity terms, and τ is a 7x1 vector of the net toques applied at the joints. Given the kinematics of the human arm $(\ddot{\Theta}, \dot{\Theta}, \Theta)$ the individual contributions on the net joint toque (τ) vector were calculated for each action of each subject. These allow one to examine the contribution of gravity in comparison to the effects on net torque from inertial, centrifugal, and Coriolis forces.

Measured subject parameters (height, weight, and segment lengths) were used to compute estimates for segment properties of mass and inertia according to Equations 20-22.

$$cm_i = L_i \cdot cm_i(L) \qquad \textbf{Equation 20}$$

$$m_i = BW \cdot m_i(BW) \qquad \textbf{Equation 21}$$

$$I_{i,j} = m_i \cdot \left[K_j(L) \cdot L_i\right]^2 \qquad \textbf{Equation 22}$$

where L_i refers to the longitudinal length of the segment, BW is the subject's bodyweight, and $K(L)$ refers to the radius of gyration expressed as a percent of the segment length. Similarly, on the right hand side of Equations 20 and 21, the center of mass is expressed as a percent of the segment length, and mass as a percent of bodyweight. Subscripts i and j indicate the segment (upper arm, lower arm, or hand) and coordinate axis of interest (x, y, or z), respectively. Equation 20 was used to calculate the longitudinal component of the center of mass, while transverse and sagittal components were represented by average values from literature [79].

Mass and inertial properties of manipulated objects were small in comparison to the hand, and for this reason were neglected in the study. Inertial values of the hand were approximated from literature by the values of an open hand [79,106,107] during all tasks.

5.2. ADL Results (N=6)

The results of the ADL study reveal several trends in arm behavior while executing common tasks. Additionally, many results from the previous pilot study are further supported.

5.2.1. Environmental Manipulation: positioning vs. orienting

Figure 5.5 shows mean and standard deviation curves for five actions from the following task categories: two reaching tasks (action 2, action 3), one functional task (action 9), and one eating tasks (action 16). One immediate observation from the plot is the involvement of the hand during functional tasks as opposed to general reaching and positioning tasks. In actions 2 and 3, the goal is to move an object from one location to another, in which case most of the movement takes place in the shoulder and elbow in order to position the wrist, while changing the orientation of the wrist is only minimally required. Contrast this with functional actions such as opening a cupboard door (action 9) or eating with a fork (action 16), and much larger ROM's are seen in forearm rotation and both wrist flexion and deviation.

5.2.2. Method of Grasp: normal vs. powered

Figure 5.6 compares results from two styles of fork handling: a typical three-fingered grasp (Figure 5.6a) and a powered grasp of a fork (Figure 5.6b) having a common handle buildup to aid in myopathic grasping. For impaired users with difficulty achieving a firm grasp, the buildup lessens the amount of palmar flexion required to grasp the fork. Comparison of the plots at each joint reveal significant increases in shoulder abduction ($p<0.005$) and shoulder flexion ($p<0.005$) to accommodate food stabbing as a result of the altered grasp. Additional trends showed increases in pronation, wrist flexion, and wrist radial deviation with the powered grasp.

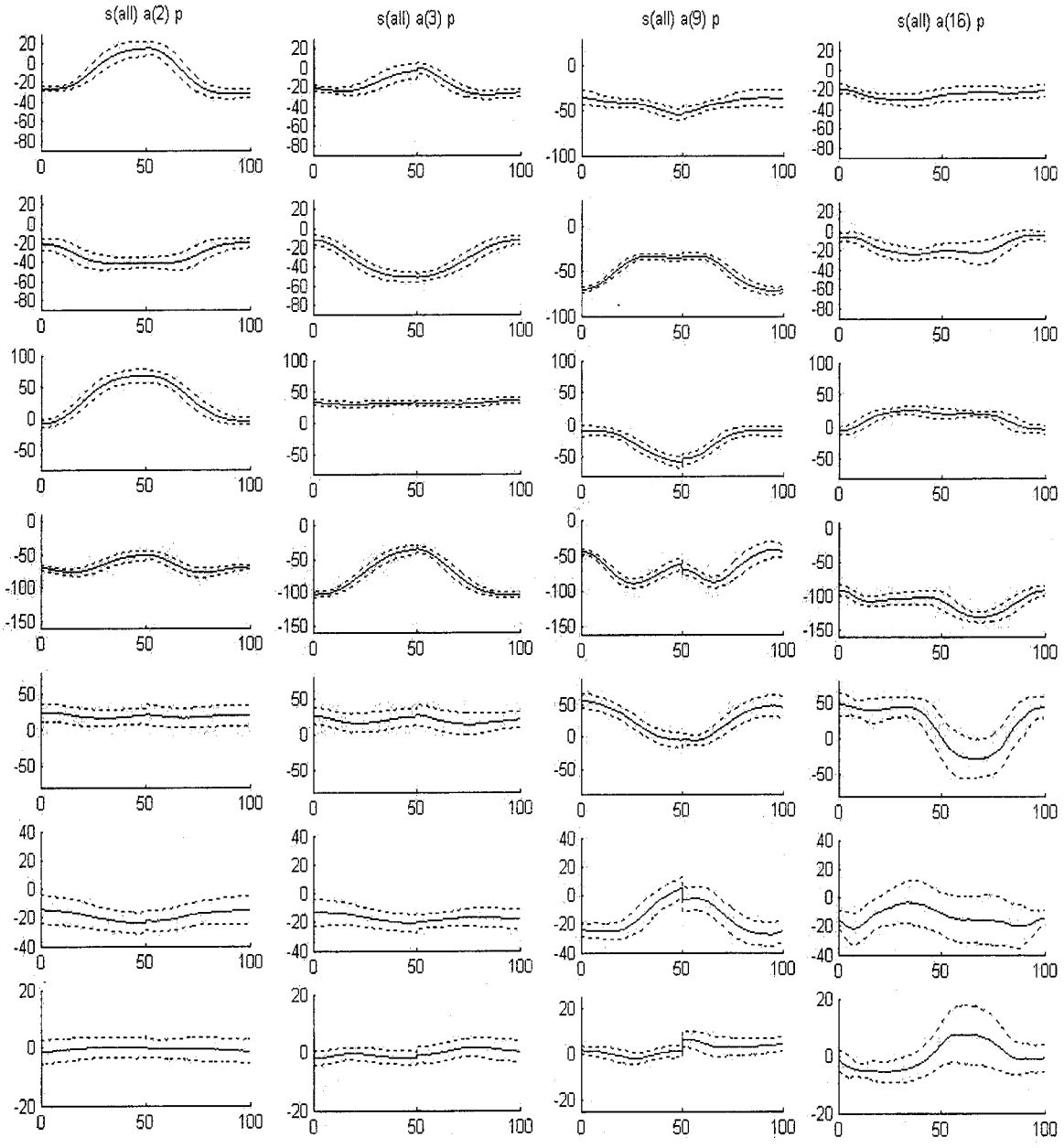

Figure 5.5: Mean (solid line), mean plus and mean minus the standard deviation (dashed lines) for segmented position data averaged over 6 subjects, 6 trials each (36 trials total), shown for actions 2, 3, 9, and 16, from left to right. All plot domains are shown from 0 to 100 percent of the segmented action, and ranges are given in degrees from top to bottom for SA, SF, SR, EF, FR, WF, and WD.

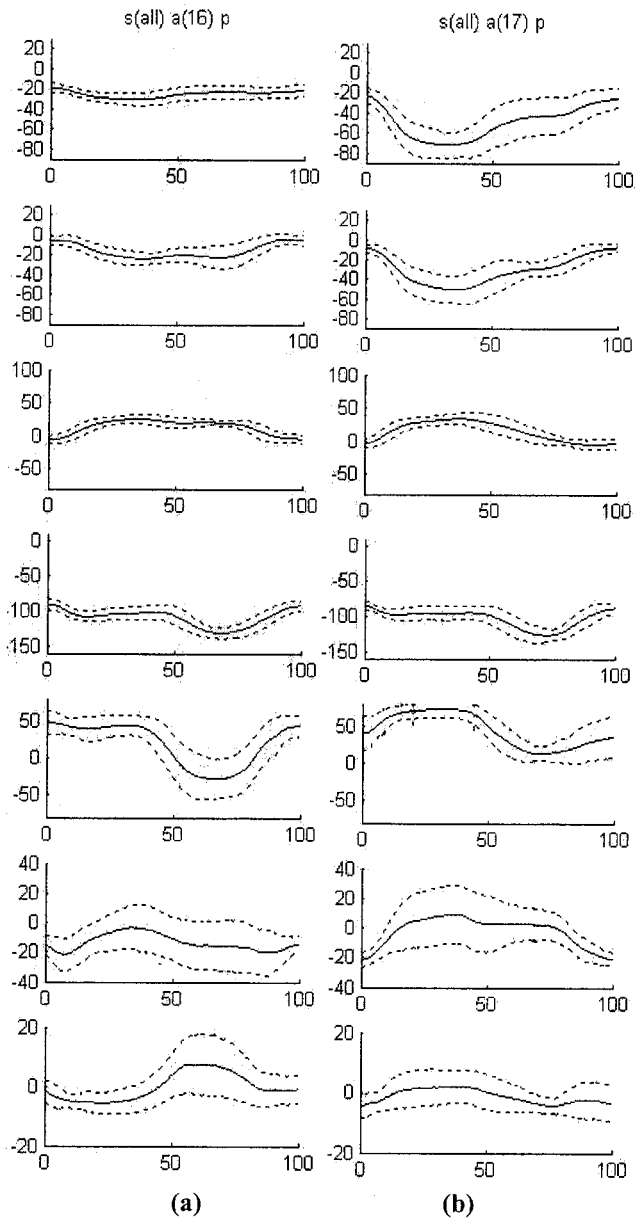

Figure 5.6: Mean (solid line), mean plus and mean minus the standard deviation (dashed lines) for segmented position data averaged over 6 subjects, 6 trials each (36 trials total), shown for (**a**) action 16 and (**b**) action 17. All plot domains are shown from 0 to 100 percent of the segmented action, and ranges are given in degrees from top to bottom for SA, SF, SR, EF, FR, WF, and WD.

5.2.3. ADL Kinematic and Dynamic Distribution of Data

5.2.3.1. Kinematic Distribution

Kinematic distribution of the ADL data, illustrated in Figure 5.7a, shows a high correlation with results of the pilot study with a few notable differences. Mean and ranges of position data are generally within 10 degrees of previous results, however, distributions are more normally distributed in the shoulder (SA, SF, SR) and wrist (WF, WD), whereas the elbow (EF) maintains the tri-modal shape with modal centers at approximately 50, 90, and 130 degrees of flexion. The distribution of forearm pronosupination (FR) possesses a widely spread distribution, extending beyond 100 degrees of supination, characteristic of the inclusion of some erroneous data trails.

5.2.3.2. Dynamic Distribution

Dynamic distributions of the ADL data, illustrated in Figure 5.7b, show a high correlation with previous results primarily in both mean and range for flexion-extension of the shoulder and elbow. There is also a strong correlation in the range for shoulder rotation. Distributions for overall are normal in shape with medians at -1, -3.9, -1.4, -1.7, -0.01, -0.14, and -0.09 Nm, according to the joint convention previously defined.

5.2.3.3. Torque Distributions

Figure 5.7c through Figure 5.7e show the contributions to total torque during ADL tasks due to gravitational effects (Figure 5.7c), Coriolis and centrifugal effects (Figure 5.7d), and inertial effects (Figure 5.7e). From the figures, it is clear that gravitational forces are the primary components of total joint torques. In comparison to gravitational effects, accelerational and velocital contributions are each respectively one and two orders of magnitude smaller in the shoulder (SA, SF, SR) and elbow (EF). At the wrist, the same ratios between components are approximately 1:2 and 1:100, while in pronosupination of the forearm, ratios are about 1:2 and 1:20 for accelerational and velocital components, respectively. The wide distribution of pronosupination velocital torque again suggests some non-physiological fitting of the models in the motion analysis software. Smaller traces of the same phenomenon to differing degrees are apparent in the other arm joints as well, resulting in large data extremes. The extent of the data is instead

shown in Table 5.2 at the 5th, 50th (median), and 95th percentiles for total and each of the three torque components for comparison.

5.2.4. ADL Task Subgroup Variations

Separating ADL results by task subgroup shows significant similarities between both position (Figure 5.8a) and torque (Figure 5.8b) distributions between subgroups. Higher percent differences of 20-40% between individual subgroups and the complete dataset (All Tasks) occur almost exclusively at the 95th percentile (rightmost bound) for most arm joints, while the 5th percentile values are generally within 10% of the torque range, with the exception of shoulder flexion while eating (Table 5.3). The 95th percentile torques correspond primarily with positive values of torque, which, for the frame orientations defined, act in the following directions of increasing motion: adduction, extension, and internal rotation of the shoulder, elbow extension, forearm pronation, wrist flexion, and wrist ulnar deviation. While percent differences of torque are mostly negative for reaching, functional, and eating tasks, suggesting lower than typical 95th percentile ADL values, values at the same percentile for hygiene tasks are positive, indicated higher than typical values for torques that generate motions in the directions defined as positive.

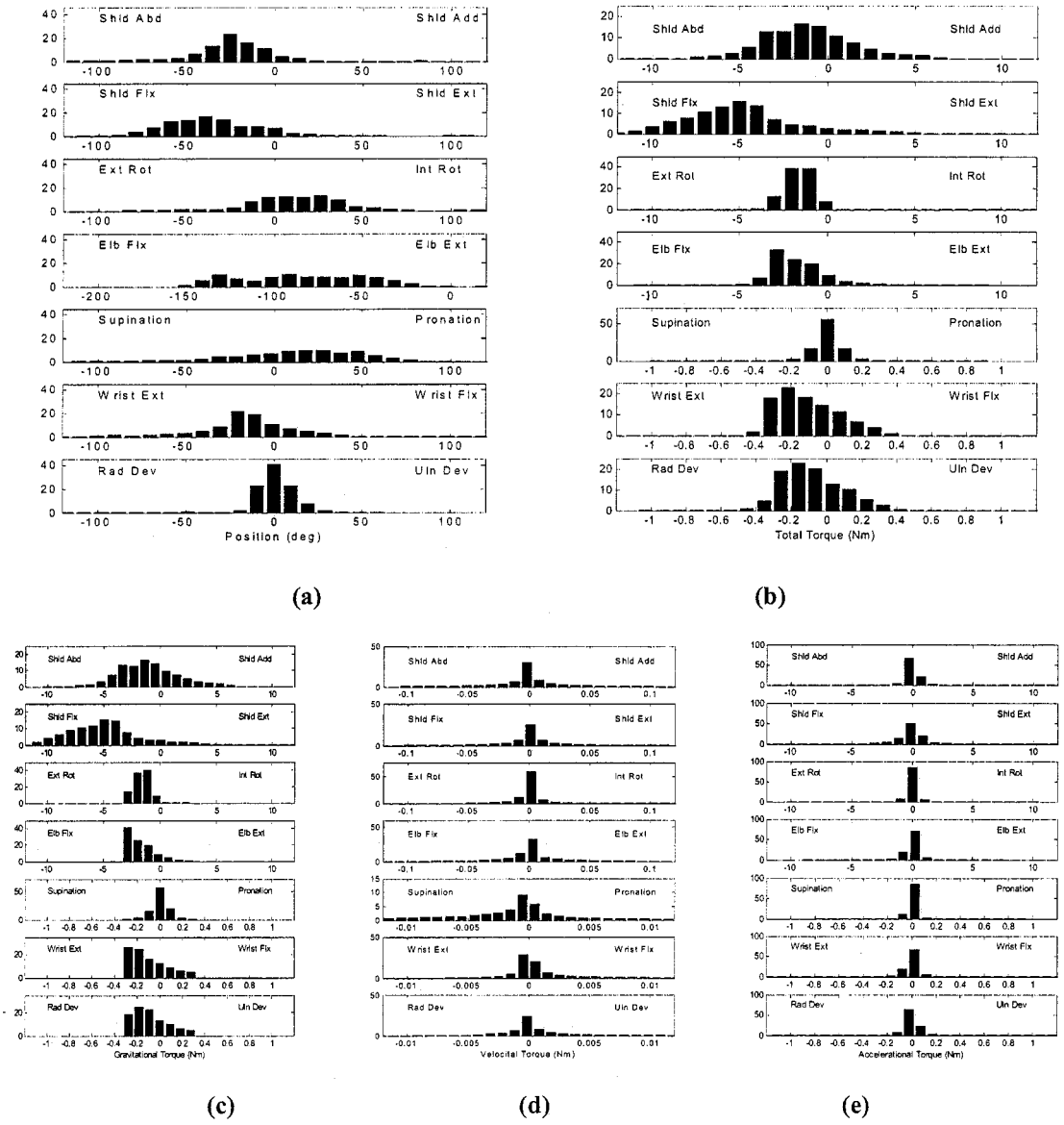

Figure 5.7: Histograms showing the distribution of joint position (a), total torque (b), gravitational torque (c), velocital torque (d), and accelerational torque (e). Each plot represents the complete set of data across all actions and subjects.

Table 5.2: The 5th, 50th, and 95th percentile values of position (deg) and torque (Nm) generated during daily activities at each of the seven degrees of freedom. Torque is expressed in terms of total torque (T_total), gravitational torque (T_grav), velocital torque (T_vel), and accelerational torque (T_accel). Mean and standard deviation (St. Dev.) also provided for joint positions.

		SA	SF	SR	EF	FR	WF	WD
Position	Mean	-24.1	-34.6	9.0	-81.0	19.2	-9.6	0.8
	St. Dev.	56.4	27.3	64.7	39.0	56.3	53.6	14.6
	5th	-91.5	-75.0	-85.0	-137.7	-76.7	-74.0	-12.9
	50th	-24.0	-36.0	8.7	-83.7	22.2	-13.7	1.0
	95th	30.0	8.7	86.3	-23.9	86.0	44.3	18.7
	90%ROM	121.5	83.7	171.3	113.8	162.6	118.3	31.6

		SA	SF	SR	EF	FR	WF	WD
T_total	5th	-4.65	-10.89	-3.80	-4.07	-0.85	-0.46	-0.39
	50th	-1.00	-3.92	-1.35	-1.65	-0.01	-0.14	-0.09
	95th	3.33	1.71	0.53	0.92	0.72	0.21	0.25
T_grav	5th	-4.70	-10.37	-3.17	-4.01	-0.12	-0.45	-0.35
	50th	-1.00	-3.94	-1.30	-1.67	0.01	-0.14	-0.09
	95th	3.31	1.71	-0.27	0.74	0.14	0.20	0.22
T_vel	5th	-0.22	-0.66	-0.05	-0.14	-0.37	-0.01	-0.04
	50th	0.00	0.00	0.00	0.00	-0.01	0.00	0.00
	95th	0.30	0.34	0.04	0.25	0.06	0.02	0.04
T_accel	5th	-0.09	-1.04	-1.91	-0.58	-0.78	-0.07	-0.13
	50th	0.00	0.00	0.00	0.00	0.00	0.00	0.00
	95th	0.06	1.02	1.76	0.61	0.83	0.08	0.12

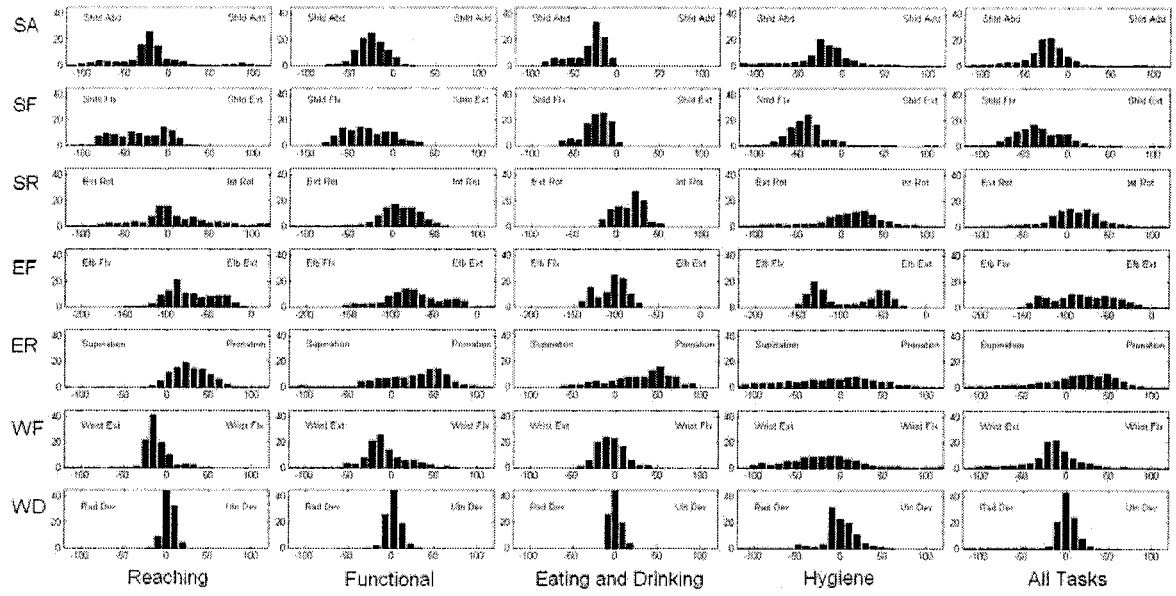

(a)

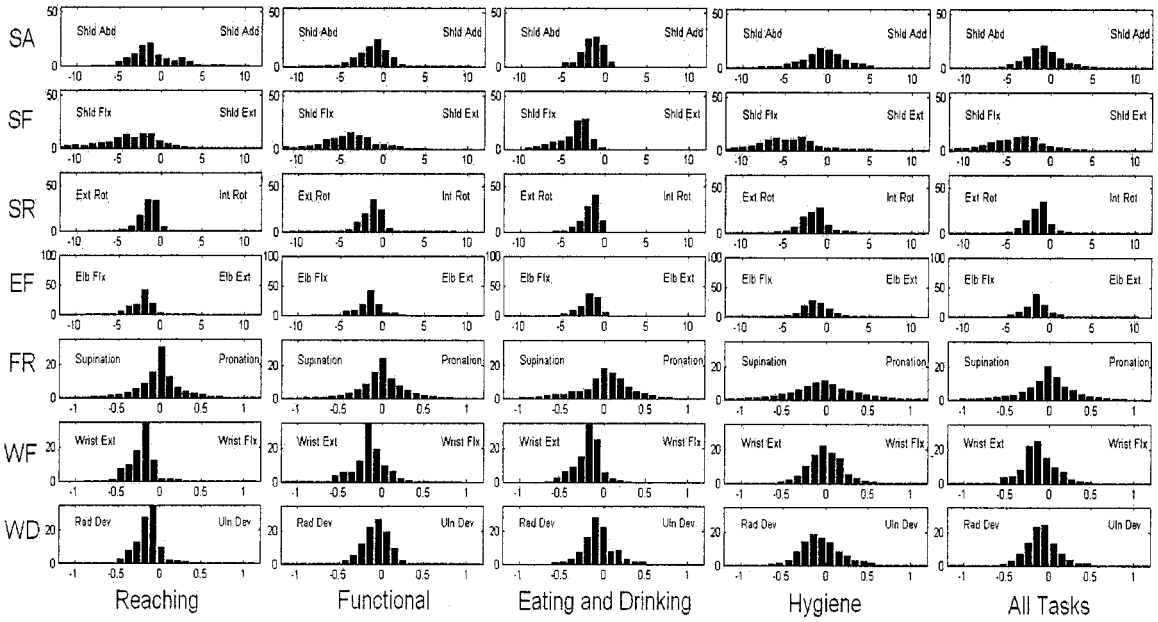

(b)

Figure 5.8: Range of motion and range of torque histograms for ADL's are represented by activity subgroup (Reaching, Functional, Eating and Drinking, Hygiene, and All Tasks Combined), for position data (a) and total torque data (b) for each arm joint. Vertical labels correspond to shoulder abd-add (SA), shoulder flx-ext (SF), shoulder int-ext rot (SR), elbow flx-ext (EF), forearm rotation (FR), wrist flx-ext (WF), and wrist rad-uln deviation (WD). Horizontal axes for (a) and (b) are in units of degrees and Nm.

Table 5.3: 5th, 50th (median), and 95th percentile values of total joint torque for each of the four task subgroups (a), and differences at those percentiles between each task subgroup and the values for all tasks (b). Each difference is expressed as a percent of the 5th to 95th percentile range. For example, the median shoulder flexion torque (SF) during reaching tasks is 40.74 % higher than the 95th percentile value for all tasks combined. Percent difference values are shaded according to shading key to the right.

(a)

		SA	SF	SR	EF	FR	WF	WD
Reaching	5th	-4.65	-10.78	-3.49	-4.28	-0.58	-0.47	-0.39
	50th	-1.43	-3.40	-1.30	-1.88	-0.01	-0.19	-0.13
	95th	4.69	1.43	0.14	-0.57	0.50	-0.05	0.05
Functional	5th	-4.86	-11.50	-3.48	-3.98	-0.61	-0.49	-0.34
	50th	-1.13	-4.15	-1.24	-1.64	-0.01	-0.17	-0.06
	95th	1.37	0.85	0.24	0.54	0.55	0.13	0.17
Eating	5th	-3.91	-6.99	-3.59	-4.04	-0.69	-0.47	-0.35
	50th	-1.49	-3.17	-1.52	-1.58	0.02	-0.18	-0.07
	95th	0.26	-1.54	-0.42	-0.31	0.50	0.01	0.29
Hygiene	5th	-5.06	-10.82	-4.42	-3.46	-1.21	-0.33	-0.44
	50th	-0.48	-4.55	-1.49	-1.32	-0.05	-0.01	-0.08
	95th	3.99	3.64	1.60	1.76	1.08	0.34	0.40
All Tasks	5th	-4.65	-10.89	-3.80	-4.07	-0.85	-0.46	-0.39
	50th	-1.00	-3.92	-1.35	-1.65	-0.01	-0.14	-0.09
	95th	3.33	1.71	0.53	0.92	0.72	0.21	0.25

(b)

		SA	SF	SR	EF	FR	WF	WD
Reaching	5th	0.02	0.86	7.26	-4.26	17.49	-1.93	-0.33
	50th	-5.45	4.11	1.19	-4.65	0.07	-6.94	-6.58
	95th	16.99	-2.21	-8.86	-29.88	-14.24	-39.56	-31.90
Functional	5th	-2.65	-4.89	7.27	1.71	15.45	-4.40	7.33
	50th	-1.58	-1.84	2.62	0.12	-0.17	-3.78	3.80
	95th	-24.56	-6.79	-6.50	-7.58	-10.79	-12.56	-13.22
Eating	5th	9.33	-30.89	4.81	0.51	10.03	-1.65	5.75
	50th	-6.18	5.91	-3.92	1.32	2.08	-4.85	3.13
	95th	-38.47	-25.80	-21.81	-24.67	-14.26	-30.24	5.82
Hygiene	5th	-5.10	0.53	-14.34	12.15	-22.77	19.93	-8.65
	50th	6.50	-5.02	-3.18	6.49	-2.22	19.21	1.36
	95th	8.33	15.36	24.95	16.84	22.57	18.91	23.02
All Tasks	5th	0	0	0	0	0	0	0
	50th	0	0	0	0	0	0	0
	95th	0	0	0	0	0	0	0

PERCENT DIFFERENCE

> 30%

> 20%

> 10%

0-10%

5.3. ADL Discussion

5.3.1. Human Arm Model

In the selection of appropriate kinematic and dynamic models of the human arm, various tradeoffs were weighed. The following discussion assumes the arm can be represented as a spherical shoulder, a perpendicular elbow axis (beta=0), and three additional axes representing the remainder of the forearm and wrist motion.

For both dynamic and kinematic models, a significant election pertained to the order of Euler rotations both at the shoulder and wrist joints. In the case of a spherical joint such as the shoulder, there are six possible permutations on the order of frame rotations (1-2-3, 1-3-2, 2-1-3...etc.) where any of the six are viable and correct regarding a representation of the resulting three-dimensional vector. The difference of course is in the relative meaningfulness of the individual rotations with respect to motion of the human arm. Human arm biomechanics are such that the int-ext rotation (SR) of the shoulder is the last of the three rotations, while shoulder flx-ext (SF) and shoulder abd-add (SA) are precursory motions that define the axis about which SR is to take place. The order of the first two rotations is less defined, however, and can be ordered in either manner with equal legitimacy, and neither a perfect correlation to the anatomical equivalent.

5.3.2. Positioning vs. Orienting

In various ADL tasks, it has been observed that joint velocities and angular excursions tend to take place in one of several joint combinations. Combinations seem to be threefold, having either high velocities in the shoulder and elbow and low velocities in the wrist, high velocities in the wrist and low velocities in the shoulder and elbow, or high velocities in all three joints. Although some complex and partially constrained tasks, such as brushing your teeth or opening a cupboard, require the simultaneous use of shoulder, elbow and wrist joints, many tasks rely primarily on the use of the shoulder and elbow for positioning an object relative to the environment or positioning the hand relative to an object. On the other hand, with the hand positioned in a desired location relative to the environment, the hand has been observed to perform high velocity manipulations in order to orient the hand and/or other objects with respect to one another.

5.3.3. Gravitational Dominance

Comparing torque contributions from the effects of gravity, centrifugal and Coriolis forces, and inertial parameters, it is clear that the influence of gravity is the most dominant effect, more so than the other two combined. In particular, the effect of velocity-dependent terms, commonly two orders of magnitude below those dependent on position. Coincidentally, the velocity-dependent terms are computationally the most expensive terms in the equations of motion, contributing more than half of the total execution time. A favorable outcome of this result is that these computationally expensive terms can legitimately be removed from the equations of motion, significantly reducing execution times of command signals without affecting the system performance.

5.3.4. Subgroup Torques

As was noted in the results of Section 5.2.4, the reaching, functional, and eating/drinking tasks yielded significantly lower positive torques than the hygiene tasks, on average 1 to 3 Nm lower for shoulder and elbow joints and 0.3-0.5 Nm lower for wrist joints. Remember that the torque directions defined as positive in the study are shoulder adduction, shoulder extension, shoulder internal rotation, elbow extension, forearm pronation, wrist flexion, and wrist ulnar deviation. For the majority of daily activities, where the arm is placed in front of the body to move or manipulate an object, the arm would generate torques of the opposite sign to counteract the forces of gravity. Clearly then, the elevated levels of torque in hygiene tasks are due instead to velocities and accelerations of limb segments.

CHAPTER 6: ROBOTICALLY-ASSISTED REHABILITATION

6.1. Brief History

Early exoskeletons were considered primarily for their appeal as human amplifiers (assistive devices) that provide healthy individuals with increased strength [2,3,108,109]. Since 1988, a number of generic upper limb exoskeleton devices have been developed for teleoperation [54-56,59,110-112] and as haptic devices for virtual reality simulation [55,56,112,113]. Despite more than 25 years of research in the field of rehabilitation robotics, there remain only a small number of assistive upper-limb exoskeletons that specifically target the disabled community [61,114]. Even smaller is the number of commercially available systems for rehabilitation research and treatment. To date, only a single system is available for purchase, the InMotion2 (MIT-Manus), while others exist only within institutes for research and development. The following review of existing systems includes only the mechanisms that are specifically used for upper limb rehabilitation.

- *Manus (MIT)* [8,38,41-43] – The Manus is a planar module that provides two translational DOF's for elbow and forearm motion (Figure 6.1a). The 2-DOF module is portable and consists of a direct-drive commercial robotic arm (SCARA).
- *MIME (VA Palo Alto RR&D Center)* [33-36] – The MIME therapy workstation is based on an industrial robotic arm (PUMA 560) that is mounted beside a table and placed in front of the patient (Figure 6.1b). When attached to the paretic limb, a 6-axis position digitizer can be used to quantify voluntary movement kinematics. When attached to the stronger limb, it provides positional control for the paretic side to follow, thereby implementing a mirror image, master/slave mode involving both limbs.
- *ARM Guide (Rehabilitation Institute of Chicago and UC Irvine)* [44-47] – The ARM guide is a single actuated, 3-DOF device designed to mechanically assist in

reaching movements that typically follow approximately straight-line trajectories (Figure 6.1c).

- *GENTLE/s (University of Reading)* [37] – GENTLE/s is an integrated system of several technologies (Figure 6.1d). The core technology is a Haptic Master from FCS Robotics, a 3-DOF arm with three passive DOF's at the wrist. The Haptic Master assists with movement patterns needed to accomplish virtual tasks in a simulated environment.

Results to date using common clinical scales suggest that robot-aided sensorimotor training does have a genuinely positive effect on reduction of impairment and offers the potential benefit of deeper insight into the process of recovery from neurological injury [32-47]. Improvements have been demonstrated in strength and Fugl-Meyer assessment of motor function, and have been shown to persist in excess of 6 months following a stroke [33-36]. Active assist therapy produced several quantifiable benefits such as active range of motion and ability to initiate movement [44-47]. Additionally, user interfaces based on VR environments could improve patient motivation for using the system [37]. This information is relevant given evidence that highly repetitive exercises may be needed for improved recovery.

Critical review of the four aforementioned systems yields three areas for improvement: firstly, each design has at most three active degrees of freedom, some having only one; secondly, the workspace of each system is significantly less than that of the human arm, limiting its capabilities as a rehabilitative device; and thirdly, regarding questions of safety in non-anthropometric designs. The lack of active degrees of freedom prevents the ability to correctly assist users in performing a variety of activities of daily living. Additionally, the choice of non-anthropometric translational and rotational joints requires complex multi-joint motions of the robot's actuators in order to track even single-joint motions of the arm. Similarly, improper constraints or coupling schemes on robot joint motions for non-anthropomorphic robots could result in injury due to non-physiological imposed motions. This is an issue of safety that must be considered

carefully if higher degrees of freedom are to be achieved using non-anthropomorphic exoskeleton designs.

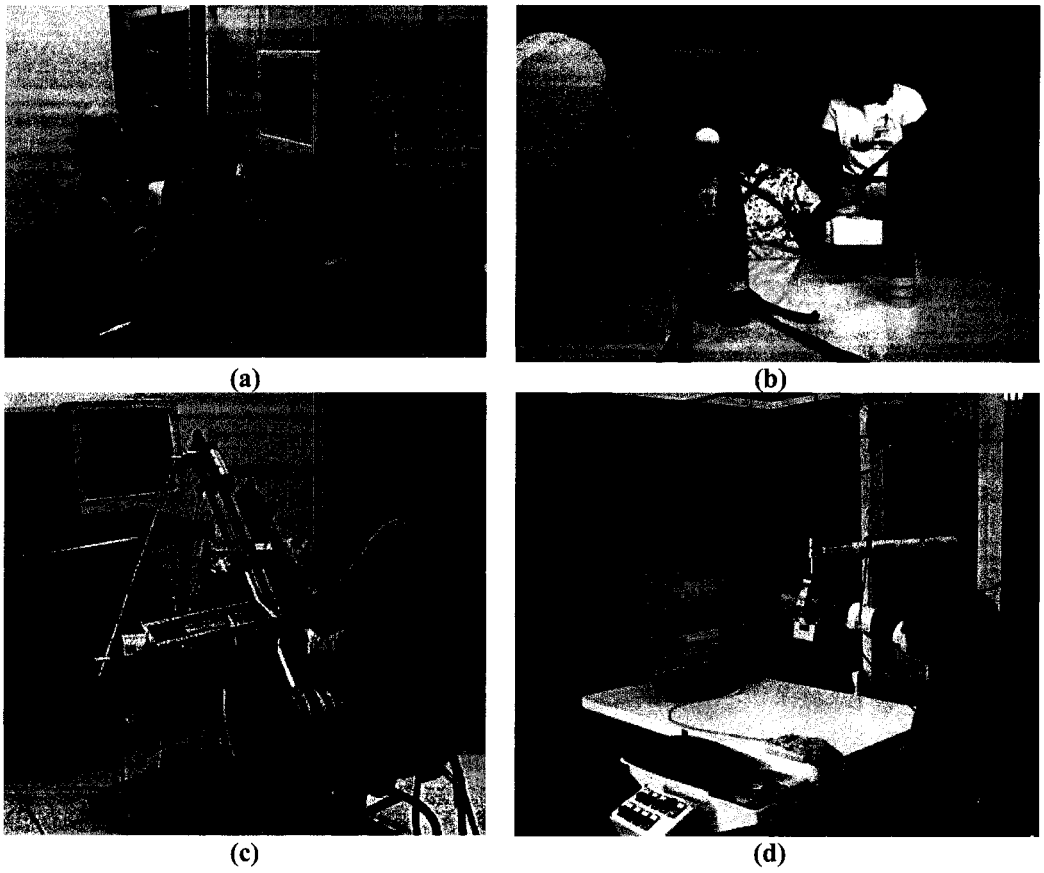

Figure 6.1: Robotics Systems Used for Rehabilitation: (a) MANUS (MIT) (b) MIME (VA Palo Alto RR&D Center) (c) ARM Guide (Rehabilitation Institute of Chicago and UC Irvine) (d) GENTLE/s (University of Reading)

6.2. Stroke Rehabilitation – Unmet Needs

Stroke is a leading cause of long-term disability in the US. Each year about 700,000 people in the US sustain a first or recurrent stroke with more than 5 million people currently living with the consequences of stroke [117,118] Reducing the degree of permanent disability remains the goal of post stroke rehabilitation programs. In 2006, the direct and indirect costs of stroke in the US were estimated at $57.9 billion, where over half of this sum resulted from direct costs [118]. This figure is nearly twice that of

estimates from 1993 (Figure 6.2). Due in part to inflation, a more significant factor is the steady rise in life expectancy, which in 2003 increased to 77.5 years [119]. To further compound this issue of rising annual cost, the first members of the generation born between 1946 and 1964 (known as the 'baby-boomers') will reach age 65 in the year 2011, initiating a rise in the global elderly population of historic proportion [120]. As a direct consequence of this approaching demographic wavefront in the very population that is most susceptible to stroke, combined with the still increasing life expectancy, the population of elderly in America is projected to triple by year 2050 (Figure 6.3). Without the vital introduction of new treatment interventions, the outlook on stroke rehabilitation for future patients is under rapid decline. If the current treatment numbers of [121] persist, then by year 2050, fewer than 5% of stroke patients will receive the treatment they need as a result of insufficiencies in the capacity for patient throughput.

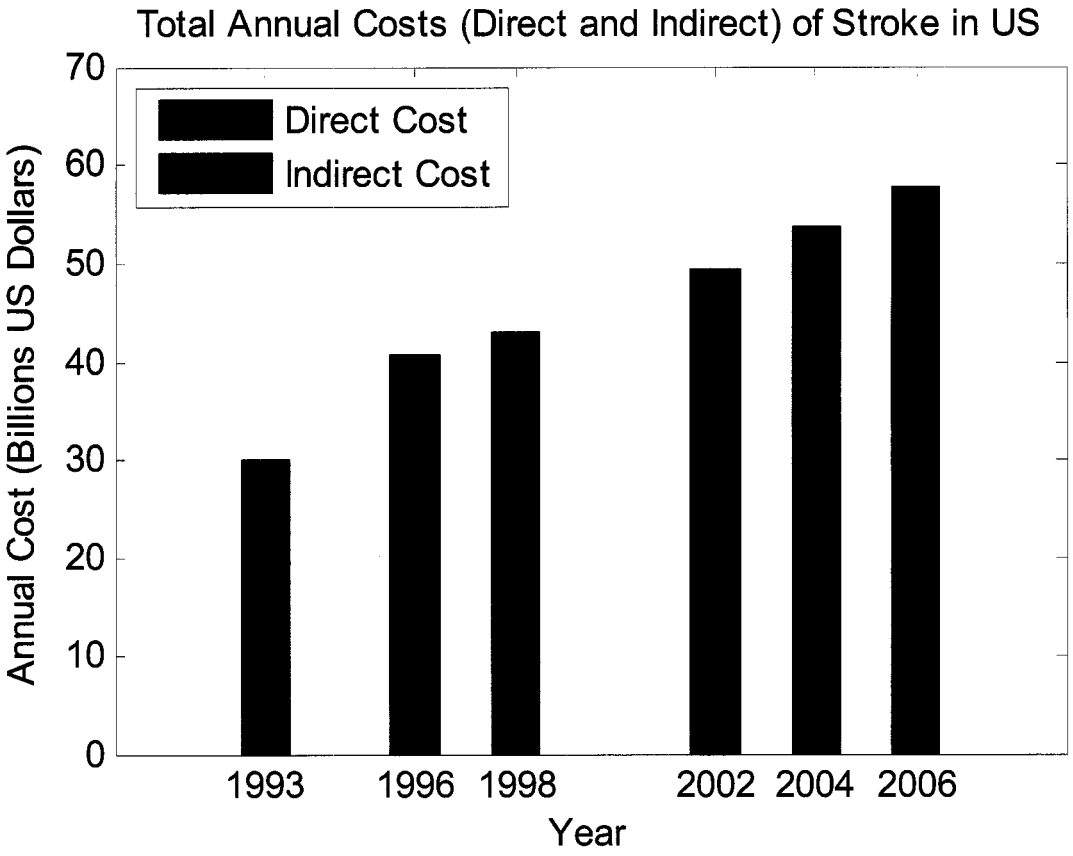

Figure 6.2: Current trends in aging populations lead to higher numbers of stroke patients and annual treatment costs: The annual cost of stroke patient care has nearly doubled to $60 billion since 1993 [117,118,123,124].

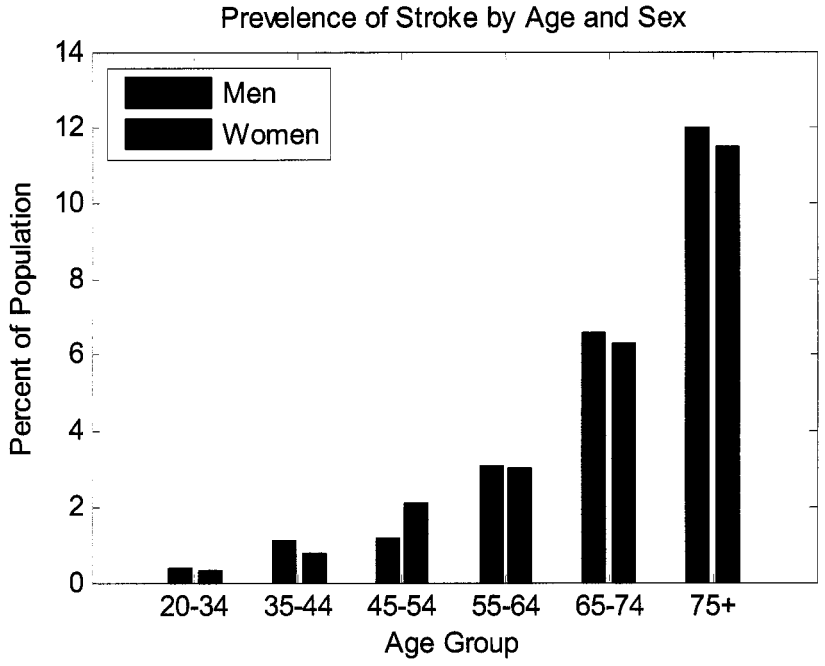

(a)

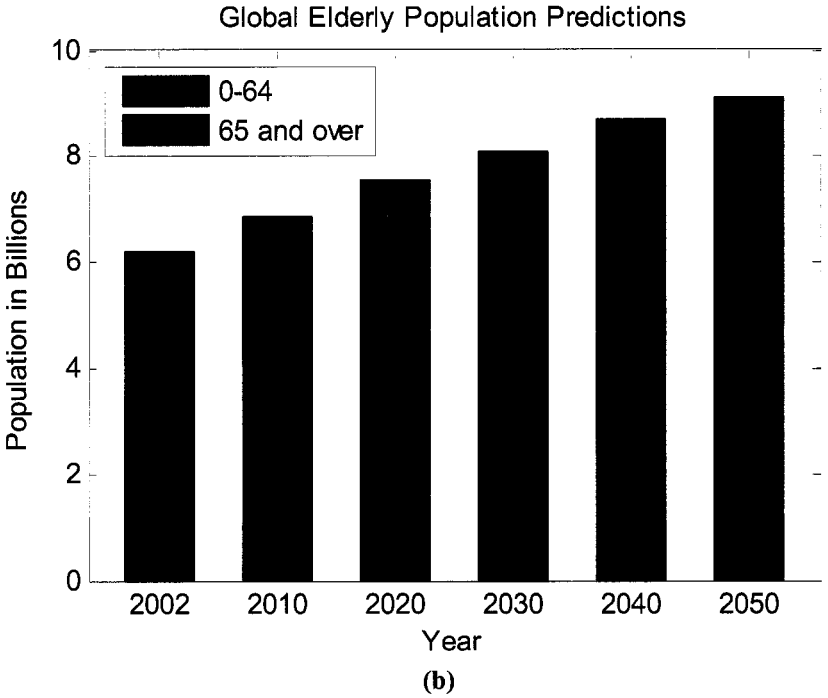

(b)

Figure 6.3: Current trends in aging populations lead to higher numbers of stroke patients: (a) probability of stroke increases dramatically with age [118], (b) global population of persons 65 years and older is projected to triple by 2050 [125].

Approximately 5% of direct costs of stroke, or nearly $2 billion, is currently spent on inpatient rehabilitation [121]. However, despite the fact that 90% of survivors are left with lifelong post-stroke deficits, existing facilities are only able to provide rehabilitation services for 10% to 15% of patients [122]. This situation creates a pressing need and opportunity. The need is for new strategies to increase productivity while optimizing the quality of care, and the opportunity is to utilize advances of robotics, sensing, and information technology to address this growing deficit in our existing health care system. Robotically assisted rehabilitation (RAR) is aimed at increasing the efficiency in the delivery of rehabilitation care for a wide variety of patients while simultaneously improving the quality of that care. For reasons of safety, affordability, and accessibility to treatment, anthropomorphic exoskeletons may be the ideal vessel to enable the successful delivery of this vital treatment.

CHAPTER 7: CONCLUSION

In this document, the development of a novel and versatile anthropomorphic exoskeleton has been introduced, with specific aims to assess and aid in the rehabilitation of neural, orthopedic, and muscular deficits of the arm. Supported by a grant from the National Science Foundation, the immediate project spanned four years, following more than fifteen years of preliminary research, and produced a pair of exoskeleton arms (left and right) to support further research.

Originally considered primarily for their appeal as human amplifiers (assistive devices) anthropomorphic exoskeletons have since been developed for such applications as master controllers, teleoperation, high-fidelity haptic devices, and virtual environment human computer interfaces. Even at present, there exist only a small number of assistive upper-limb exoskeletons dedicated to the disabled community, despite more than 25 years of research in the filed of rehabilitation robotics. Even smaller is the number of commercially available systems for rehabilitation research and treatment.

The CADEN-7 (Cable-Actuated Dexterous Exoskeleton for Neuro-rehabilitation) exoskeleton system begins a new generation of capabilities. The combination of actuated anthropomorphic segments and sensored human-machine interfaces permits the ability to assess and quantify physiologic capabilities of the human arm in a way never before possible. Results from both impaired and healthy populations can be directly compared to lay the foundations for improved strategies in rehabilitation, muscle modeling, neural control, and much more.

With applications in rehabilitation medicine and virtual reality simulation, anthropomorphic exoskeletons offer benefits for both disabled and healthy populations. A pilot database defining the kinematics and dynamics of the upper limb during daily living activities was one among several factors guiding the development of the CADEN-7 anthropomorphic, seven degree-of-freedom (DOF), powered exoskeleton. Additional design inputs included anatomical and physiological considerations, workspace analyses, and upper limb joint ranges of motion. The database was compiled from 19 arm activities

of daily living (ADL). Utilizing a model of the human arm, represented as a 7-DOF system, the equations of motion were used to calculate joint torques from measured arm kinematics. A second ADL study including six subjects (N=6) and 24 daily actions confirmed prior result of the pilot study toward the compilation of the design requirements.

The CADEN-7 exoskeleton arm offers remarkable opportunities as a versatile human-machine-interface and as a new generation of assistive technology. Proximal placement of motors and distal placement of cable-pulley reductions were incorporated into the design, leading to low inertia, high-stiffness links, and back-drivable transmissions with zero backlash. The design enables full glenohumeral, elbow, and wrist joint functionality. Potential applications of the exoskeleton as a wearable robot include use as: (1) a therapeutic and diagnostics device for physiotherapy, (2) an assistive (orthotic) device for human power amplifications, (3) a haptic device in virtual reality simulation, and (4) a master device for teleoperation.

In addition to the applications listed above, the neural-controlled exoskeleton system serves as a versatile tool for a multitude of studies. A 64-channel EMG amplifier allows for simultaneous collection of up to 32 surface electromyography signals and joint kinematic data, providing the capacity for comprehensive study of such areas as muscle recruitment and stimulation patterns, post-deficit kinematic behavioral adaptations, and effects of neural plasticity. Load cells positioned at four discrete locations simultaneously record forces transmitted between the user and exoskeleton under varying external loads applied to the exoskeleton, enabling the rendering of haptic forces at each point of contact. Such rendering capabilities allow for full immersion in virtual environments where haptic feedback can be applied along the length of the arm to simulate collisions with virtual objects such as walls or parts in an assembly.

The research and development work presented in this document represents a significant contribution not only to the fields of haptics, neurophysiology, and human computer interfaces, but also toward the advancement of human understanding. The CADEN-7 exoskeleton is a unique but versatile high-performance two-way interface,

manufactured to the highest industry standards, that will support further research along a number of academic pathways toward a deeper understanding of the human body, the neuromuscular system, and the optimal modalities for neuromuscular rehabilitation.

REFERENCES

1. American Heritage Dictionary, Houghton Mifflin Company, Boston, 2nd Ed. 1982.
2. General Electric Company (1966), "exoskeleton prototype project, final report on phase I," Report S-67-1011, Schenectady, NY.
3. General Electric Company (1968), "Hardiman I prototype project, special interim study," Report S-68-1060, Schenectady, NY.
4. Makinson, B.J. (1971), "Research and development prototype for machine augmentation of human strength and endurance, Hardiman I project," Report S-71-106, GE Company, Schenectady, NY.
5. Emery, AE, "Population frequencies of inherited neuromuscular diseases--a world survey." Neuromuscul Disord. 1991; 1(1): pp.19-29. Review.
6. Kelly-Hayes, M. et. al. The American Heart Association Stroke Outcome Classification, AHA Scientific Statement, June 1998.
7. Volpe, B T et. al., "Robotics and Other Devices in the Treatment of Patients Recovering From Stroke." *Cur Atheroscler Rep.* 2004 July; 6(4): p. 314-319.
8. Volpe, B.T., H.I. Krebs, and N. Hogan, "Is Robot-Aided Sensorimotor stroke Rehabilitation a Realist Option," *Curr Opin Neurol*, 2001 Dec; 14(6): p. 745-752.
9. Glasser, L., "Effects of isokinetic training on the rate of movement during ambulation in hemiparetic patients." *Phys Ther*, 1986; 66(5): p. 673-6.
10. Sharp, S.A. and B.J. Brouwer, "Isokinetic strength training of the hemiparetic knee: effects on function and spasticity." *Arch Phys Med Rehabil*, 1997; 78(11): p. 1231-6.
11. Wilder, P.A. and J. Sykes, "Using an isokinetic exercise machine to improve the gait pattern in a hemiplegic patient. A case report." *Phys Ther*, 1982; 62(9): p. 1291-5.
12. Weiss, A., et al., "High intensity strength training improves strength and functional performance after stroke." *Am J Phys Med Rehabil*, 2000; 79(4): p. 369-76.
13. Mercier, C., et al., "Description of a new motor re-education programme for the paretic lower limb aimed at improving the mobility of stroke patients." *Clin Rehabil*, 1999; 13(3): p. 199-206.
14. Sjogaard, G., et al., "Muscle involvement during intermittent contraction patterns with different target force feedback modes." *Clin Biomech* (Bristol, Avon), 2000; 15 Suppl 1: p. S25-9.
15. Bourbonnais, D., et al., "Effect of force-feedback treatments in patients with chronic motor deficits after a stroke." *Am J Phys Med Rehabil*, 2002; 81(12): p. 890-7.

16. Dean, C.M. and R.B. Shepherd, "Task-related training improves performance of seated reaching tasks after stroke. A randomized controlled trial." *Stroke*, 1997; 28(4): p.722-8.

17. Smith, G.V., et al., ""Task-oriented" exercise improves hamstring strength and spastic reflexes in chronic stroke patients." *Stroke*, 1999. 30(10): p. 2112-8.

18. Whitall, J., et al., "Repetitive bilateral arm training with rhythmic auditory cueing improves motor function in chronic hemiparetic stroke." *Stroke*, 2000; 31(10): p. 2390-5.

19. Bayona, N.A., J. Bitensky, K. Salter, and R. Teasell, "The role of task-specific training in rehabilitation therapies," *Topics in Stroke Rehabil.*, Summer 2005; 12(3): p. 58-65.

20. Riener, R., T. Nef, and G. Colombo, "Robot-aided neurorehabilitation of the upper extremities," *Med Biol Eng Comput*, 2005 Jan; 43(1): p. 2-10.

21. Kelly, J.L., M.P. Baker, and S.L. Wolf, "Procedures for EMG biofeedback training in involved upper extremities of hemiplegic patients." *Phys Ther*, 1979; 59(12): p.1500-7.

22. Wolf, S.L. and S.A. Binder-MacLeod, "Electromyographic biofeedback applications to the hemiplegic patient. Changes in upper extremity neuromuscular and functional status." *Phys Ther*, 1983; 63(9): p.1393-403.

23. van der Lee, J.H., et al., "Forced use of the upper extremity in chronic stroke patients: results from a single-blind randomized clinical trial." *Stroke*, 1999; 30(11): p. 2369-75.

24. Willis, J.K., et al., "Forced use treatment of childhood hemiparesis." *Pediatrics*, 2002; 110(1 Pt 1): p. 94-6.

25. Wolf, S.L., et al., "Forced use of hemiplegic upper extremities to reverse the effect of learned nonuse among chronic stroke and head-injured patients." *Exp Neurol*, 1989; 104(2): p.125-32.

26. Gelber, D.A. and D.R. Jeffery, Clinical Evaluation and Management of Spasticity, Humana Press, Feb. 11, 2001, p. 94

27. Hartkopp, A, et al., "Effect of training on contractile and metabolic properties of wrist extensors in spinal cord-injured individuals." *Muscle Nerve*. 2003 Jan; 27(1): p. 72-80.

28. Nursing Practice Related to Spinal Cord Injury and Disorders, Ed. A. Nelson, C.P. Zejdlik, L. Love, Demos Medical Publishing, LLC, Aug. 1, 2001; p. 498

29. Bourbonnais, D., et al., "Effect of force-feedback treatments in patients with chronic motor deficits after a stroke." *Am J Phys Med Rehabil*, 2002; 81(12): p. 890-7.

30. Rakos, M., et al., "Electromyogram-controlled functional electrical stimulation for treatment of the paralyzed upper extremity." *Artif Organs*, 1999. 23(5): pp. 466-9.

31. Hogan, N., et al., "MIT-MANUS: a workstation for manual therapy and training. I," *IEEE Proc. Intl. Workshop on Robot and Human Communication*, 1992 Sept; p. 161-165.

32. Reinkensmeyer, D.J., et al., Chapter 38 - Rehabilitators, robots, and guides: new tools for neurological rehabilitation. In: "Biomechanics and Neural Control of Posture and Movement," Ed. J.M. Winters & P.E. Crago, Springer-Verlag, New York, 2000

33. Lum, P.S., et al., "A mechanically assisted method for quantification of upper-limb move-ment deficits in post-stroke hemiparesis." IEEE Trans on Biomedical Engineering, 1998

34. Lum, P.S., et al., "Quantification of force abnormalities during passive and active-assisted upper-limb reaching movements in post-stroke hemiparesis. *IEEE Transactions on Biomedical Engineering*, 1999; 46(6): p. 652-662,

35. Burgar, C.G., et al., "Development of robots for rehabilitation therapy: the Palo Alto VA/Stanford experience." *J Rehab Res Dev*, 2000; vol. 37: p. 663-673.

36. Lum, P.S., et al., "Robot-assisted movement training compared with conventional therapy techniques for the rehabilitation of upper limb motor function after stroke." *Arch Phys Med Rehab*, 2002; vol. 83: p. 952-959.

37. Loureiro, R., et al., "Upper Limb Mediated Stroke Therapy - GENTLE/s Approach," *Special Issue on Rehabilitation Robotics Journal of Autonomous Robots*, 2003

38. Krebs, H.I., et al., "Increasing Productivity and Quality of Care: Robot-Aided Neuro-rehabilitation," *VA J of Rehabil Research and Development*, 2000; 37(6): p. 639-652.

39. Fasoli, S. E., et al., "Effects of Robotic Therapy on Motor Impairment and Recovery in Chronic Stroke"; *Archives of Physical Medicine & Rehabilitation*, 2003; 84: p. 477-82.

40. Krebs, H.I., et al., "Robotic Applications in Neuro-motor Rehabilitation," *Topics in Spinal Cord Injury Rehabilitation*, 1999; 5(3): p. 50-63.

41. Krebs, H.I., et al., "Robot-Aided Neuro-Rehabilitation: From Evidence-Based to Science-Based Rehabilitation"; *Topics in Stroke Rehabilitation*, 2002; 8(4): p. 54-68.

42. Volpe, B.T., et al., "Robot Training Enhanced Motor Outcome in Patients with Stroke maintained over 3 years," *Neurology*, 1999; 53: p.1874-1876.

43. Krebs, H.I., et al., "Rehabilitation Robotics: Pilot Trial of a Spatial Extension for MIT-Manus," *Journal of NeuroEngineering and Rehabilitation*, 1:5 Biomedcentral (2004).

44. Reinkensmeyer, D.J., J.P.A Dewald, and W.Z. Rymer, "Guidance-based quantification of arm impairment following brain injury: A pilot study," *IEEE Trans on Rehabilitation Engineering*, 1999; 7(1): p.1-11.

45. Reinkensmeyer, D.J., et al., Understanding and treating arm movement impairment after chronic brain injury: Progress with the ARM Guide, *J Rehab Research and Development*, 2000; 37(6): p. 653-662.

46. Kamper, D.G., et al., "Alterations in reaching after stroke and their relationship to movement direction and impairment severity," *Archives of Physical Medicine and Rehabilitation*, 2002; 83: p. 702-7.

47. Reinkensmeyer, D.J., P.S. Lum, and J. Winters, 'Emerging Technologies for Improving Access to Movement Therapy Following Neurologic Injury', in "Emerging and Accessible Telecommunications, Information and Healthcare Technologies: Engineering Challenges in Enabling Universal Access," (ed) Winters J, Robinson C, Simpson R., Vanderheiden G. (eds), IEEE Press, 2002.

48. Schleenbaker, R.E. and A.G. Mainous, 3rd, "Electromyographic biofeedback for neuromuscular reeducation in the hemiplegic stroke patient: a meta-analysis." *Arch Phys Med Rehabil*, 1993; 74(12): p. 1301-4.

49. Mathieu, P.A., and S.J. Sullivan, "Changes in the hemiparetic limb with training. I. Torque output." *Electromyogr Clin Neurophysiol*, 1995; 35(8): p. 491-502.

50. Pette, D, and G. Vrbova, "What does chronic electrical stimulation teach us about muscle plasticity," *Muscle Nerve* 1999 June; 22(6): p. 666-77. Review

51. Nuhr, M, et al., "Functional and biochemical properties of chronically stimulated human skeletal muscle." *Eur J Appl Physiol*, 2003; Apr; 89(2): p. 202-8.

52. Cavallaro, E., J. Rosen, J.C. Perry, S. Burns, and B. Hannaford, "Hill-based model as a myoprocessor for a neural controlled powered exoskeleton arm – parameters optimization," *Proc. Intl. Conf. on Robotics and Automation*, ICRA'05, April 2005

53. Gray, H., Anatomy of the Human Body. Philadelphia: Lea & Febiger, 1918; Bartleby.com, 2000. www.bartleby.com/107/.

54. Jau, B.M., "Anthropomorhic exoskeleton dual arm/hand telerobot controller," *IEEE International Workshop on Intelligent Robots,* 1988; p. 715-718.

55. Bergamasco, M., et al., "An arm exoskeleton system for teleoperation and virtual environments applications," *Proc. IEEE Intl. Conf. on Robotics and Automation,* 1994; vol. 2: p. 1449-1454.

56. Caldwell, D.G., O. Kocak, and U. Andersen, "Multi-armed dexterous manipulator operation using glove/exoskeleton control and sensory feedback," *Proceedings of the IEEE/RSJ Int. Conf. on Intelligent Robots and Systems*. 'Human Robot Interaction and Cooperative Robots', 1995; vol. 2: p. 567-572.

57. Repperger, D.W., et al., "Human tracking studies involving an actively powered augmented exoskeleton," *Proc 15th Southern Biomed Engineering Conf*, 1996; p. 28-31.

58. Umetani, Y., et al. ""Skil Mate", wearable exoskeleton robot," *Proceedings of the IEEE International Conference on Systems, Man, and Cybernetics*, 1999; vol.4: p. 984-988.

59. Sooyong, L., et al. "A new exoskeleton-type masterarm with force reflection: controller and integration," *Proceedings of the IEEE/RSJ International Conference on Intelligent Robots and Systems*, IROS 1999; vol.3: p.1438-1443.

60. Repperger, D.W., S.J. Remis, G. Merrill. "Performance measures of teleoperation using an exoskeleton device," *Robotics and Automation, 1990. Proc IEEE Int Conf*, 13-18 May 1990; vol.1: p.552-557.

61. Kiguchi, K., T. Tanaka, and T. Fukuda. "Neuro-fuzzy control of a robotic exoskeleton with EMG signals," *Fuzzy Systems, IEEE Transactions on,* 2004 Aug; 12(4): p. 481-490.

62. Frisoli, A., et al., "A new force-feedback arm exoskeleton for haptic interaction in virtual environments," *First Joint Eurohaptics Conf. and Symp. on Haptic Interfaces for Virtual Environment and Teleoperator Systems*, pp. 195-2005, March 2005.

63. Carignan, C., and M. Liszka. "Design of an arm exoskeleton with scapula motion for shoulder rehabilitation," *Proc. 12th Int Conf on Advanced Robotics*, July 18-20, 2005; p. 524-531.

64. Kazerooni, H., "The human amplifier technology at the university of California, Berkeley," *Robotics and Autonomous Systems*, 1996; vol. 19: p.179-187.

65. Rosen, J., M. B. Fuchs, and M. Arcan, "Performances of Hill-Type and Neural Network Muscle Models - Towards a Myosignal Based exoskeleton," *Computers and Biomedical Research*, 1999 October; 32(5): p. 415-439.

66. Rosen, J., et al., "A myosignal-based powered exoskeleton system," *IEEE Trans. On Systems, Man and Cybernetics-Part A: Systems and Humans*, 31(3), May 2001.

67. Hannaford, B., 'Feeling is Believing: Haptics and Telerobotics Technology', In "The robot in the garden: telerobotics and telepistemology in the age of the Internet," J.K. Goldberg, Ed., MIT Press, Cambridge, MA, 2000.

68. Burdea, G.C., Force and touch feedback for virtual reality, John Wiley & Sons, Inc. NY, 1996: p.339

69. Hannaford, B., and S. Venema, 'Kinesthetic display for remote and virtual environment', In "Virtual environment and advanced interface design," W. Barfield and T. A. Furness, Oxford University Press, Oxford p. 415-436, 1995.

70. Jacobsen, S.C., et al., "High performance, high dexterity, force reflective teleoperator," *Proc 38th conf on remote systems technology*, Washington DC, 1990; p.180-185

71. Workshop on Medical Robotics, International Advanced Robotics Program. Hidden Valley, Pennsylvania, May 19-22, 2004

72. Winter, D. A., Biomechanics and motor control of human movement," 2ed edition, John Wiley & Sons Inc., N.Y, 1992

73. Norman, RW, and P.V. Komi, "Electromechanical delay in skeletal muscle under normal movement conditions." *Acta Physiol Scand.* 1979 Jul;106(3):241-8.

74. Cavanagh, P.R., and P.V. Komi, "Electromechanical delay in human skeletal muscle under concentric and eccentric contractions." *Eur J Appl Physiol Occup Physiol.* 1979 Nov; 42(3):159-63.

75. Stanger, C.A., et al., "Devices for assisting manipulation: a summary of user task priorities," *IEEE Trans on Rehabil Engineering*, 1994 Dec; 2(4):256–265

76. Ramanathan, R., S. Stroud, and M.D. Alexander, "Powered Orthosis Project Forum," ASEL. Tech. Rep. TR #ROB9405. [Online]

77. Romilly, D.P., et al., "A functional task analysis and motion simulation for the develop-ment of a powered upper-limb orthosis," *IEEE Trans on Rehabil Engr*, 2(3):119-129

78. Military Handbook Anthropometry of US Military Personal, DODHDBK-743A, 1991

79. Investigation of Internal Properties of the Human Body, DOT HS-801 430, 1975

80. Basmajian, J. and A. Blumenstien, Electrode Placement in EMG Biofeedback. William & Wilkins, 1980.

81. Cram, J.F. and G. S. Kasman, Introduction to Surface Electromyography. Aspen Publishing, 1998.

82. Winters, J.M. and L. Stark, "Estimated mechanical properties of synergistic muscles involved in movements of a variety of human joints," *J biomech*, 1988; vol. 21: p. 1027-1041.

83. Lemay, M.A. and P. Crago, "A dynamic model for simulating movements of the elbow, forearm and wrist," *J biomech*, 1996; vol. 29: p. 1319-1330.

84. Garner, B.A. and M. G. Pandy, "A kinematic model of the upper limb based on the visible human project (vhp) image dataset," *Computer methods in biomechanics and biomedical engineering*, 1999; vol. 2: p.107-124.

85. Garner, B.A. and M. G. Pandy, "Musculoskeletal model of the upper limb based on the visible human male dataset," *Computer methods in biomechanics and biomedical engineering,* 2001; vol. 4: p. 93-126.

86. Garner, B.A. and M. G. Pandy, "The obstacle-set method for representing muscle paths in musculoskeletal models," *Computer methods in biomechanics and biomedical engineering*, 2000; vol. 3: p.1-30.

87. Winters, J.M., "Multiple muscle systems: biomechanics and movement organization, ch. Hill based muscle models: a system engineering perspective," p. 69-93. Springer-Verlag, N.Y., 1990

88. Zajac, F.E., "Muscles and tendons: properties, models, scaling, and application to biomechanics and motor control," *Critical Reviews in Biomedical Engineering*, 1989.

89. Yarden, O., "Dynamics of racket-arm interaction applied to tennis elbow." PhD thesis, University of Tel-Aviv, 1996.

90. Buchanan, T.S., G. P. Rovai, and W. Z. Rymer, "Strategies for muscle activation during isometric torque generation at the human elbow," *J Neurophysiol*, 1989.

91. Tax, A.A., J.J.D. van der Gon, C.C. Gielen, and C.M.V. den Tempel, "Differences in the activation of m. biceps brachii in the control of slow isotonic movements and isometric contractions," *Exp Brain Res*, 1989.

92. Holland, J., Adaptation In Natural and Artificial Systems. The University of Michigan Press, Ann Arbour, 1975.

93. Michalewicz, Z., Genetic algorithms + data structures = Evolution programs. Springer, 1996.

94. Houk, C.R., J.A. Joines, and M.G. Kay, "A genetic algorithm for function optimization: a matlab implementation," tech. rep., North Carolina State University, 1995.

95. Virtual Reality: Scientific and Technological Challenges, Ch. Telerobotics, pp. 304-361, National Research Council, National Academies Press, Jan. 1, 1994

96. Robot Analysis and Control, sec. The Modeling/Performance Trade-Offs, pp. 165-169. H. Asada, J.-J. E. Slotine. Wiley-IEEE, April 11, 1986

97. Virtual Reality: Scientific and Technological Challenges, ch. Position Tracking and Mapping, pp.188-204, Natl. Res. Council, National Academies Press, Jan. 1, 1994

98. Kazerooni, H., "Human-Robot Interaction via the Transfer of Power and Information Signals," *Trans on Systems, Man, and Cybernetics*. March/April 1990; 20 (2)

99. Brooks, T.L., "Telerobotic Response Requirements," *Proc Intl Conf On Systems, Man and Cypernetics*, Los Angeles, CA, Nov. 1990; p.113-120

100. Yokoi, K., et al., "Design and control of a seven-degrees-of-freedom manipulator actuated by a coupled tendon-driven system." Intelligent Robots and Systems '91.

'Intelligence for Mechanical Systems, *Proc IROS '91. IEEE/RSJ International Workshop*, 3-5 Nov. 1991; vol.2: p. 737 - 742

101. Ma, S., S. Hirose, and H. Yoshinada, "Design and experiments for a coupled tendon-driven manipulator," *Control Systems Magazine*, IEEE 13(1), Feb. 1993; pp. 30 - 36

102. Salisbury, K., W. Townsend, B. Eberman, and D. DiPietro, "Preliminary design of a whole-arm manipulation system (WAMS)," *Proc IEEE Intl Conf On Robotics and Automation*, April 1988; vol. 1: p. 254-260,.

103. Miller, L., "Gravity Compensation for a 7 DoF upper limb exoskeleton," Thesis, University of Washington, 2006

104. Davis, B., "Velocity Control of a Seven Degree-of-Freedom Exoskeleton Arm," Thesis, University of Washington, 2006

105. Murray, R.M., Z. Li, and S.S. Sastry, A Mathematical Introduction to Robotic Manipulation. CRC Press, Boca Raton, Florida, 1994

106. de Leva, P. "Adjustments to Zatsiorsky-Seluyanov's segment inertia parameters." *J Biomechanics*, Sept. 1996; 29(9), p.1223-30,

107. McConville, J.T., C.E. Clauser, J. Cuzzi, "Anthropometric Relationships of Body and Body Segment Moments of Inertia," Report No. AFAMRL-TR-80-119, Aerospace Medical Research Laboratory, Wright-Patterson Air Force Base, Dayton, Ohio, 1980

108. Kazerooni, H. and T.J. Snyder, "Case study on haptic devices: Human-induced instability in powered hand controllers," *Journal of Guidance Control and Dynamics*, 1995; 18 (1): p.108-113.

109. Kazerooni, H., "The human amplifier technology at the university of California, Berkeley," *Robotics and Autonomous Systems*. 1996; vol. 19: p.179-187.

110. Remis, S.J., "Design of an Exoskeleton with Kinesthetic Feedback: Lessons Learned." *IEEE Intl Conf On Systems Engineering*, Aug 9-11, 1990; p.109-112

111. Kim, Y.S., J. Lee, S. Lee, and M. Kim, "A Force Reflected Exoskeleton-Type Masterarm for Human- Robot Interaction." *IEEE Trans On Systems, Man, and Cybernetics* – Part A: Systems and Humans, March 2005, 35(2): p.198-212

112. Frisoli, A., et al., "A new force-feedback arm exoskeleton for haptic interaction in virtual environments." *First Joint Eurohaptics Conference and Symposium on Haptic Interfaces for Virtual Environments and Teleoperator Systems*, March 18-20 2005; p.195-201

113. Tsagarakis, N., D.G. Caldwell, and G.A. Medrano-Cerda, "A 7 dof pneumatic Muscle Actuator (pMA) powered Exoskeleton," *Proc. Of the 1999 IEEE Intl Workshop on Robot and Human Interaction*, Pisa, Italy. Sept. 1999; p. 327-333

114. Johnson, G.R., et al., "The design of a five-degree-of-freedom powered orthosis for the upper limb." *Proc Instn Mech Engrs,* 2001; vol. 215, part H: p. 275-284

115. Kapandji, I.A., The Physiology of the Joints: Annotated Diagrams of the Mechanics of the Human Joints, Churchill Livingstone; 5th Revise edition, 1982

116. Morrey, B.F. and K.N. An, The Shoulder, Ch. 6: Biomechanics of the Shoulder. Vol. 1, Ed. C.A. Rockwood, F.A. Matsen. WB Saunders Company, Philadelphia, PA. 1990.

117. Kelly-Hayes, M., et. al., The American Heart Association Stroke Outcome Classification: Executive Summary. AHA Scientific Statement. *Circulation J Amer Heart Assoc.*, June 1998.

118. Thom, T., et al., Heard Disease and Stroke Statistics – 2006 Update. AHA Statistical Update; *Circulation J Amer Heart Assoc,* Feb. 14, 2006

119. Arias, E, United States Life Tables, 2003. National Vital Statistics Reports, Centers for Disease Control and Prevention, April 19, 2006; 54(14): p. 1-40

120. Centers for Disease Control and Prevention. Public Health and Aging: Trends in Aging – United States and Worldwide. MMWR 2003; 52(06): p. 101-106

121. Clinical Neuropsychology and Cost Outcome Research, Ed. Prigatano G.P., Pliskin, N.H. Psychology Press, Inc. New York, NY, 2003; p. 113-115,

122. Dobkin, B., The economic impact of stroke. *Neurology*, 1995; 45(2) S6-S9,

123. Diringer, et al.; Predictors of Acute Hospital Costs for Treatment of Ischemic Stroke in an Academic Center. *J Amer Heart Assoc*, April 1999; p. 724-728

124. Taylor, T.N.; Lifetime Cost of Stroke in the United States. *Stroke*, 1996; 27: p. 1459-1466

125. US Census Bureau, Global Population Profile: 2002, March 2004, p. 49

126. Perry, J.C., J. Rosen, "Design of a 7 Degree-of-Freedom Upper-Limb Powered Exoskeleton," *First IEEE Intl Conf On Biomedical Robotics and Biomechatronics*, Feb. 20-22, 2006; p. 805-810

APPENDIX A: ADDITIONAL RENDERINGS AND PHOTOGRAPHS

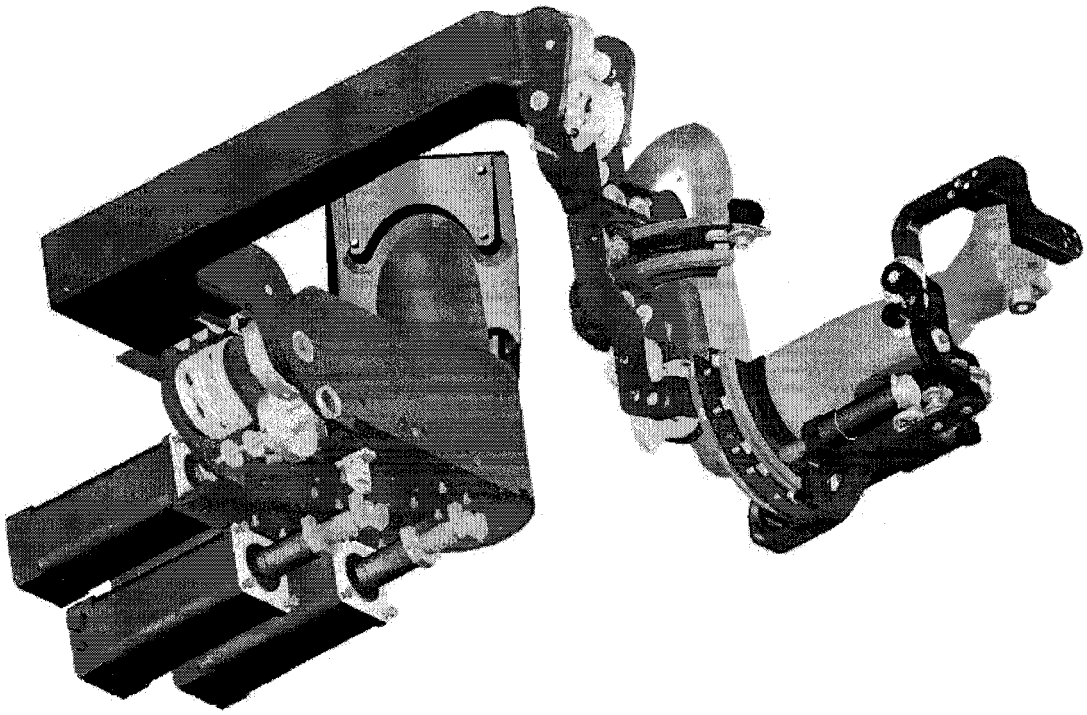

Figure A.1: 3-dimensional CAD rendering (Solidworks) of a human arm wearing the CADEN-7 exoskeleton arm.

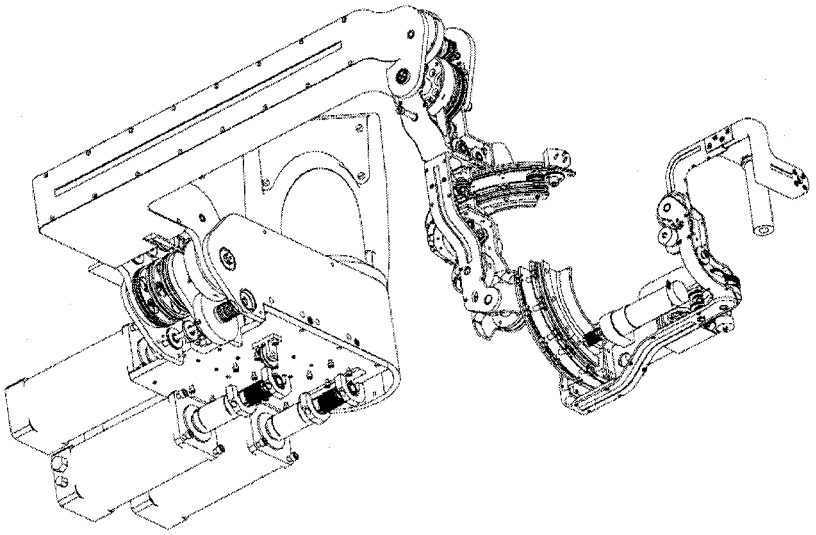

Figure A.2: The 7 degree-of-freedom exoskeleton is composed of a wall-mounted stationary base and seven articulating rigid link subassemblies (see Fig. A.3).

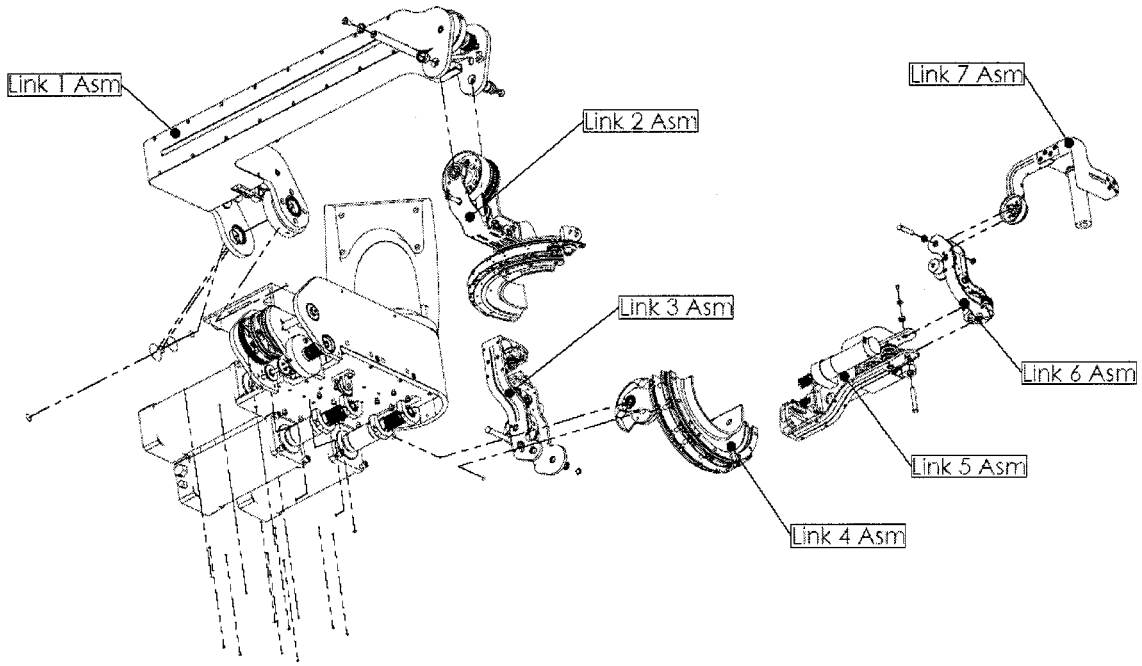

Figure A.3: An exploded wireframe view of the CADEN-7 exoskeleton arm illustrate the various subassembly components, labelled sequentially from the base..

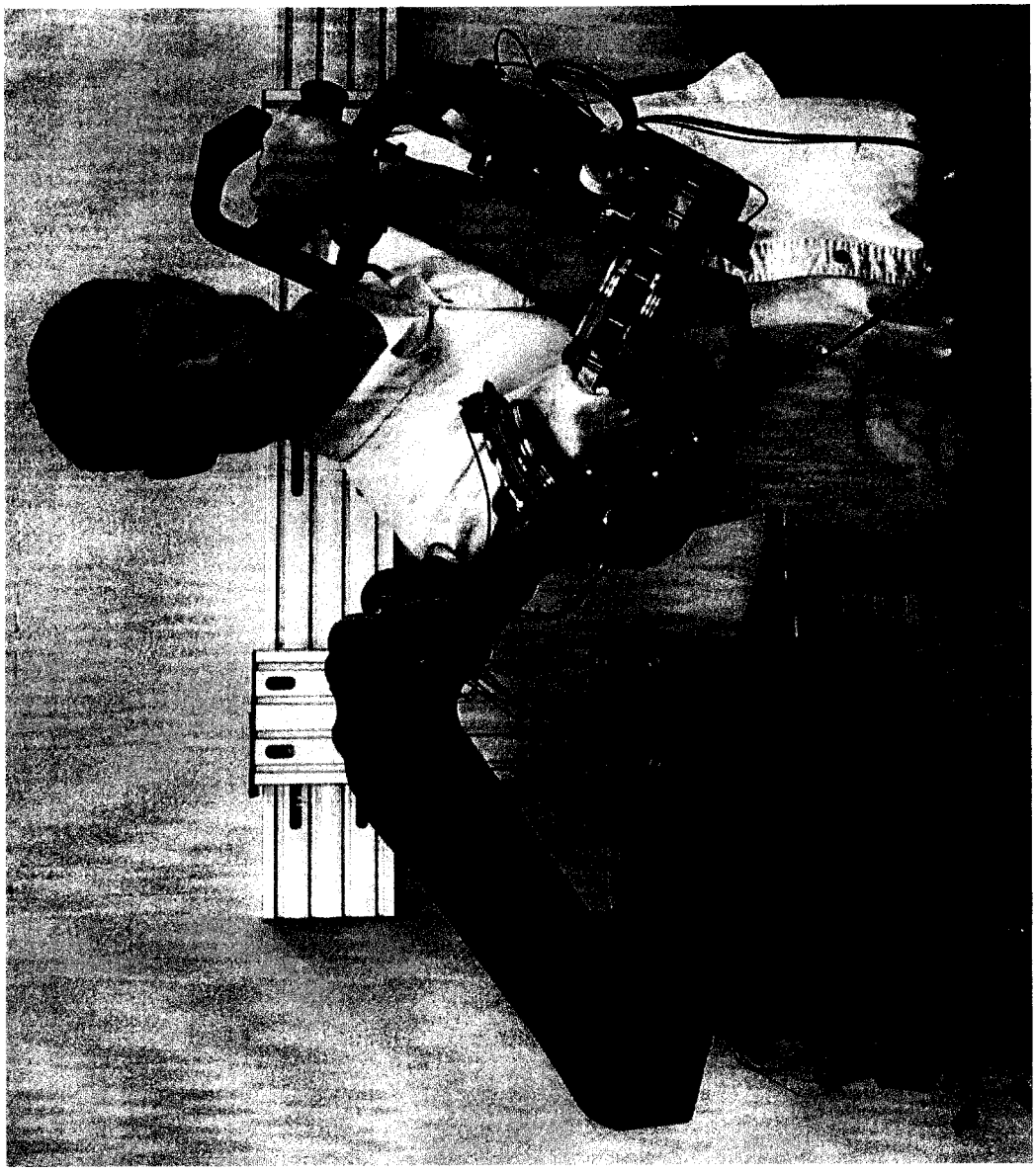

Figure A.4: The CADEN-7 exoskeleton arm enables users to achieve full glenohumeral, elbow, and wrist joint functionality [126].

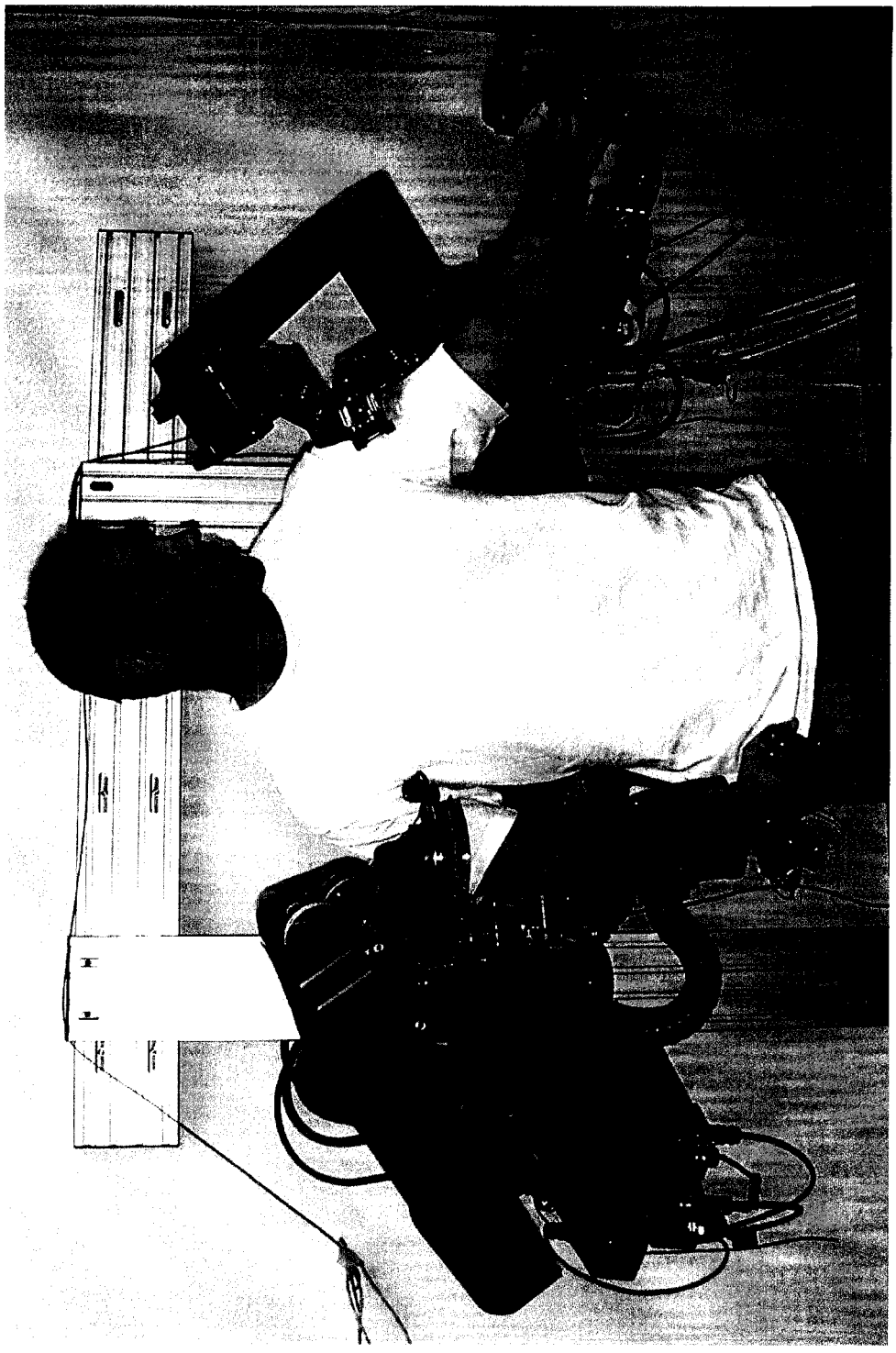

Figure A.5: The dual-arm CADEN-7 exoskeleton system offers assessment, treatment, and neuro-muscular research capabilities on patient populations with either left or right arm afflictions.

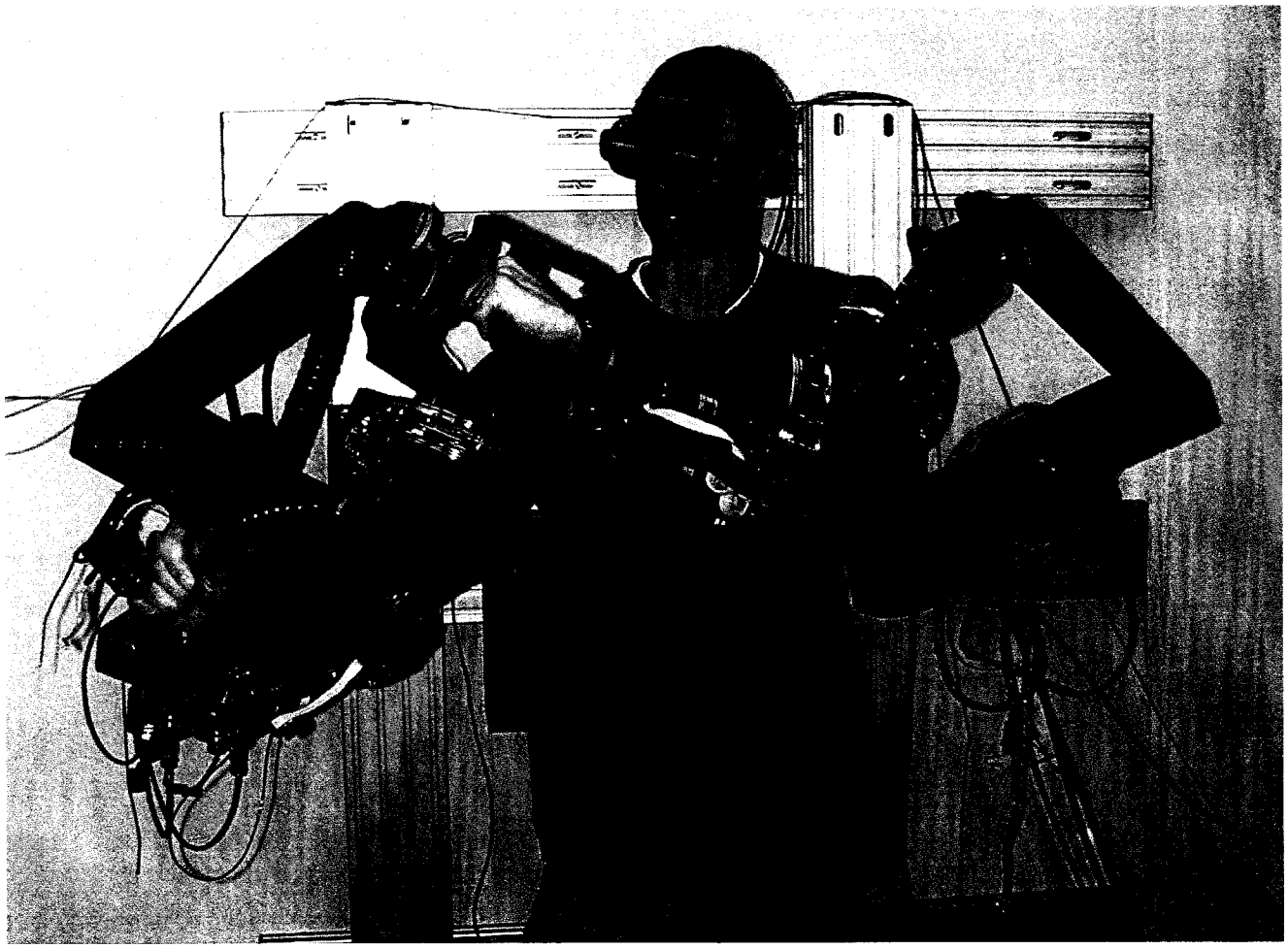

Figure A.6: Other applications of the dual-arm CADEN-7 exoskeleton system include total arm haptic force rendering in virtual environments. With the use of VR eyewear, a user can experience a virtual representation of his arms and physically feel forces and collisions with virtual objects in a simulated environment. Such environments could serve as platforms for therapeutic rehabilitation, complex operator training, gaming, and much more.

CURRICULUM VITAE

JOEL C. PERRY

EDUCATION

University of Washington, Seattle, WA — PhD Mechanical Engineering
Granted Research Assistantship — August 2006

University of Washington, Seattle, WA — M.S. Mechanical Engineering
Granted Teaching Assistantship — December 2002

Gonzaga University, Spokane, WA — B.S. Mechanical Engineering
Awarded Trustees and Engineering academic merit scholarships — August 2000

WORK EXPERIENCE

Postdoctoral Researcher, University of Washington — Autumn 2006-Present
Research and development of advanced medical robotics. Review of designs for manufacturability, assemblability, and functionality. Technical writing for publication. Grant proposal preparation.

Research Assistant, University of Washington — Winter 2002-Summer 2006
Research and development of 7 degree-of-freedom powered exoskeleton robotic arm. Design of custom parts for low-inertia, high-stiffness operation under 10 Hertz bandwidth. FEA analysis of stress and deformation for design evaluation. Development of back-drivable power transmissions with zero backlash.

Research Assistant, University of Washington — Summer 2001-Winter 2002
Research and development of variable stiffness ankle prosthesis for the VA Center of Excellence in Limb-Loss Prevention and Prosthetic Engineering. Literature searches via Medline, Compendex, IEEE Xplore. Retrofit of pneumatic muscle actuators on existing single axis ankle prosthesis.

Research Assistant, University of Washington — Spring-Summer 2001
Design work in Bio-Robotics lab on training device for minimally-invasive surgery

Teaching Assistant, University of Washington — Autumn 2000-Spring 2001
Engineering Graphics lab instructor. Discuss 3D modeling concepts and present features of Solidworks 2000 to groups of 20-30 students. Address homework questions, troubleshoot modeling errors, and hold office hours.

Whitewater Engineering Corp, Cordova, Alaska — Summer 1999
Field Engineer. Interpreted blueprints and worked with several others to build a bridge. Worked as part of a team that surveyed grade, directed heavy equipment, and operated heavy equipment.

Haskell Corporation, Bellingham, Washington — Summers 1997 and 1998
Pipefitting apprentice. Prepared pipes for: welding, measuring, and cutting. Forklift operator. Interpreted pipe spool drawings, pressure tested, and sandblasted. Secured loads.

ACTIVITIES

- University of Washington Sports – Track and Field Team 2000-2001
- Campus Ministry – Coordinator of Gonzaga Search Program 1999-2000
- Member of American Society of Mechanical Engineering 1996-2000
- Gonzaga Sports – Track Team and Intramural Basketball 1997-1999
- American Legion Evergreen Boys State – Junior Counselor 1996-1998
- Volunteer Groups: Esperanza, Habitat for Humanity, April's Angels
- National Honor Societies: Alpha Sigma Nu, Tau Beta Pi

PUBLICATIONS

1. "Hill-Based Model as a Myoprocessor for a Neural Controlled Powered Exoskeleton Arm – Parameters Optimization." Ettore Cavallaro, Jacob Rosen, Joel C. Perry, Stephen Burns, Blake Hannaford. Proc. Intl. Conf. on Robotics and Automation. Barcelona, Spain. April 18-22, 2005; Page(s): 4514-4519

   – ICRA 2005 (published)

2. "The Human Arm Kinematics and Dynamics During Daily Activities – Toward a 7 DOF Upper Limb Powered Exoskeleton." Jacob Rosen, Joel C. Perry, Nathan Manning, Stephen Burns, Blake Hannaford. Proc. 12th Intl. Conf. on Advanced Robotics. Seattle, USA. July 18-20, 2005; Page(s): 532-539.

   – ICAR 2005 (published)

3. "Design of a 7 Degree-of-Freedom Upper-Limb Powered Exoskeleton." Joel C. Perry, Jacob Rosen. Proc. 1st Intl. Conf. on Biomedical Robotics and Biomechatronics. Pisa, Italy. February 20-22, 2006.

   – BioRob 2006 (published)

4. "Real-time Myoprocessors for a Neural Controlled Powered Exoskeleton Arm." Ettore Cavallaro, Jacob Rosen, Joel C. Perry, Stephen Burns, Blake Hannaford. IEEE Trans. on Biomedical Engineering.

   – 2006 (accepted for publication)

5. "Upper-Limb Powered Exoskeleton Design." Joel C. Perry, Jacob Rosen, Stephen Burns. IEEE ASME Trans. on Mechatronics. Focused section on Medical Mechatronics.

   – 2006 (submitted for publication)

6. "Gravity Compensation for a 7 DoF Exoskeleton: A Theoretical and Experimental Approach." Levi Makaio Miller, Joel C. Perry, Jacob Rosen. IEEE Int. Conf. On Robotics and Automation. Rome, Italy. April 10-14, 2007.

   – 2006 (submitted for publication)

CURRENT RESEARCH INTERESTS

Research interests include medical device development, rehabilitation robotics, biologically-inspired robotics, and assistive technologies for the disabled.